MICROCOPY RESOLUTION TEST CHART
NATIONAL BUREAU OF STANDARDS 1963 A

AFWAL-TR-80-3132, PART IV

ALTERNATE T-38 TRANSPARENCY DEVELOPMENT
PART IV, PARAMETRIC STUDIES

Richard A. Nash
Blaine S. West

University of Dayton
Research Institute
Dayton, Ohio 45469

June 1983

Final Report for Period: January 1980 - February 1981

Approved for public release; distribution unlimited.

DTIC
ELECTE
AUG 0 0 1983

FLIGHT DYNAMICS LABORATORY
AIR FORCE WRIGHT AERONAUTICAL LABORATORIES
AIR FORCE SYSTEMS COMMAND
WRIGHT-PATTERSON AIR FORCE BASE, OHIO   45433

082

NOTICE

When Government drawings, specifications, or other data are used for any purpose other than in connection with a definitely related Government procurement operation, the United States Government thereby incurs no responsibility nor any obligation whatsoever; and the fact that the Government may have formulated, furnished, or in any way supplied the said drawings, specifications, or other data, is not to be regarded by implication or otherwise as in any manner licensing the holder or any other person or corporation, or conveying any rights or permission to manufacture use, or sell any patented invention that may in any way be related thereto.

This report has been reviewed by the Office of Public Affairs (ASD/PA) and is releasable to the National Technical Information Service (NTIS). At NTIS, it will be available to the general public, including foreign nations.

This technical report has been reviewed and is approved for publication.
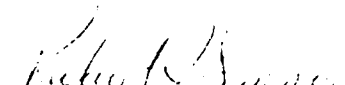
1Lt ROBERT J. SIMMONS
Project Manager
Improved W/S Protection ADPO
Vehicle Equipment Division
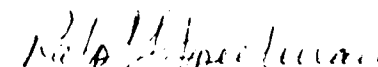
RALPH J. SPEELMAN
Program Manager
Improved W/S Protection ADPO
Vehicle Equipment Division

FOR THE COMMANDER:

SOLOMON R. METRES
Director
Vehicle Equipment Division

REPORT DOCUMENTATION PAGE		READ INSTRUCTIONS BEFORE COMPLETING FORM
1. REPORT NUMBER AFWAL-TR-80-3132,Part IV	2. GOVT ACCESSION NO.	3. RECIPIENT'S CATALOG NUMBER
4. TITLE (and Subtitle) ALTERNATE T-38 TRANSPARENCY DEVELOPMENT PART IV, PARAMETRIC STUDIES		5. TYPE OF REPORT & PERIOD COVERED Final Report January 1980-February 1981
		6. PERFORMING ORG. REPORT NUMBER UDR-TR-82-25
7. AUTHOR(s) Richard A. Nash Blaine S. West		8. CONTRACT OR GRANT NUMBER(s) F33615-76-C-3103 F33615-80-C-3401
9. PERFORMING ORGANIZATION NAME AND ADDRESS University of Dayton Research Institute 300 College Park Avenue Dayton, Ohio 45469		10. PROGRAM ELEMENT, PROJECT, TASK AREA & WORK UNIT NUMBERS Project 2202 Project 1926
11. CONTROLLING OFFICE NAME AND ADDRESS Air Force Wright Aeronautical Laboratories (AFWAL/FIEA) Wright-Patterson Air Force Base, OH 45433		12. REPORT DATE June 1983
		13. NUMBER OF PAGES 96
14. MONITORING AGENCY NAME & ADDRESS(If different from Controlling Office)		15. SECURITY CLASS. (of this report) Unclassified
		15a. DECLASSIFICATION. DOWNGRADING SCHEDULE

16. DISTRIBUTION STATEMENT (of this Report)

Approved for public release; distribution unlimited.

17. DISTRIBUTION STATEMENT (of the abstract entered in Block 20, if different from Report)

18. SUPPLEMENTARY NOTES

19. KEY WORDS (Continue on reverse side if necessary and identify by block number)

Acrylic	Materially Nonlinear	MAGNA
Polycarbonate	Analysis	T-38 Transparencies
Parametric Study	Finite Element	T-38 Student
Geometrically Nonlinear	Analysis	Windshiled
	Birdstrike	Static Analysis

20. ABSTRACT (Continue on reverse side if necessary and identify by block number)

..Studies conducted to examine the effect of structural parameter variations on the nonlinear, dynamic response of the T-38 student windshield/support structure system to bird impact are described. The studies were conducted using the Materially And Geometrically Nonlinear Analysis (MAGNA) finite element computer program. Both static and transient dynamic analyses were conducted, examining the effects of changes to the transparency and support structure

DD $_{1}^{FORM}_{JAN\ 73}$ 1473 EDITION OF 1 NOV 65 IS OBSOLETE

Continuation of Block 19.

Bird Impact
Impulse-Momentum
Transient Dynamic Analysis

Continuation of Block 20.

stiffness, intensity of the applied load both coupled and
uncoupled, and duration of the impact event. Significant results
of the finite element analysis include transparency deflection,
peak load versus transparency stiffness, and resultant force
plots both along the aft arch and around the impact area. A
discussion of application of the finite element method to the
birdstrike problem is also presented.

FOREWORD

Accession For

NTIS GRA&I	X
DTIC TAB	☐
Unannounced	☐
Justification	

Distribution/

Availability Codes

Dist | Avail and/or Special

A

iii

TABLE OF CONTENTS

LIST OF ILLUSTRATIONS

LIST OF ILLUSTRATIONS (continued)

LIST OF ILLUSTRATIONS   (concluded)

LIST OF TABLES

LIST OF SYMBOLS

A_t	Area under applied load at time t (in.^{2})
b,h,ℓ,d	Linear dimensions (in)
E_T	Elastic modulus, transparency (lb/in^2)
E_F	Elastic modulus, frame (lb/in^2)
F_{AVE}	Average force (lb)
F_{Peak}	Peak force (lb)
F_t	Force at time t (lb)
F_{TY}	Yield tensile strength (lb/in^2)
F_{TU}	Ultimate tensile strength (lb/in^2)
F_{BRU}	Ultimate bearing strength (lb/in^2)
G	Shear modulus (lb/in^2)
I_x	Moment of inertia along horizontal axis (in^4)
I_y	Moment of inertia along vertical axis (in^4)
I_{xy}	Product of inertia (in^4)
K	Force constant (lb$^{1/3}$-sec^2/ft^2)
K_T	Transparency stiffness (lb-in^2)
K_F	Frame stiffness (lb-in^2)
$ℓ_{EFF}$	Effective length (in)
m	Mass (lb-sec^2/ft)
P	Pressure (lb/in^2)
t	Time (sec)
t_t	Transparency thickness (in)
u_t	Transparency deflection (in)
V	Velocity (ft/sec)
ρ	Volumetric density (lb/in^3)

σ_E Equivalent stress (lb/in^2)

ϵ_F Frame strain   (in/in)

ν Poisson's ratio

θ Angle (degrees)

T_S Squash up time (sec)

SECTION I

INTRODUCTION

The structural analysis parametric studies of the T-38 forward transparency system (Figure 1) were conducted in support of the T-38 Improved Transparency Development (Reference 1). With the increased use of the T-38 aircraft in low level flight, the problem of birdstrike becomes a primary concern with regard to possible loss of life and loss of aircraft. The present impact resistance of the T-38 aircraft student windshield for a four pound bird impacted along the centerline of the aircraft near the intersection of the student windshield and canopy is 190 knots (Reference 2). This capability would be adequate for low speed landings, but for high speed, low level flight it is inadequate. This effort addresses the problem of improved capability and contributes to its solution as illustrated in Figure 3, Part I of this report.

This report presents the results of parametric studies, encompassing a range of design variables which evaluate the ability of the transparency structural system to absorb impact loading effectively. The objective of these parametric studies was to examine the effect of variations in the transparency and support structure in the performance of the total system during the birdstrike event.

The studies reported herein involve the application of new technology to the birdstrike problem; specifically, the application of the nonlinear finite element method to the dynamic response analysis of the T-38 structural system. The use of the finite element method in a parametric study of this type has not previously been extended to include the nonlinear response characteristics of a transparency system of this complexity (see Figures 1, 2, and 3). Some of the problems associated with nonlinear coupled load application, nonlinear material response, and problem size are discussed.

1

Front
(Student) Windshield

REAR
WINDSHIELD

NORTHROP DWG
2-13000
3-13000
3-13014

NORTHROP DWG
3-13100

FRONT CANOPY

NORTHROP DWG
2-13201

REAR CANOPY

NORTHROP DWG
2-13300
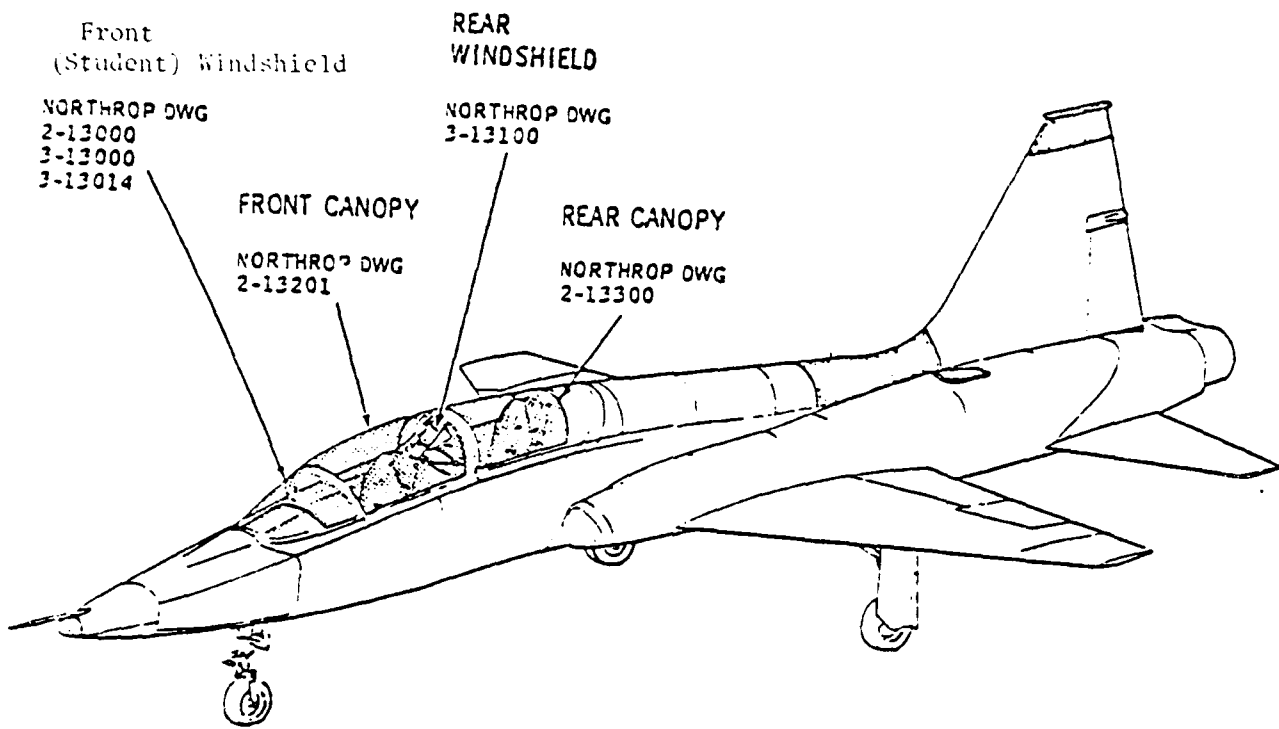
Figure 1.   T-38 Aircraft.

2
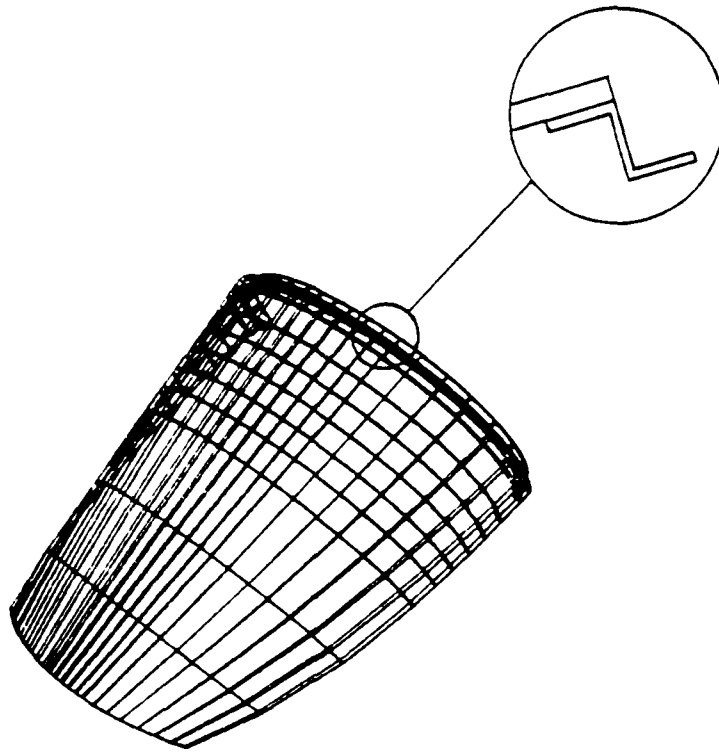
Figure 2.   Student Windshield Finite Element Model -
             Undeflected.
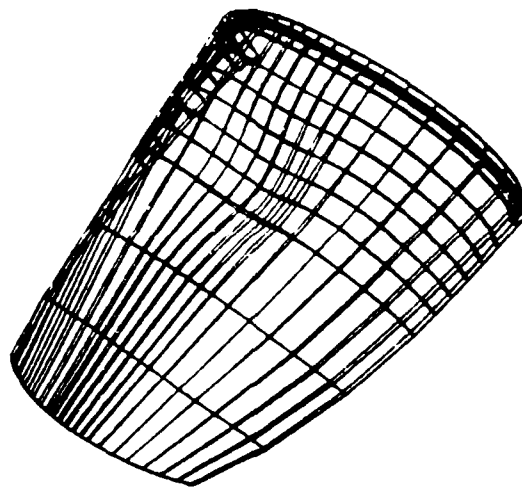
Figure 3.   Student Windshield Finite Element Model -
             Deflected.

Details related to assembly of the finite element model, preparation of the necessary input data (material properties, loads, element types, etc.), solution techniques, and methods used to interpret the results are presented. The organization is such that the information is presented in a chronological sequence. The sequence proceeds from definition of the design data such as the applied loads and mechanical and sectional properties to the parametric study matrix, a description of the finite element model and analysis, and finally to presentation of the results.

SECTION II

PRELIMINARY CONSIDERATIONS

The T-38 transparency development program was initiated with the ground rule that structural changes should be minimized (see Reference 1). Any alteration to the windshield structural system should involve field or depot level retrofit only. The resulting recommended candidate transparency design configurations for the forward windshield, as defined in Reference 1, are:

a. Monolithic polycarbonate with inside and outside coatings;

b. Monolithic polycarbonate structural ply with thin outer acrylic ply and inside coating;

c. Monolithic polycarbonate structural ply with inside and outside acrylic plies; and

d. Increased thickness (0.9 inch) monolithic stretched acrylic.

For this parametric study, concentration was focused on the range of stiffness provided by single ply transparencies, the existing 0.6 inch and candidate 0.9 inch stretched acrylic, and the 0.45 inch polycarbonate. The 0.45 inch polycarbonate was part of recommendation (b) above, with the elimination of the thin acrylic and interlayer materials.

All finite element studies reported herein were made using a geometrically and materially nonlinear analysis computer program MAGNA (Reference 9). The MAGNA computer program is a large scale, general purpose finite element system intended for the nonlinear analysis of complex engineering structures. Unlike many available nonlinear analysis software packages, MAGNA has been developed primarily for the efficient solution of three dimensional problems, involving many degrees of freedom and large bandwidth. Isoparametric modeling techniques and state-of-the-art numerical solution methods are combined in MAGNA to provide effective

analytical capabilities for three-dimensional structures experiencing large displacements, finite strains, arbitrary rotations, and elastic-plastic behavior. Both static and transient dynamic solution options may be performed with the program, as well as natural frequency/normal mode calculations, and steady-state forced harmonic vibrations of viscoelastically damped structure. Analyses were accomplished on the ASD CDC CYBER 175/750 computer system located in Building 676, Wright-Patterson Air Force Base, Ohio.

Performance of the parametric studies was facilitated by the use of computer programs developed for interactive use on the computer. Two of the major efforts involved the generation of MAGNA program input data in correct form and order, and the computation of resultant forces from the postprocessing capabilities in MAGNA. All geometry, material, element, constraint, and loading data were assembled and submitted to the computing facilities interactively. The Resultant Forces Program provided the necessary means to interpret the load distribution data both lengthwise and along the student windshield/student canopy support arch. Some of this data is presented in Section 5, Analytical Studies.

The difference between stretched acrylic and polycarbonate material properties, as input to the finite element program for an elastic-plastic material, are minimal as shown in Table 2. However, the material failure mechanisms associated with the two materials are significantly different. A brittle material will generally fail when the maximum principal stress reaches the ultimate strength of the material. A ductile material will yield when the combination of principal stresses, expressed in terms of an equivalent uniaxial tensile stress, produces the same level of octahedral shear stress as does a uniaxial tensile specimen at yield. This is referred to as the octahedral shear stress theory and is incorporated into the MAGNA computer code. These two failure mechanisms were used to interpret the acrylic and polycarbonate material response, respectively.

6

Another important consideration in the analytical process is the energy transformation between the bird and the aircraft. As the aircraft strikes the bird, energy is imparted to the bird through the transparency structural system. During the impact event the bird mass is accelerated to the velocity of the aircraft (normal component) with no significant change in the velocity of the aircraft. During impact, at relatively high velocities, the bird is compressed and behaves as a viscous fluid (Reference 4), loading the transparency. The design approach to absorbing the energy resulting from a bird-aircraft collision can be accomplished through different design philosophies. One approach is to design a very stiff transparency and supporting structure to deflect the path of the bird mass without introducing significant deflections or stresses in the transparency/support structure system. A second approach is to design a very flexible system in an attempt to accelerate the bird mass to the aircraft velocity and absorb the resulting energy. Previous experience (Reference 5) indicates that the most efficient and practical approach for providing safety to the aircraft crew in high performance aircraft is a compromise between these two extremes.

SECTION III

DESIGN DATA

1. LOADS - STATIC ANALYSIS

Preliminary bird loading of the T-38 student windshield for the static analysis was based on the recommendations of References 4, 6, 7, and 8. Formulae for each of the four methods and the basic assumptions associated with each are presented in the Appendix. The results of these loads calculations (summarized in Table 1) established a range of bird loading for use with the MAGNA static analysis option. The calculated peak loading ranged from a high of 284,240 lb. to a low of 31,025 lb. During preliminary analysis, the structural response of the system more closely resembled the experimental results of Reference 2 when the latter values were used. A range of pressure (load) levels corresponding to the range of peak loads was used in the parametric study. The pressures ranged from a low of 250 psi to a high of 750 psi in steps of 100 psi. The analysis was discontinued at the pressure level which indicated ductile failure.

For the parametric study, the impact point location investigated is shown in Figure 4. The axis of an assumed cylindrical bird was concentric with the load point for determining load location. The targeted point is on the aircraft center-line 6-1/4 inches in the forward direction, down the transparency from the intersection of FS 169.0 and the outer mold line of the student windshield of the T-38 aircraft. Previous experience (References 2 and 5) indicates that the worst case condition is at this location where the birdstrike is in close proximity to the constrained edge of the transparency.

2. LOADS - TRANSIENT DYNAMIC ANALYSIS

Based on the results of the static analysis and review of the loading formulae of the Appendix, the load intensity and time duration for the transient dynamic analysis was derived from

TABLE 1

BIRD LOADING CALCULATIONS

Calculation Method	Bird Weight (lbs)	Bird Speed (knots)	Angle Incidence (degrees)	Average Force (lbs)	Peak Force (lbs)
A[5,6]*	4	400	27 1/2		284,420
B[3]	4	400	27 1/2		31,025
C[3]	4	400	27 1/2		129,935
D[4]	4	400	27 1/2	29,280	37,610

* Superscripts refer to referenced documents.
  Also see Appendix
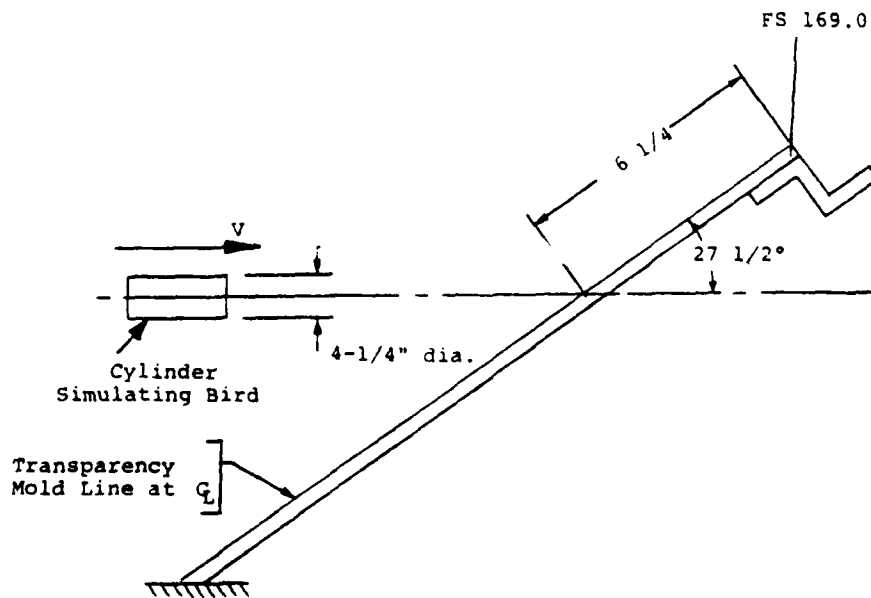
Figure 4. Load Application Location.

9

impulse and momentum relationships. The peak load-time curve was assumed to be a sawtooth type distribution as depicted in Figure 5. The spatial distribution of the load along the center-line of the transparency was assumed triangular in shape. The distribution transverse to the centerline was assumed to be rectangular in shape. These assumptions were based on preliminary analyses, the data in References 4 and 6 and experimental films of the T-38 baseline birdstrike testing (Reference 2). The impulse and momentum relationship is

$$mv = \frac{1}{2} F_{peak} \, t \, .$$

A plot of the two variables t (time) and F (peak load) is shown in Figure 6 for a four pound bird.

For the dynamic analysis a time of 4.75 milliseconds was used with Figure 6 to determine the proper peak load to be used in conjunction with Figure 5. This time was estimated from experimental observation of AEDC test number 641. This was a 190 knot impact on 0.6 in. acrylic windshield at impact point shown on Figure 4 of this report. The shot was a pass. See Reference 2 for further details. The 4.75 millisecond time includes the entire birdstrike event from the first point of contact between bird and transparency to the resulting bird mass breaking contact with the transparency.

3.   SECTIONAL PROPERTIES

The student windshield aft arch support structure of the T-38 aircraft has the cross-section shown in Figure 7(a). During the transparency parametric study the Z-shaped arch shown in Figure 7(b) was used to simulate the actual frame. This Z configuration provided an adequate representation of the frame stiffness and required only three elements, whereas a model of the original cross-section would have required five elements. The five element aft arch simulation shown in Figure 7(c) was used in

F (Force-lbs)
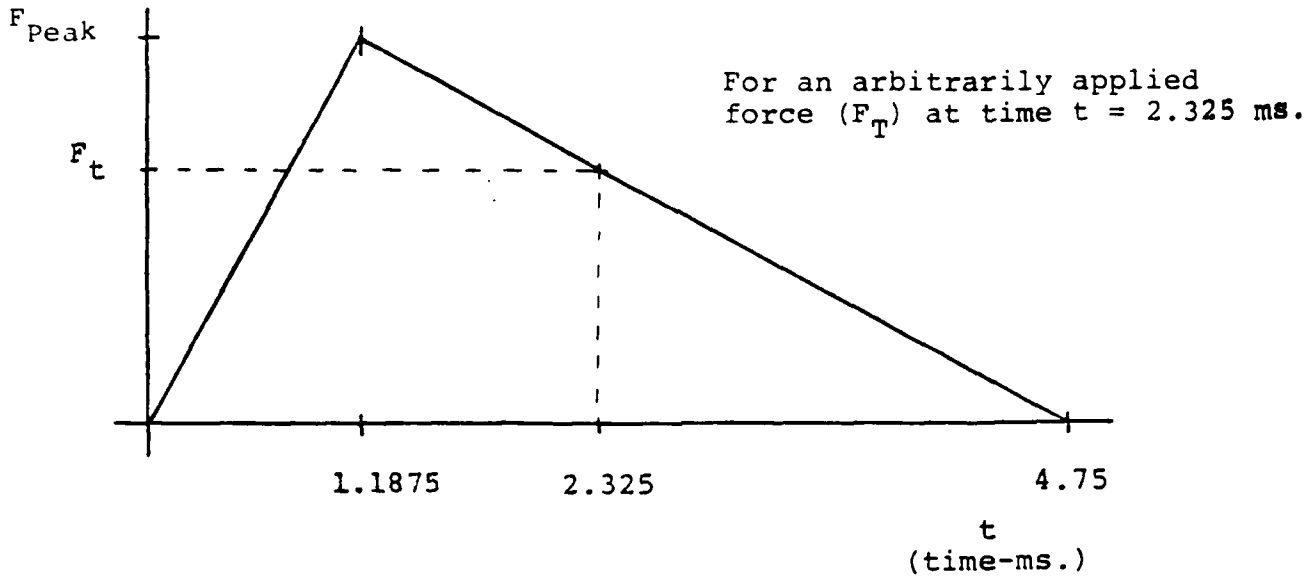
Temperal Distribution

P (Pressure-psi)

P_n - Average Pressure on Element n

A_T - Total Area Under Applied Force (Area of Element Top Surface)

*Finite Element Number
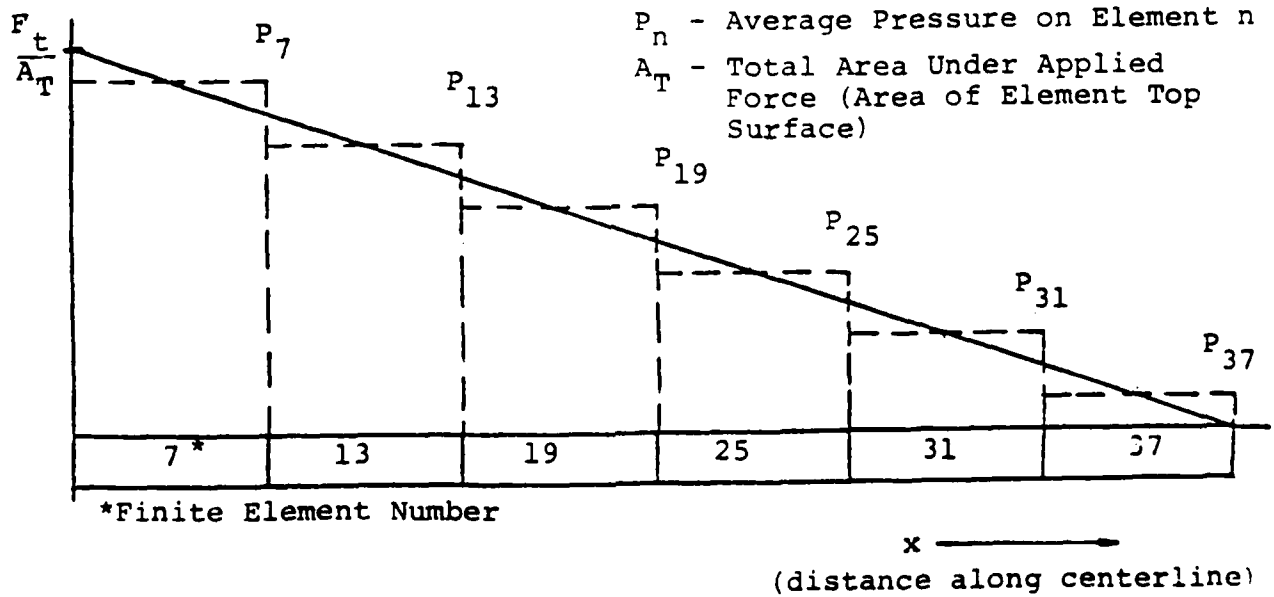
Spatial Distribution
@ t = 2.325 ms.

Figure 5.   Typical Dynamic Loading Curves.

11
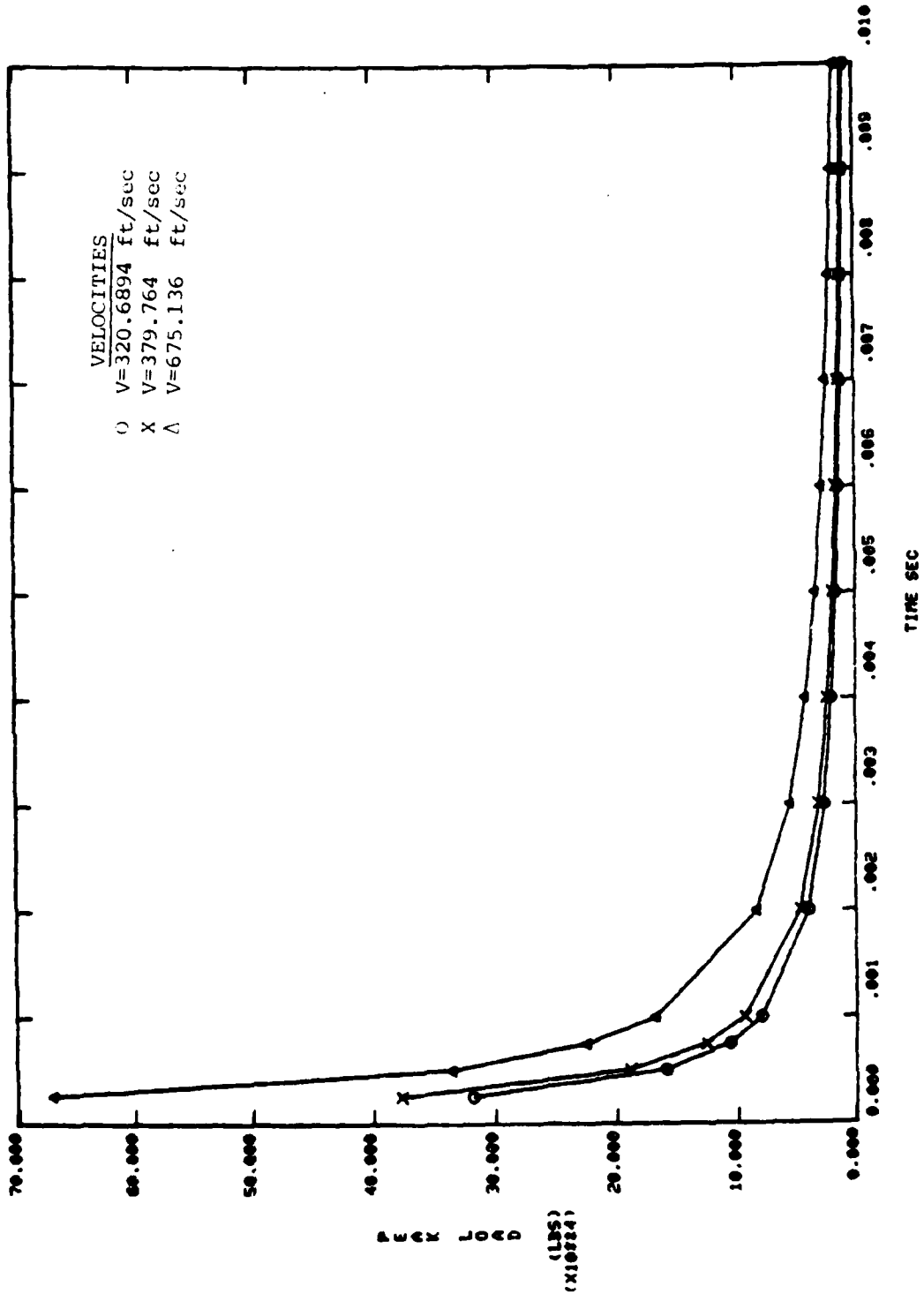
Figure 6. Impulse-Momentum Curve.

12
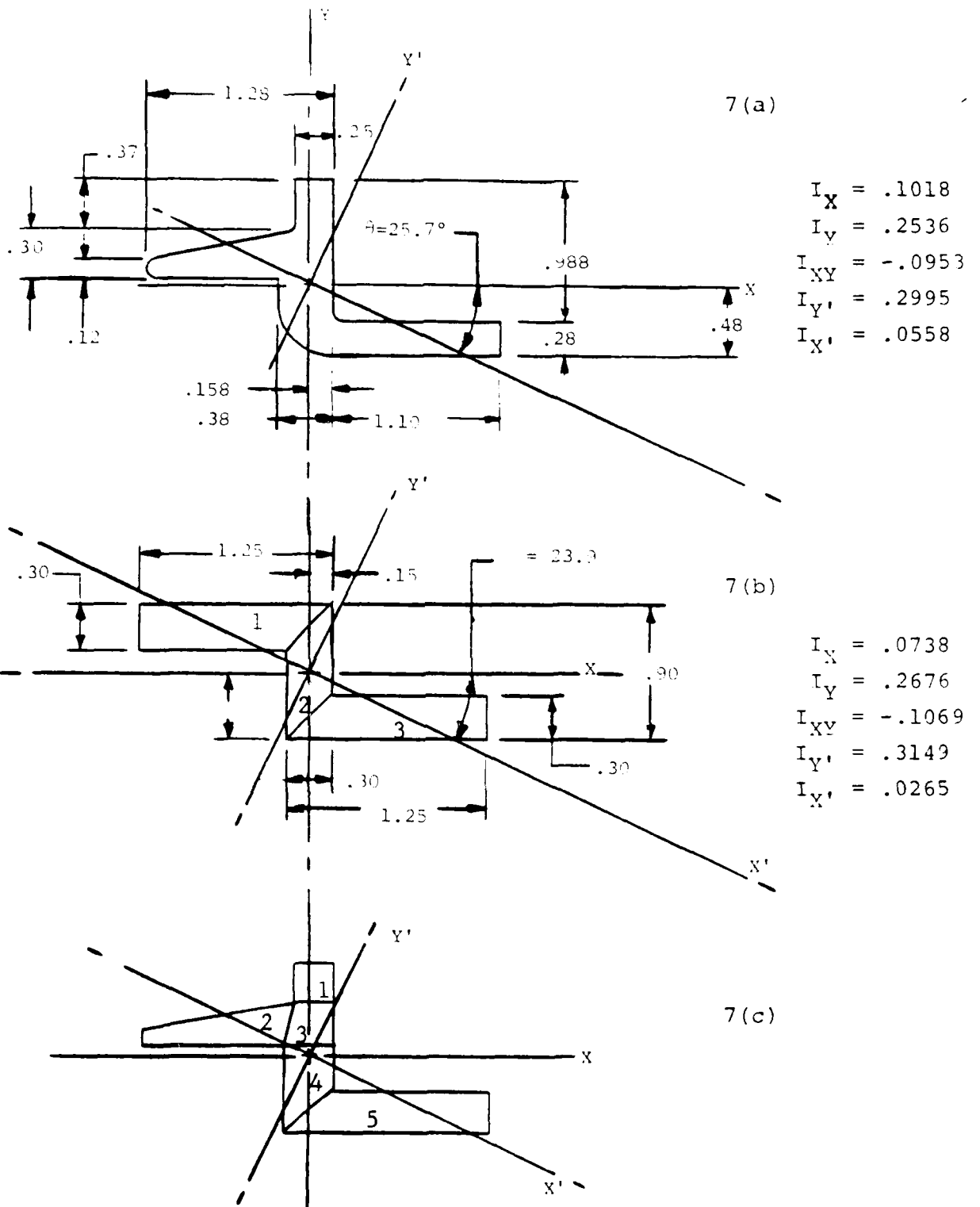
Figure 7. Arch Cross Sections.

The following data appear alongside the figure:

Section 7(a):
$$I_X = .1018$$
$$I_Y = .2536$$
$$I_{XY} = -.0953$$
$$I_{Y'} = .2995$$
$$I_{X'} = .0558$$

Section 7(b):
$$I_X = .0738$$
$$I_Y = .2676$$
$$I_{XY} = -.1069$$
$$I_{Y'} = .3149$$
$$I_{X'} = .0265$$

the frame stiffness parametric study (see Section 4) so that the frame nonlinear behavior could be adequately simulated.

The transparency sectional properties were determined using basic formulas and are documented in Figure 8 for comparison.

4. MECHANICAL PROPERTIES

Design data for the AZ91C-T6 magnesium alloy casting material (aft arch structure) was taken from MIL-HNDBK-5C. Relevant data is presented below.

$$E_F = 6.5 \times 10^6 \text{ psi}$$
$$G = 2.4 \times 10^6 \text{ psi}$$
$$\nu = .354$$
$$F_{TU} = 34,000 \text{ psi}$$
$$F_{TY} = F_{cy} = 16,000 \text{ psi}$$
$$F_{BRU} = 65,000 \text{ psi}$$
$$\rho = .066 \text{ lb/in}^3$$

The nonlinear material stress-strain curve appears as Figure 4.3.3.4.6 on page 4.67 of MIL-HNDBK-5C (see also Table 2). This room temperature curve was used in the parametric study. Based on the data available in the Aerospace Materials Handbook, it was assumed that stress-strain data and Young's modulus did not change significantly as a function of strain rate.

The transparency properties used are from MIL-HNDBK-17A, supplemented with data from References 8 and 10. Properties for the transparency materials are not well established for high strain rates. Thus assumptions were made. These include:

a. An elastic-perfectly plastic transparency material (as illustrated in Table 2),

b. F_{TY} = 9900 psi for both polycarbonate and stretched acrylic material,

14

	.45 Polycarbonate	.6 Acrylic	.9 Acrylic
I_y	7.594×10^{-3} in^4	1.8×10^{-2} in^4	6.075×10^{-2} in^4

b
unit width

Y

Y h
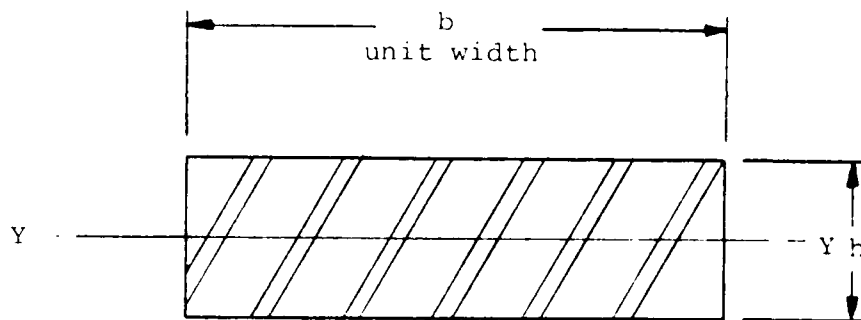
$$I = \frac{bh^3}{12}$$

Figure 8. Transparency Moment of Inertia.

15

TABLE 2

MECHANICAL PROPERTIES FOR TRANSPARENCY MATERIALS

Material	Tensile Yield Strength (psi)	Ultimate Tensile Strength (psi)	Young's Modulus (psi)	Poisson's Ratio	Izod Impact Notched
MIL-P-25690 Stretched Acrylic	9900.	10500.	4.5×10^5	.35	1.5-3.0
MIL-P-83310 Polycarbonate	9900.	10500.	6.5×10^5	.35	12-18*

* 1/8" thick

Transparency Materials

Magnesium Material

16
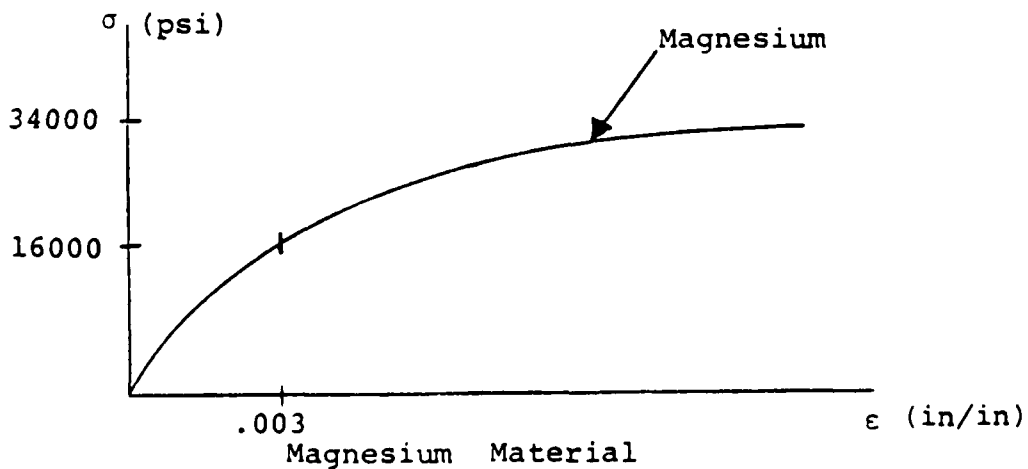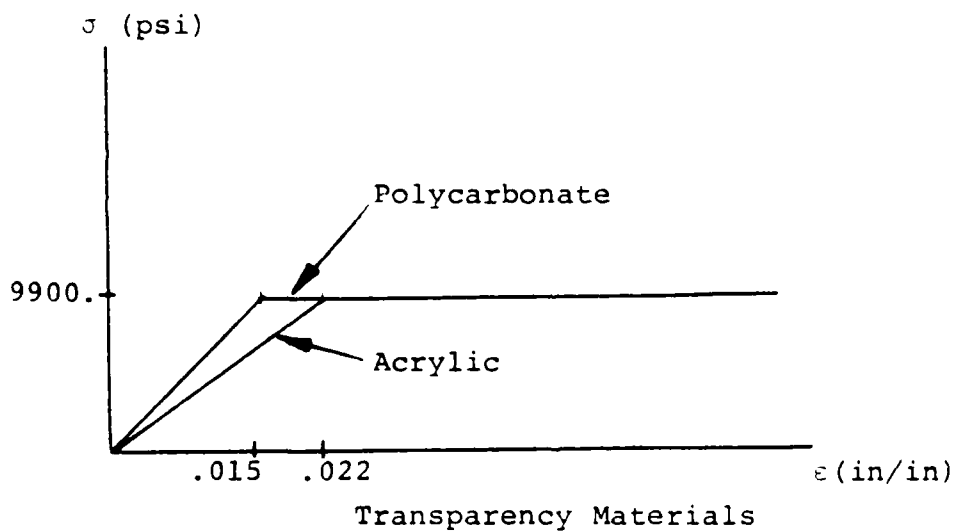
c. Young's modulus is a constant value over the range of strain rates encountered for the two materials.

A summary of the properties for the acrylic and polycarbonate materials used in the analyses are shown in Table 2. The difference in relative impact strength for a notched Izod specimen is shown for comparison. The ultimate strength is shown as a comparison to yield strength, illustrating that very little strain hardening occurs (thus supporting the elastic-perfectly plastic material representation).

SECTION IV
ANALYTICAL STUDY MATRIX

A parametric study was planned to determine the effects of
structural component stiffness and load magnitude on internal
load distribution and stress (strain) level. Three studies were
defined: a transparency stiffness study (static analysis), a
frame stiffness study (static analysis), and a transient dynamic
study to examine the effects of load intensity and time duration
as a function of transparency stiffness.

1. TRANSPARENCY STUDY

The transparency stiffness study matrix was formulated using
the 0.60 inch stretched acrylic as the baseline and building the
study around it as shown in Table 3. The 0.45 inch polycarbonate
transparency is about half as stiff in bending, and the 0.9 inch
stretched acrylic has approximately three times the bending
stiffness as the nominal 0.60 inch acrylic transparency. The
other two points in the matrix are to establish the behavior of
the structure for limiting values of the transparency bending
stiffness.

2. FRAME STUDY

For the frame stiffness study, the stiffness associated
with two principal transparencies were included as the primary
transparency variables as shown in Table 4 (0.60 inch stretched
acrylic and 0.45 inch polycarbonate). The objective was to
evaluate the effect of variations in frame stiffness on load path
distribution and stress. Variations about the nominal stiffness
of 6.5×10^6 psi were planned as shown in Table 4. Normally in
a practical design situation, the frame stiffness would be changed
by changing the frame geometry and/or material. A geometry change
would require the design of a new frame for each stiffness to be
investigated. To facilitate this study, it was decided to achieve

18

TABLE 3

TRANSPARENCY PARAMETRIC STUDY

NONLINEAR STATIC ANALYSIS

TRANSPARENCY STIFFNESS

LOAD AT 6-1/4 INCHES FROM FRAME

Pressure (psi)	$E_T = 1.625\times10^5$ $K_T = 1.233\times10^3$ $t_t = 0.45$	$E_T = 6.5\times10^5$ $K_T = 4.936\times10^3$ $t_t = 0.45$	$E_T = 4.5\times10^5$ $K_T = 8.1\times10^3$ $t_t = 0.60$	$E_T = 4.5\times10^5$ $K_T = 2.734\times10^4$ $t_t = 0.90$	$E_T = 1.8\times10^6$ $K_T = 3.24\times10^4$ $t_t = 0.60$
250	X	X		X	X
350		X	X	X	
450			X	X	
550				X	
650					
750				X	

TABLE 4
FRAME PARAMETRIC STUDY
NONLINEAR STATIC ANALYSIS

Transparency Stiffness, K_T	FRAME STIFFNESS P = 10 psi			
	$E_F=6.5\times10^5$ $K_F=4.8\times10^4$	$E_F=3.25\times10^6$ $K_F=2.4\times10^5$	$E_F=6.5\times10^6$ $K_F=4.8\times10^5$	$E_F=13.0\times10^6$ $K_F=9.6\times10^5$
1×10^3			X	
4.936×10^3 $t_t = 0.45$	X	X	X	X
8.1×10^3 $t_t = 0.60$		X	X	X
5×10^4			X	

substantial changes in stiffness using Young's modulus. Note that
a change in the modulus of elasticity implies a change in material,
which is not compatible with the guidelines established in
Reference 1 for the T-38 Alternate Transparency Development
Program.

3.   TRANSIENT DYNAMIC STUDY

It was planned to study the behavior of the transparency/support
structure system using stiffnesses associated with 0.6 and 0.9 inch
stretched acrylic and 0.45 inch polycarbonate transparencies. Due
to cost factors associated with the anticipated large computer run
times, only a limited study was planned.

The parameters involved in this study include the effect of
intensity and time duration on the dynamic response.

SECTION V
ANALYTICAL STUDIES

The analytical studies were conducted to compare the behavior of three different transparency systems under the application of time independent, uncoupled, and time dependent, structurally coupled bird impact loads. These analyses were performed using the finite element computer code MAGNA (Reference 9).

STRUCTURAL MODEL

The geometry for the T-38 student windshield model was developed using the data provided by the Northrop Aircraft Corporation (Drawings 2-13000, 3-13000, 3-13014). Use of a conical surface for the transparency mold line provided an equation which was easily programmed into the computer. Symmetry of the windshield and loading eliminated the need to model the entire transparency structure. Figure 9 provides an overview of the finite element model (FEM) geometry.

The two elements used in the FEM were a three-dimensional isoparametric solid element with a variable number of nodes and a thin shell element with eight nodes. The variable node solid element was used around the load application area and along the aft arch, which are the primary areas of interest. The use of thin shell elements in non-critical areas greatly reduced computer resource and time requirements. Typically, for a materially nonlinear static solution using the MAGNA program, the ratio of central processing unit (cpu) seconds per integration point per element is on the order of 2.5. Thus, for every cpu second used in the solution of a problem modeled with thin shell elements, there are 2.5 cpu seconds used in an identical analysis modeled with the variable node isoparametric solid element (Reference 9) (assuming the same number of elements). The unique capability of MAGNA to provide compatibility between the thin shell elements and the variable node solid element provided for a more efficient solution.

22
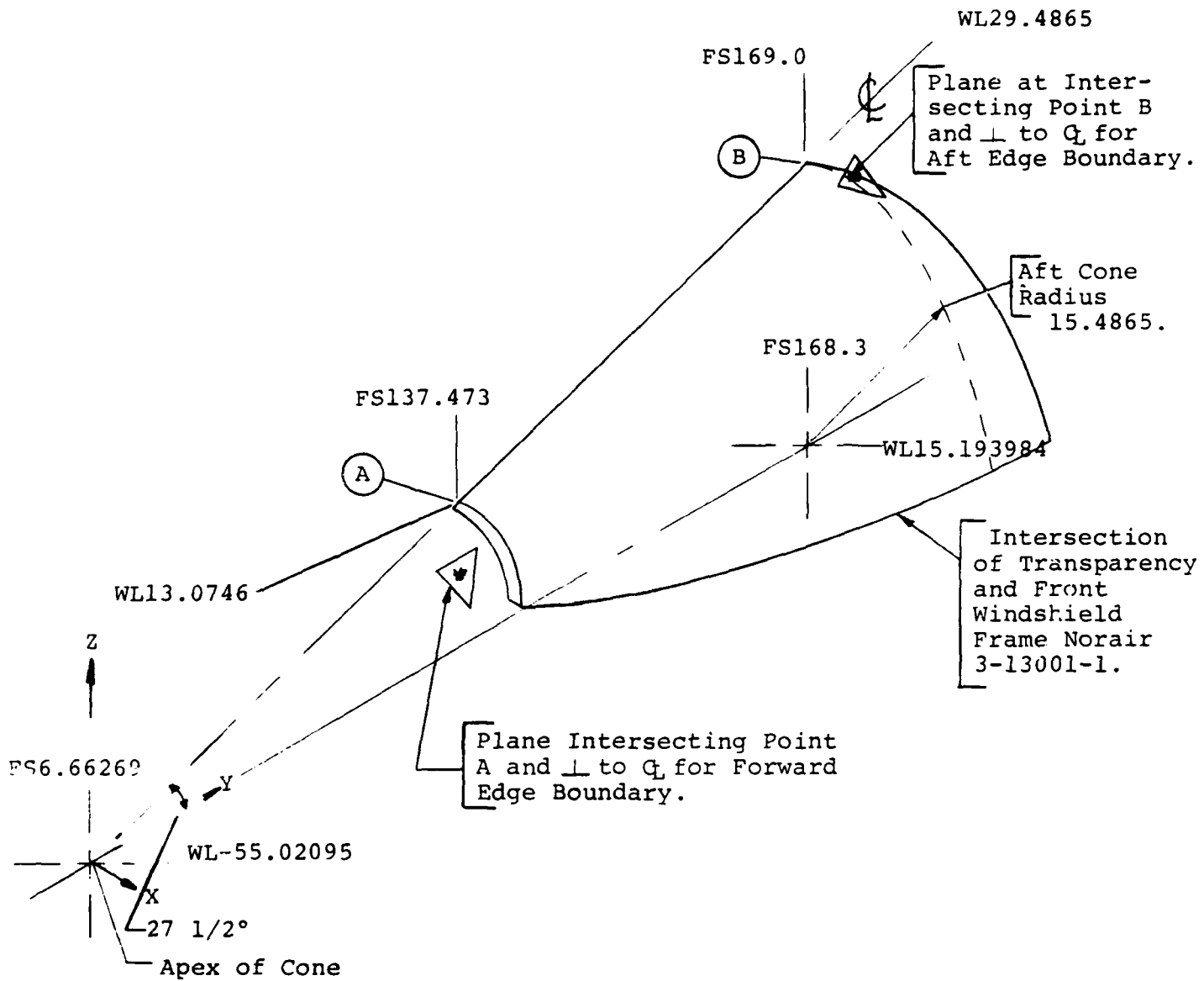
Figure 9. Transparency Geometry.

23

The final configuration of the FEM elements was determined from preliminary computer analyses (see Figure 10). These linear static analyses results (deflection and stress) were used to locate areas of high stress (strain) and high stress (strain) gradients. The T-38 FEM is shown in Figures 11 and 12. This FEM consists of 130 total elements, of which 44 are thin shell elements and 86 are isoparametric solid elements. There is a continuous boundary between the two element types. The division line in the fore and aft direction occurs between the top six elements and the bottom four elements. The displacement gradient is small in this area, indicating that a change from a solid element to a thin shell element would provide acceptable results (reference Figure 10). The more rapid change in displacement occurs in the vicinity of the target point. The first two rows of elements on the left in Figures 11 and 12 (transparency forward edge) are sufficiently far away from the impact point and are modeled as thin shell elements. The other boundary between thin shell and variable node solid elements occurs near the aft frame section. One of the desired results from the computer finite element analysis was to define the resultant force distribution along the arch. The isoparametric solid elements provide this capability, and are used for the two rows of transparency elements adjacent to the arch. The entire frame section consists of variable node solid elements which provide the required materially-nonlinear response characteristics. The thin shell elements did not have nonlinear capability in MAGNA at the time of this study.

All of the elements except those in the immediate vicinity of the load use the two point Gaussian rule for numerical integration. Elements 13, 14, 19, 20, 25, 26, 31, and 32 in the static analysis, and elements 7, 8, 13, 14, 15, 19, 20, 21, 22, 25, 26, 27, 28, 31, 32, 33, 37, and 38 in the dynamic analysis use the three point integration rule. This selective reduced integration provided increased solution efficiency.

Symmetrical boundary conditions were modeled along the centerline, i.e., the nodal points along the centerline are
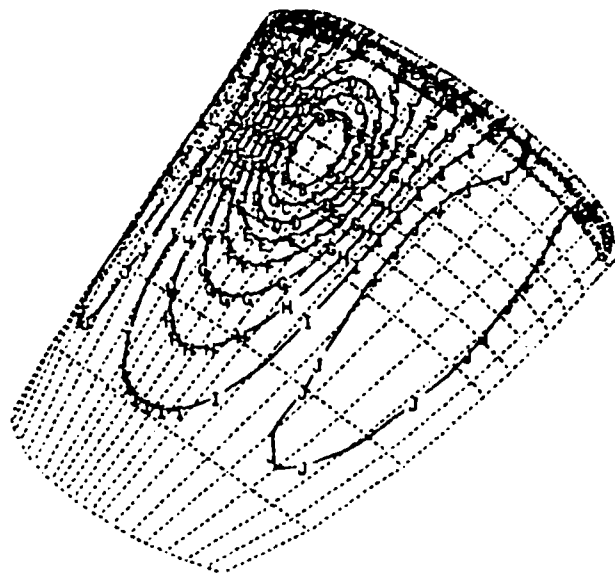
Figure 10. Z Deflection Contours - Linear Static Analysis.

AFT ARCH

F.S. 164.00

B.L.0

WL 29.4865

ELEMENT TYPE 1
(isoparametric
solid elements)

F.S. 176.86

B.L. 18.55

WL 14.12

F.S. 137.473

W.L.
13.0746

B.L. 0

ELEMENT
TYPE 5
(thin shell element)
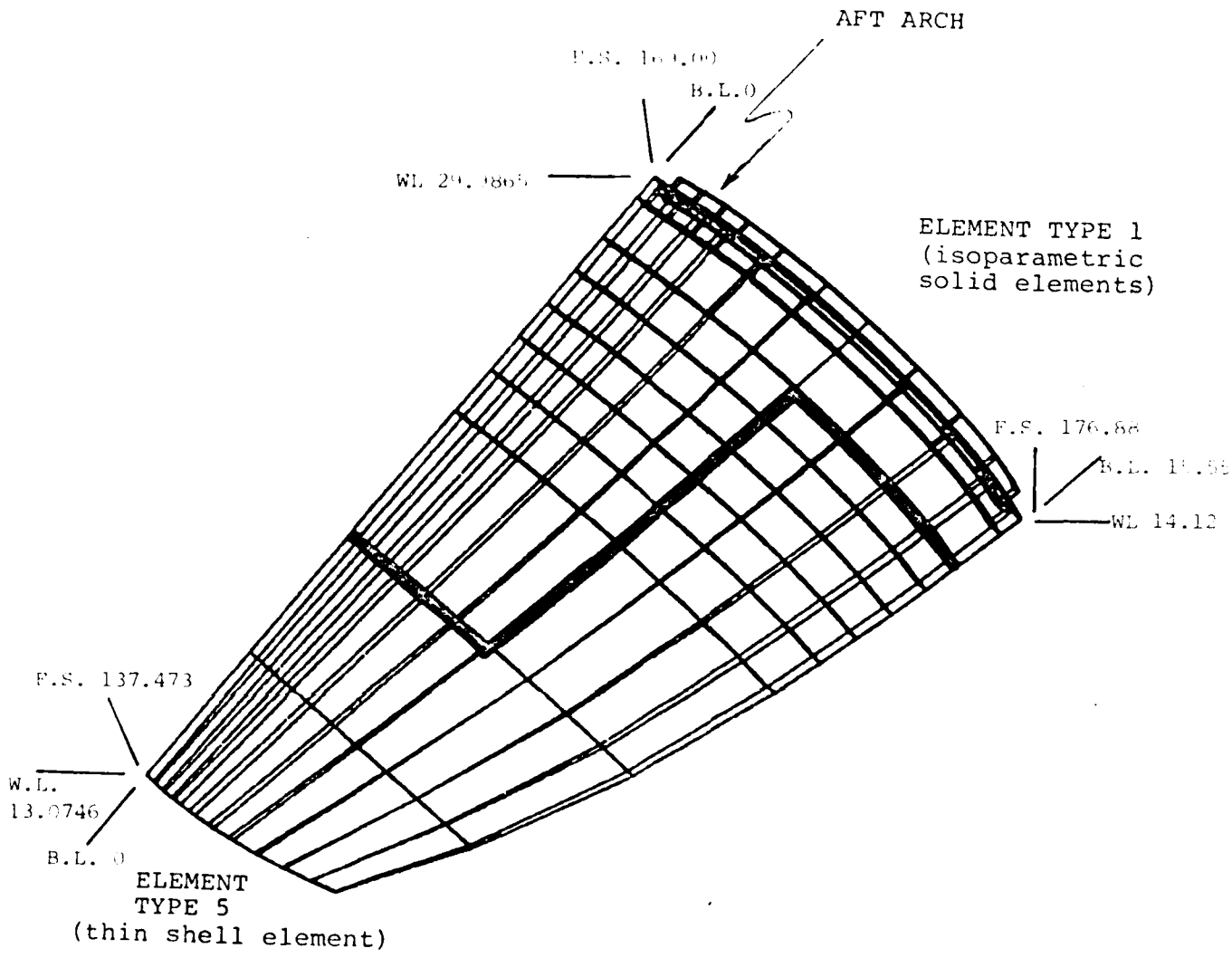
Figure 11.   Student Windshield - Element
             Configuration.

1	11	1	7	13	19	25	31	37	47
2	12	2	8	14	20	26	32	38	48
3	13	3	9	15	21	27	33	39	49
4	14	4	10	16	22	28	34	40	50
5	15	5	11	17	23	29	35	41	51
6	16	6	12	18	24	30	36	42	52
7	17	21	25	29	33	37	41	43	53
8	18	22	26	30	34	38	42	44	54
9	19	23	27	31	35	39	43	45	55
10	20	24	28	32	36	40	44	46	56

ELEMENT TYPE 5

10	20	24	28	32	36	40	44	46	56

66   76

FORWARD EDGE   AFT ARCH   86
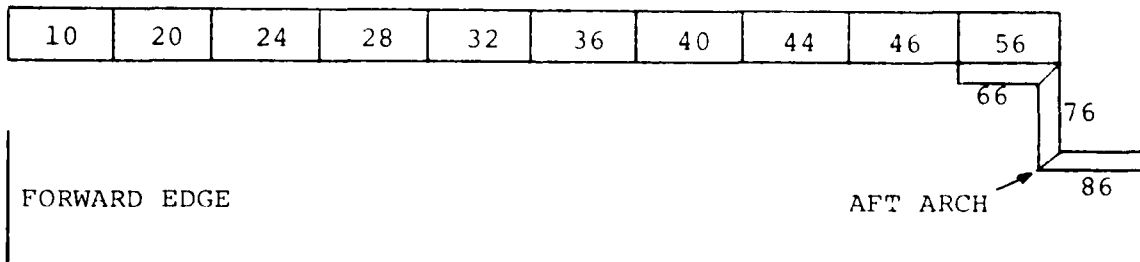
Figure 12.   Element Configuration.

27

constrained to movement in the Y-Z plane. The outer boundary of
the transparency along the forward bulkhead and sill and the
support face of the frame have complete fixity.

For the static solution option, surface tractions were
applied over an elliptical area, decreasing in intensity radially
from the center of impact as shown in Figure 13. The element
distributed loads option was utilized for the transient dynamic
analysis. The pressure was distributed over an area approximat-
ing a half circle with a 6.0 inch radius. The elements falling
within this area were loaded in a sequential manner as time
progressed. The numbers on the elements in Figure 14 indicate
the sequence of loading (area 1 loaded first, area 6 loaded last).
The larger numbers represent node numbers of the upper surface of
the elements.

2.   METHOD OF ANALYSIS

The results from the MAGNA (Reference 9) finite element
computer program for three-dimensional solid elements include the
total strain tensor, plastic strains, total stress tensor, principal
stresses, yield functions, equivalent stresses, and estimated error
at each integration point. The total strain and stress tensors at
a point are listed in their global direction, the plastic strains
are cumulative within each element, and the yield function and
equivalent stresses are used to determine plastic behavior. The
yield function will remain negative within a material's elastic
region and become zero or positive for its plastic region. The
equivalent stress (Reference 9) is a combination of principal
stresses. For a ductile elastic-plastic material undergoing deforma-
tion, the material is assumed to become plastic when the equivalent
stress is equal to or greater than the uniaxial tensile yield stress,
and failure can be estimated at a specific integration point when
the equivalent stress reaches the ultimate strength of the material.
This theory was used for the magnesium frame.
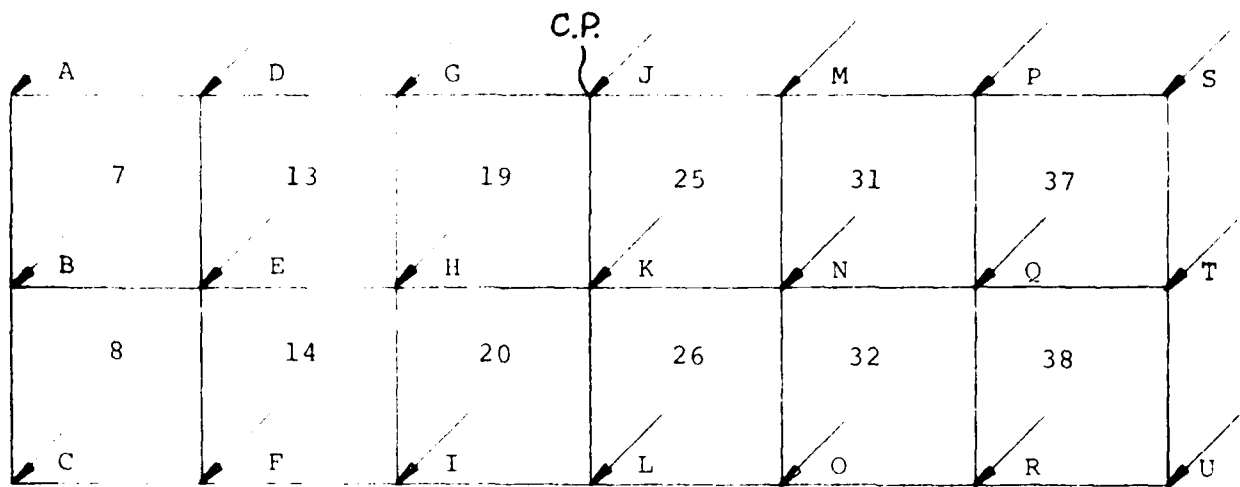
NODE	NODAL FORCE
A	0.13215
B	0.05806
C	0.0
D	1.14309
E	1.04216
F	0.01021
G	1.33049
H	1.93685
I	0.10485
J	1.37485
K	2.1451
L	0.15791
M	1.41888
N	1.88915
O	0.06692
P	1.25063
Q	0.94989
R	0.00227
S	0.14101
T	0.04950
U	0.0

Figure 13.   Element Nodal Loads, Static Solution.

29
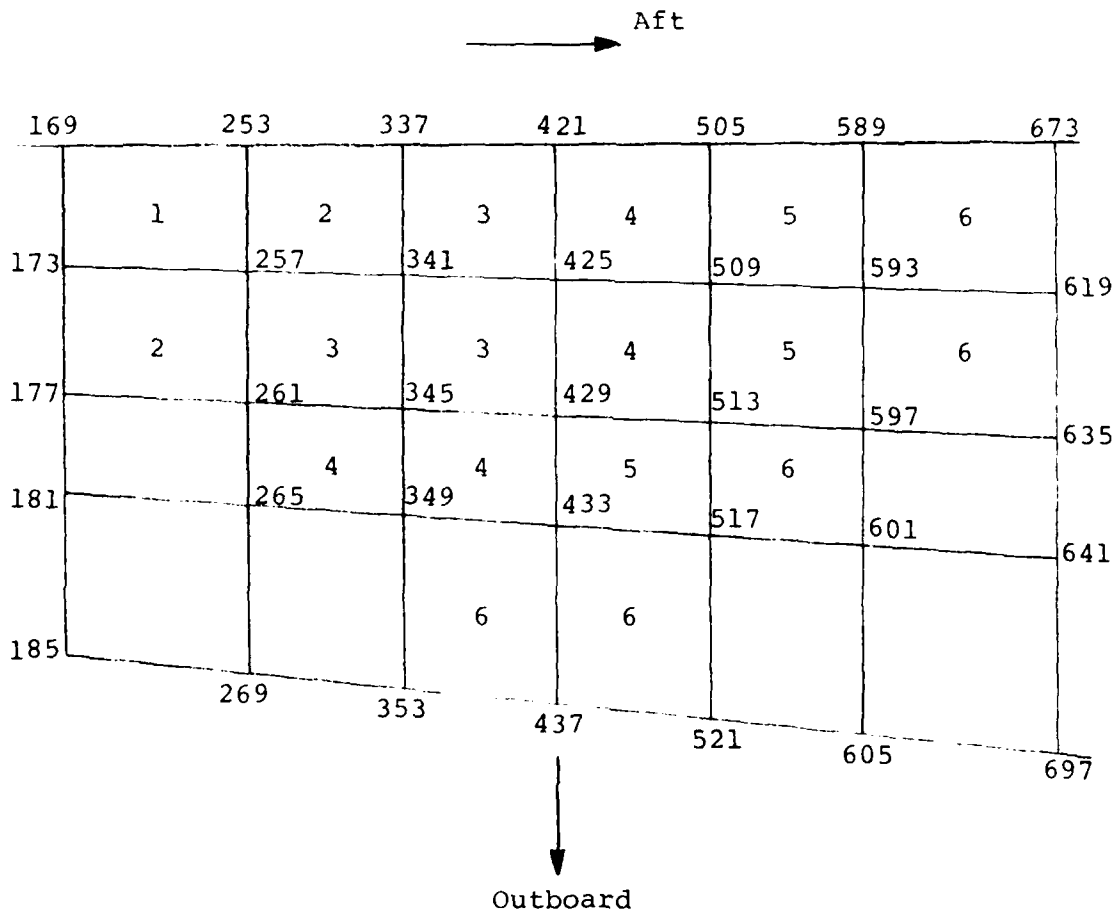
Figure 14.   Element Distributed Loads, Transient Dynamic Analysis.

The number of integration points per isoparametric element is eight, except for the elements directly beneath the impact area where 27-point integration is used. These points are located in the interior of the elements, which means that an extrapolation of the resultant stress and an integration over their respective areas is required to determine surface stresses and resultant loads. The resultant loads were determined per unit length of the transparency. Although 86 solid elements and 44 shell elements were used to simulate the structure, only 34 elements were used to develop resultant load distributions. Calculations were performed along the periphery of the impact area and along the aft frame. This provided information on the load distribution and peak load magnitude at critical locations.

Calculation of the resultant forces involved an assumption that the stress distribution through the thickness of the element is in the form of a polynomial. Figure 15 shows a typical approximation for determination of resultant forces. The order of the curve is determined by the order of integration. For 27-point integration a second order equation was used and for the eight-point integration a linear approximation was used for the extrapolation. The formulas resulting from the integration of the force/stress relationships are also presented in Figure 15. With the stresses at each integration point taken from the MAGNA postprocessor file and with thicknesses known, the resultant loads were computed.

An interactive computer code, STRESS, was written which performs the calculation and prints the results. Input to the program consists of the postprocessor file from MAGNA as local file TAPE99. Other data is obtained through interactive prompts in the program, such as the increment to be analyzed, the element type, the first element, last element, and element i· . ·ement, along with the element face number and transparency thickness, and finally the beginning node number, ending node number, and nodal increment are given. The face number determined which side of the element was to be analyzed (Figure 16). Faces one and two are the aft and

31

Outer Surface

σ_u

σ_3 3

3 x 3 Integration

σ_2 2 σ

1

σ_1

$\sigma = ay^2 + by + c$

σ_L

Inner Surface

Outer Surface

σ_u

σ_2

$\sigma = ay + b$

σ

2 x 2 Integration

σ_1

σ_L

Inner Surface
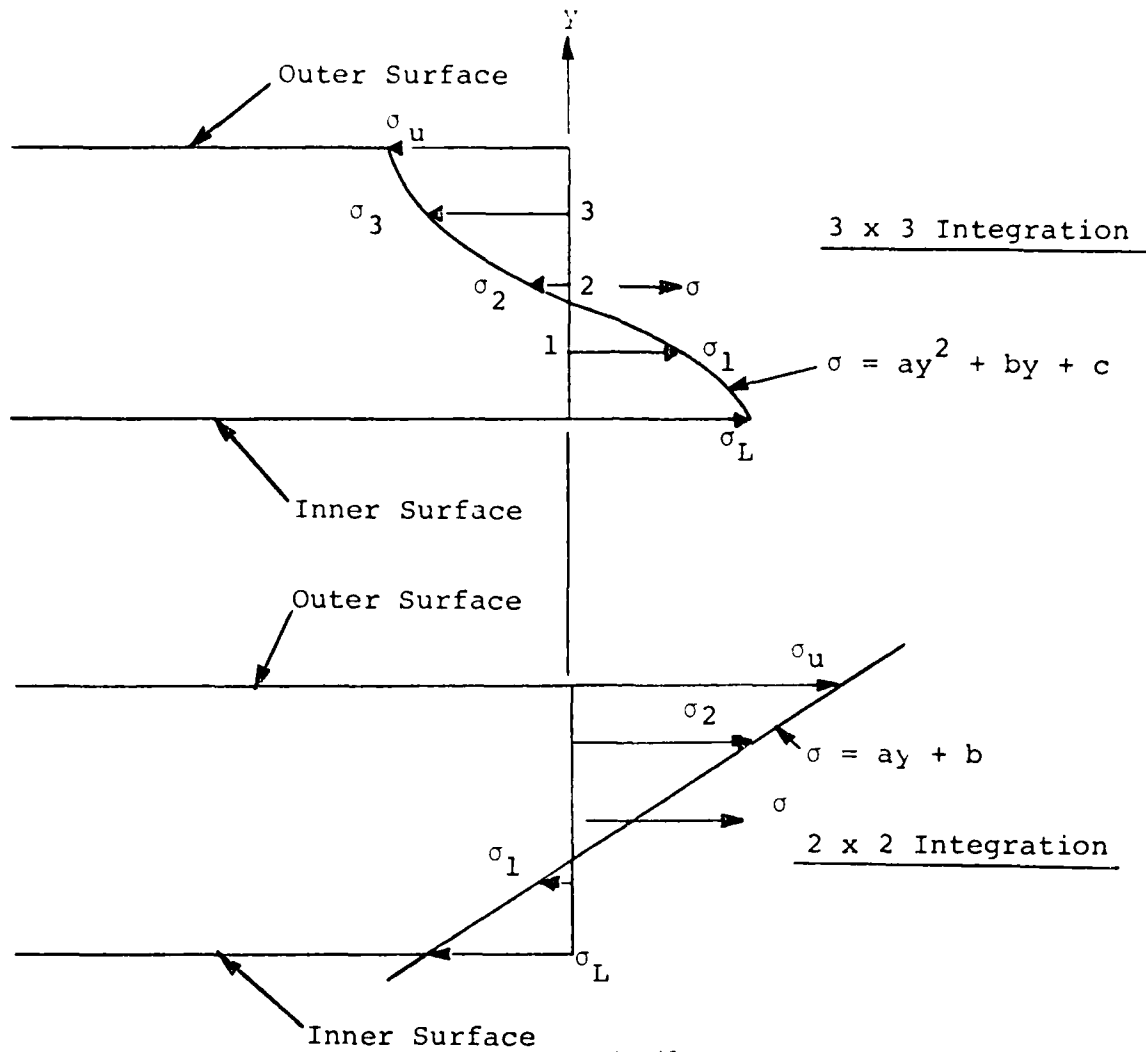
$$\text{Force} = \int_{-t_t/2}^{+t_t/2} \sigma\, dy$$

$$\text{Bending Moment} = \int_{-t_t/2}^{+t_t/2} \sigma y\, dy$$

(3 x 3 Int) Force $(\frac{lb}{in}) = \frac{20}{72}(\sigma_3 + \sigma_1 - 2\sigma_2)t + \sigma_2 t$

(2 x 2 Int) Force $(\frac{lb}{in}) = \frac{1}{2}(\sigma_2 + \sigma_1)t_t$

(3 x 3 Int) Bnd Mom $(\frac{in-lb}{in}) = \frac{\sqrt{5}}{12\sqrt{3}}(\sigma_3 - \sigma_1)t_t^2$

(2 x 2 Int) Bnd Mom $(\frac{in-lb}{in}) = \frac{\sqrt{3}}{12}(\sigma_2 - \sigma_1)t_t^2$

Figure 15.   Resultant Forces.
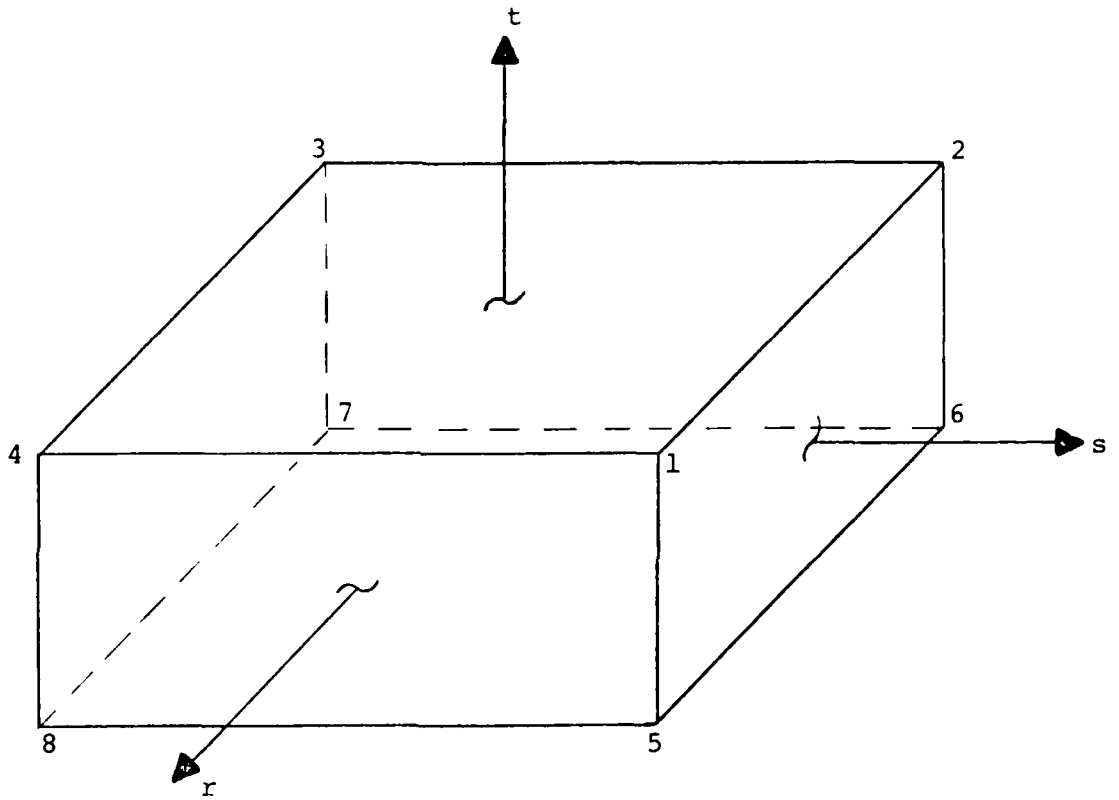
| SURFACE	LOCATION	CORNER NODES
1	-r	2-3-7-6
2	r	1-4-8-5
3	-s	3-4-8-7
4	s	2-1-5-6

Figure 16. Surface Numbers for Resultant Force
Calculations.

33

forward faces, and faces three and four are the inboard and
outboard faces, respectively. The nodal data was used to determine
the arch length along the specified face of the element. The
arch length was the independent variable in all of the resultant
plots. The output of the computer code consists of the element
type, surface or face number, integration point, arch length
coordinate, normal, tangential, transverse forces, and bending and
twisting moments. Standard sign convention for stress at a point
is used throughout. A negative bending moment is interpreted as
tension in bottom fibers, compression in top fibers. This resulted
from the sign convention for the stress tensors (reference Figure 17).

3.   DIMENSIONAL ANALYSIS

An effort was made to relate the analytical stress output to
the various structural parameters of each respective transparency
for the static analysis. The purpose of this dimensional analysis
was to relate, in a linear manner, critical variables which might
play a significant role in the response characteristics of the
structure. These variables include the maximum equivalent stress
in the transparency, the elastic modulus of the transparency,
transparency thickness, maximum transparency deflection, peak frame
strain, frame stiffness, and transparency stiffness. Using stress
as the dependent parameter, four groups of dimensionless quantities
were derived.

The four dimensionless groups consists of a pseudo transparency
strain (equivalent stress divided by the elastic modulus), σ_E/E_T,
the frame strain, ϵ_F, the ratio of the transparency to frame
stiffness, K_T/K_F, and the ratio of transparency thickness to
transparency deflection, t_t/u_t. The frame stiffness was a constant
for this analysis. Each relationship is a function of the other
relationships and thus presents general tendencies of different
transparency/frame systems. Examination of these quantities
resulted in the five graphical representations shown in Figures 18
through 22.

34
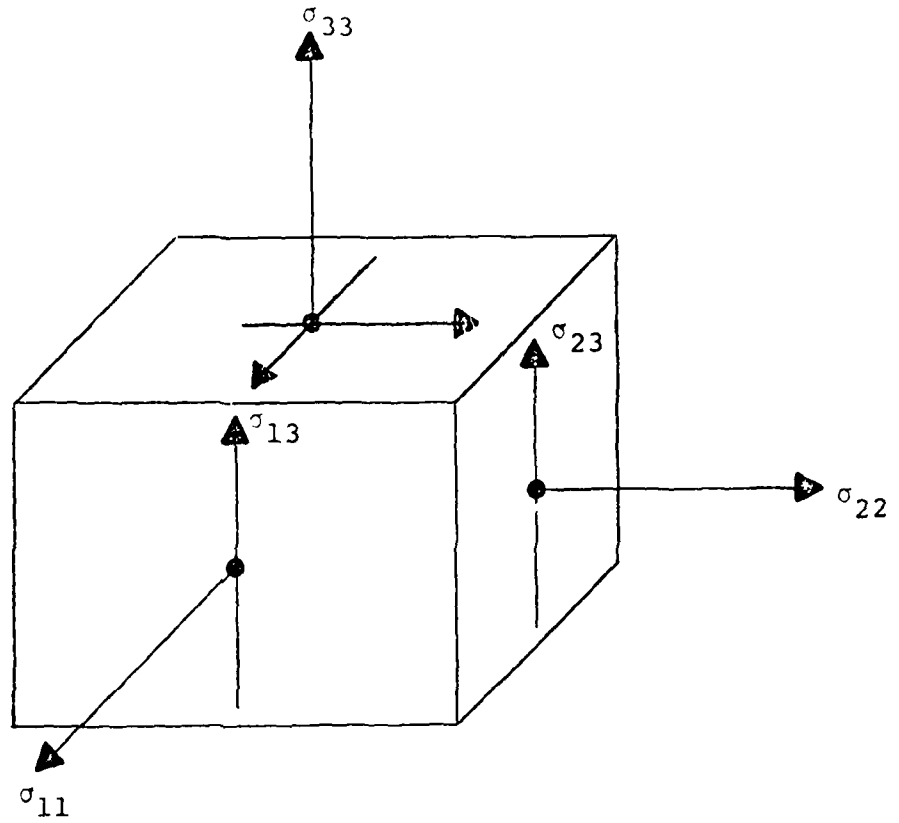
NOTE: Positive stress directions are shown.

Figure 17. Stress at a Point.
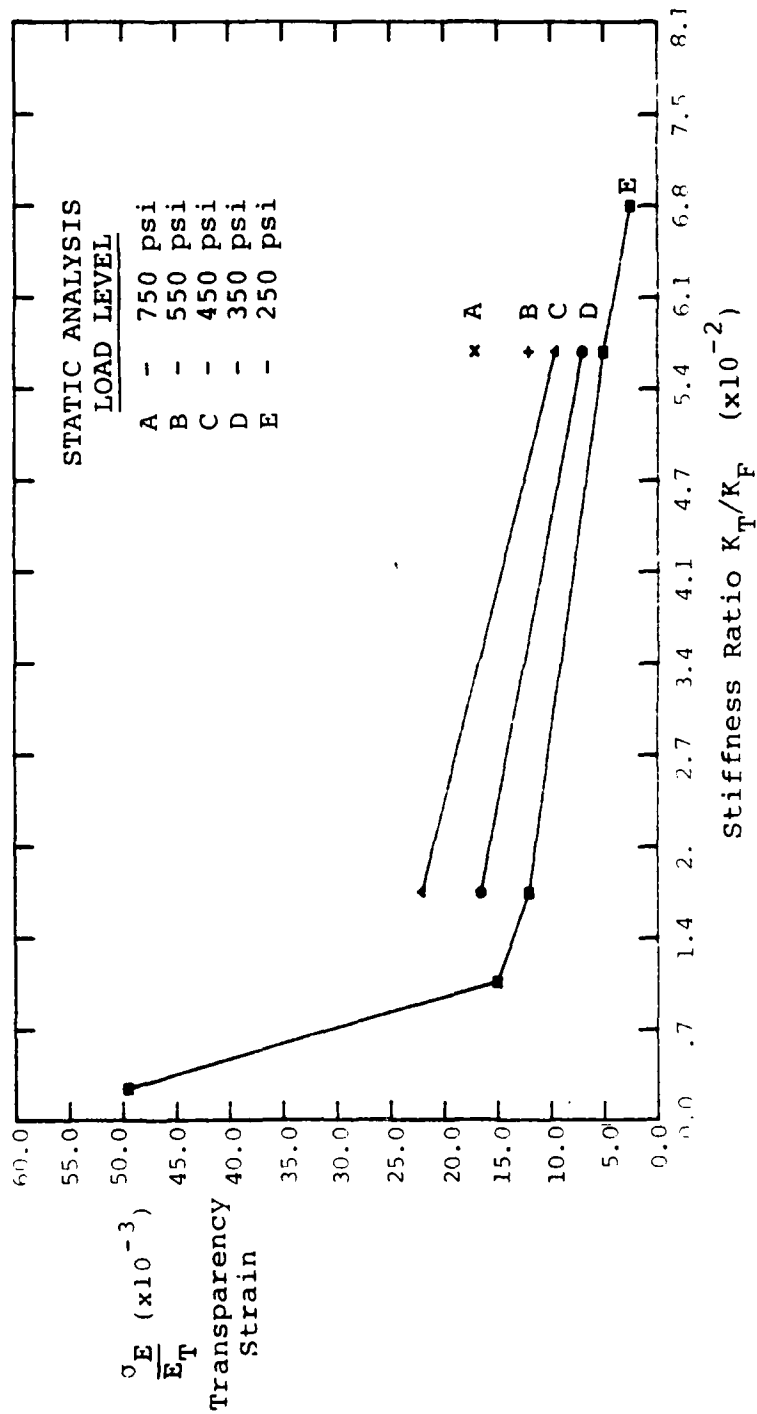
Figure 18. Transparency Strain versus Stiffness.

36
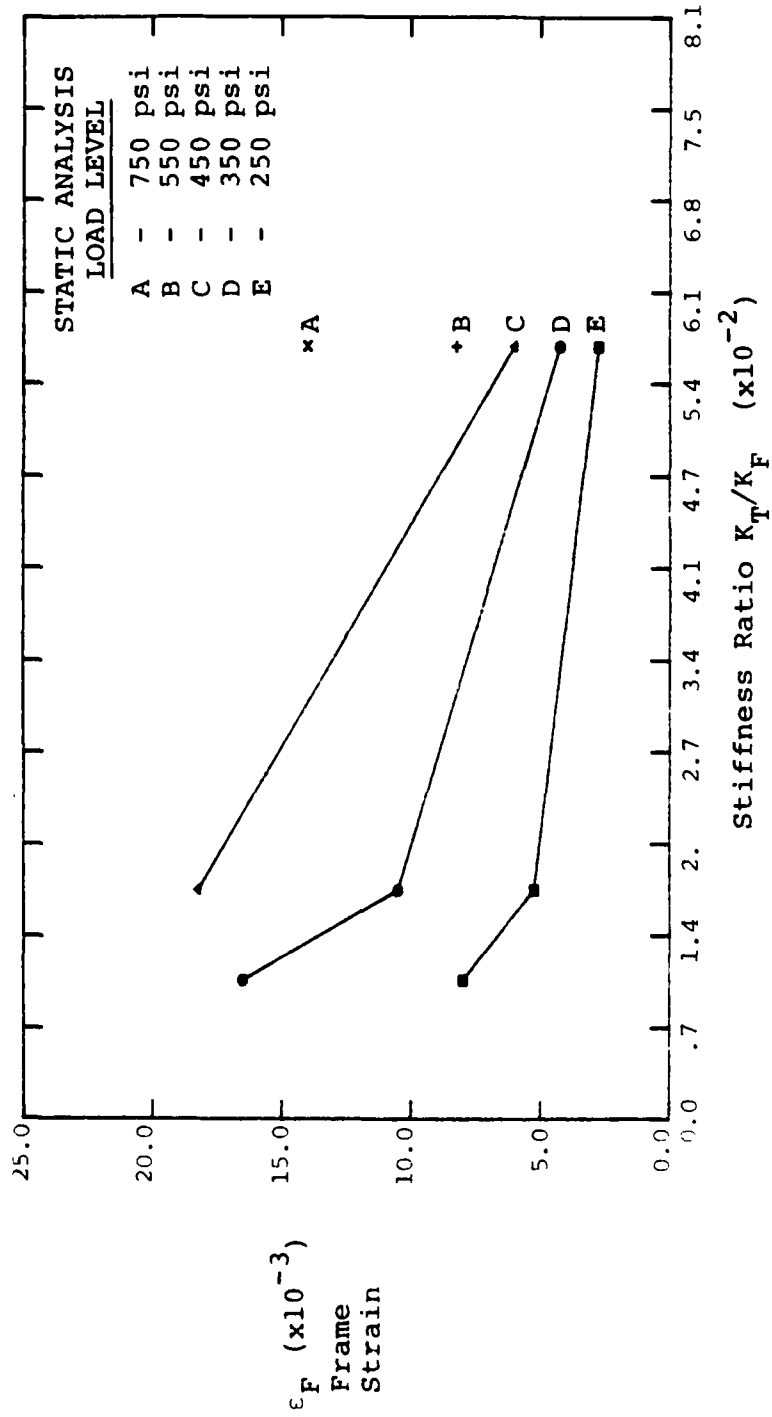
Figure 19. Frame Strain versus Stiffness.

37

Figure 2. Transparency Strain versus Frame Strain.

38
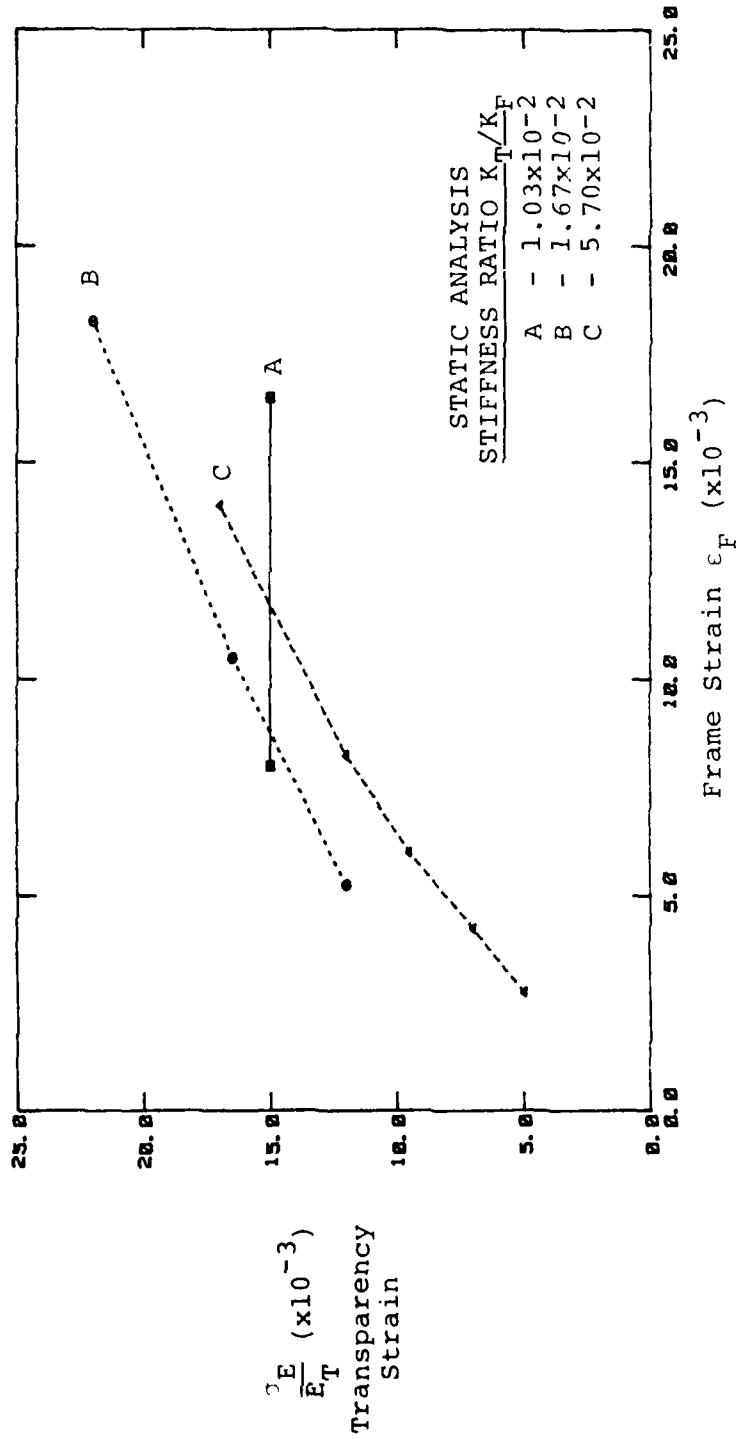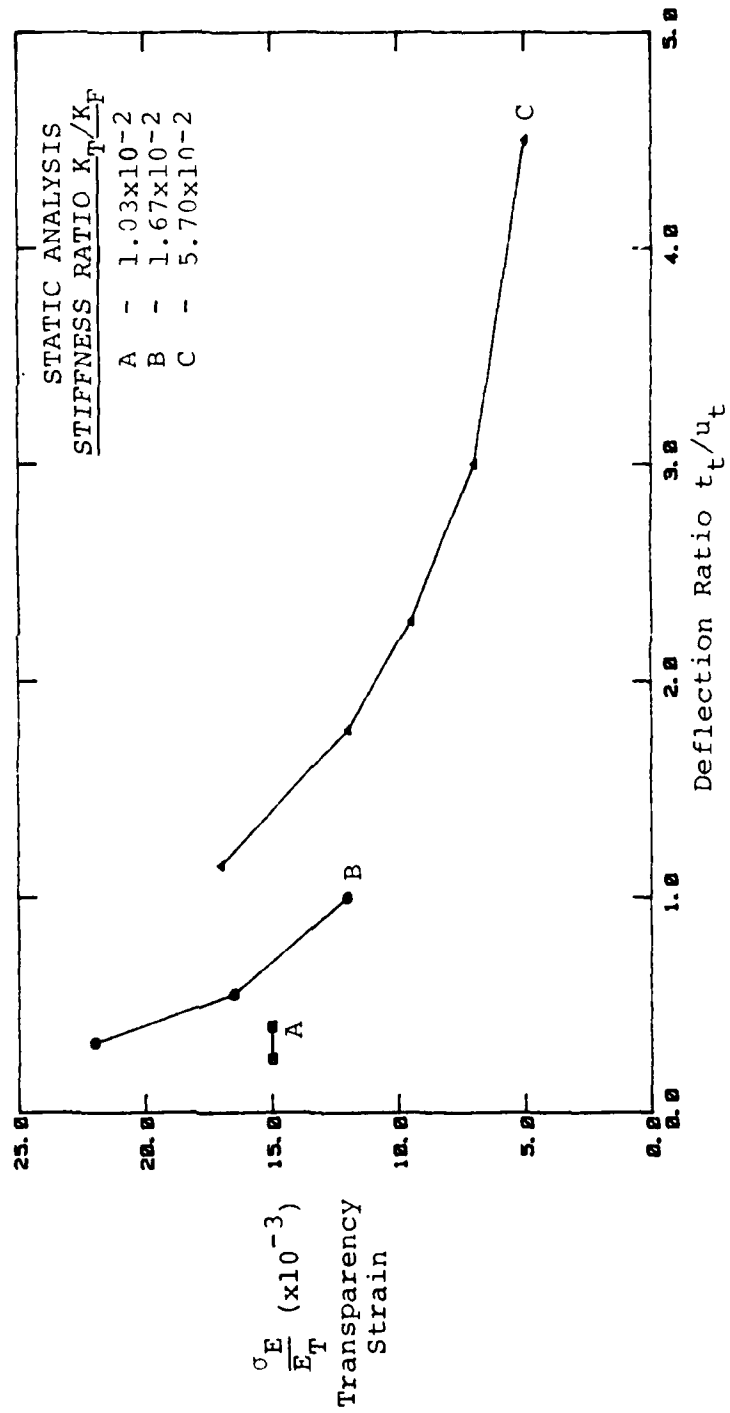
Figure 21. Transparency Strain versus Deflection.

39
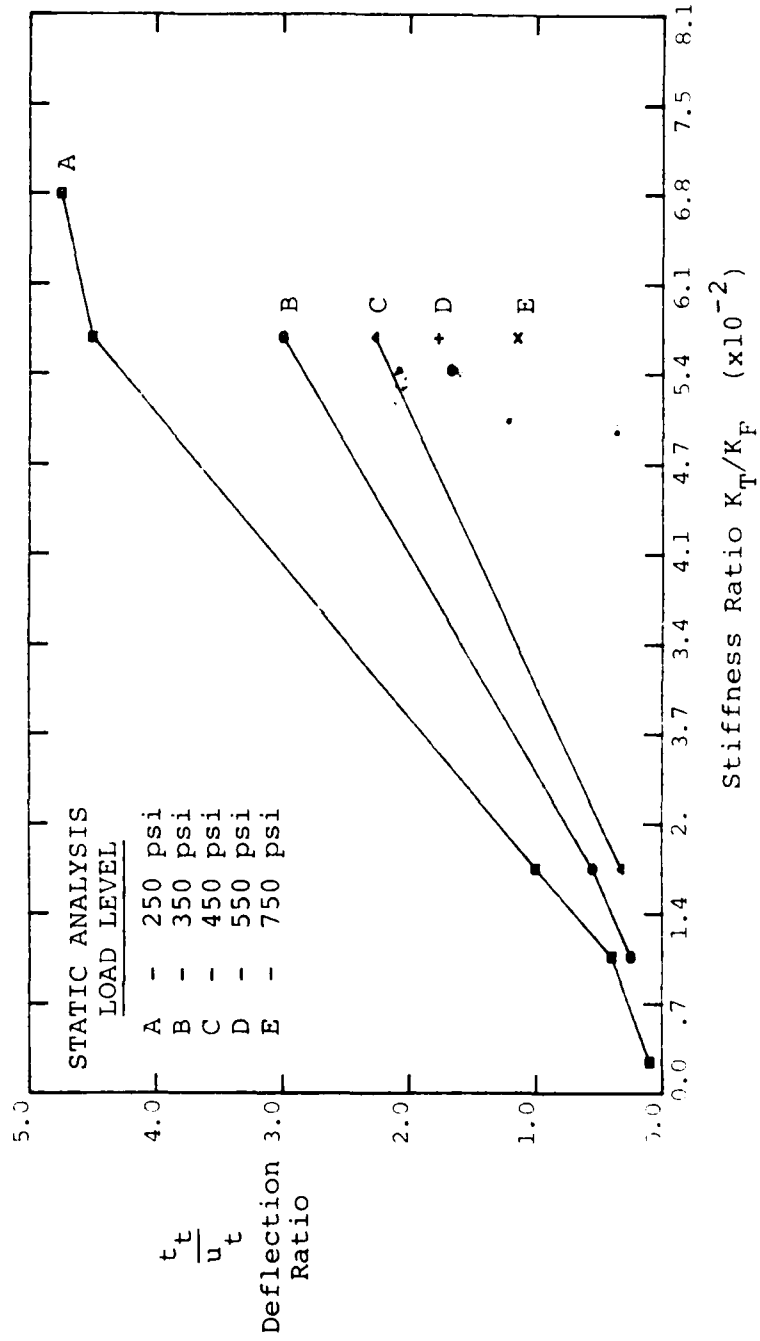
Figure 22. Deflection versus Stiffness.

40

Figure 18 represents a relationship between a representative transparency strain and the ratio of the transparency stiffness and the frame stiffness. These transparency stiffness values are as described in Section 3.3. The frame stiffness value, as used **here**, is $E_F I_X$, where I_X is defined on Figure 7(b). The larger values of the stiffness ratio represent stiffer transparencies, the 0.9 inch thick acrylic transparency as an example. For a static solution the maximum transparency strain decreases when the transparency stiffness, K_T, is increased.

Figure 19 presents the frame strain, ε_F, as a function of the stiffness ratio, K_T/K_F. The peak frame strain decreases with increasing transparency stiffness. Figure 20 is a cross-plot of Figures 18 and 19. This plot shows the variation of the transparency strain with the frame strain for different ratios of K_T/K_F. The zero degree slope on Curve A is due to the fact that the polycarbonate transparency has yielded for the load levels shown. All these curves should extrapolate to the origin.

Figure 21 shows the pseudo strain as a function of the deflection ratio t_T/u_T. Again, the data points for the yielded polycarbonate material show no change in the pseudo strain with deflection. Figure 22 shows the deflection ratios as a function of the stiffness ratio for different load levels. The lower values of the deflection ratios correspond to the lower values for the transparency stiffness.

The dynamic solution was not analyzed in this manner because of the nonlinear behavior. Both transparency materials displayed inelastic behavior at relatively low load levels (only the polycarbonate material displayed nonlinear material behavior for the static solution). Therefore, establishing linear relationships between the specified parameters was not meaningful.

4.   RESULTANT FORCES

One of the primary interests in the parametric studies was the determination of the load transfer throughout the structure.

Generally, the load will seek the stiffer load paths of a structural system. In general, a combined load condition exists throughout the structure. Individual plots of normal force, bending moment, and transverse shear are presented at selected locations.

Graphical plots of the resultant force data were generated for the static and dynamic analyses. For the static analysis, ten sets of data were interpreted in this manner and are presented in Reference 14. Each set refers to a specific load level for a specific transparency material. The high and low transparency stiffness analyses identified in Table 3 were not included in this group. Each data set contains normal force, bending moment, and transverse shear resultants in both forward/aft and inboard/outboard directions. Referring to Figure 23, fourteen sectional cuts, starting with elements 1 through 4 and progressing toward and ending with the row of elements along the aft arch (elements 37 through 46), were used to indicate the distribution of the load in the forward/aft direction. Eight sectional cuts, starting with elements 1, 7, 13, 19, 25, and 31, and progressing outboard and ending with elements 4, 10, 16, 22, 28, and 34, were also made to indicate the distribution of the load in the outboard direction. All sectional cuts were normal to the transparency and through integration points located within each element.

The dynamic analysis results were plotted for sixteen sets of data, and are presented in Reference 14. Each set refers to a different load level, at a specific time increment, for a specific transparency stiffness, as shown in Table 5. The location of each of the twenty-two section cuts for calculating the resultant forces in the dynamic analysis are exactly as described for the static analysis.

Each set of data in Reference 14 is arranged with the first fourteen graphs representing load distribution in the forward/aft direction (location 1 through 14) and the last eight graphs
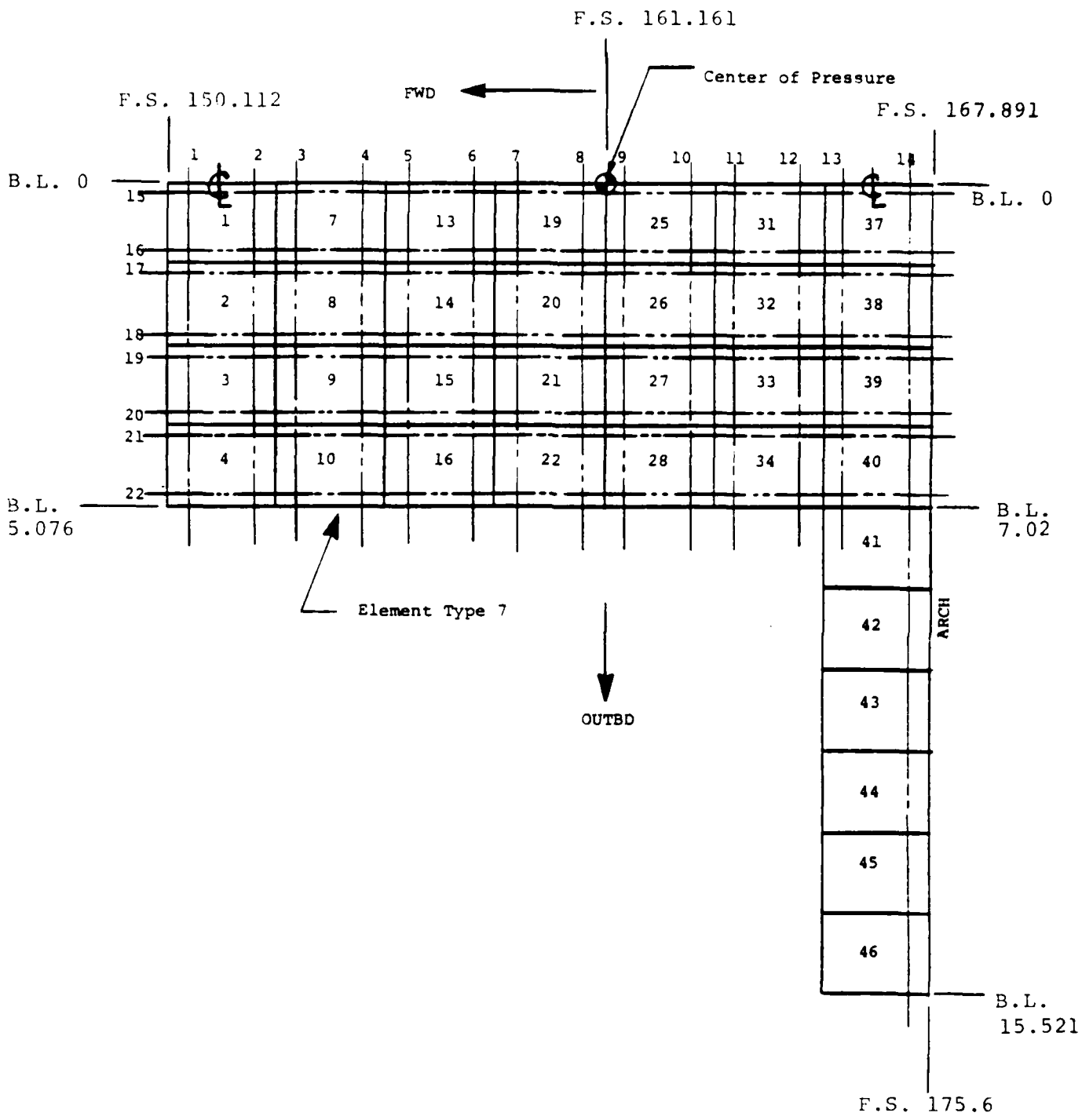
Figure 23. Locations Used for Resultant Force Calculations.

TABLE 5

TRANSPARENCY PARAMETRIC STUDY MATERIALLY NONLINEAR
TRANSIENT DYNAMIC ANALYSIS

	TRANSPARENCY STIFFNESS					
	$K_T = 4.936 \times 10^3 b$ $t_t = 0.45$ inch		$K_T = 8.1 \times 10^3 b$ $t_t = 0.60$ inch		$K_T = 2.734 \times 10^4 b$ $t_t = 0.90$ inch	
PRESSURE (PSI)	INCR 2	INCR 4	INCR 2	INCR 4	INCR 2	INCR 4
70	X	X	X	X	X	X
94	X	X	X	X	X	X
140	X	X	X	X		

representing load distributions in the outboard directions (locations 15 through 22). The first graph represents forces in the forward/aft direction, distributed along the arch of the transparency and depicts the distribution of load near the forward end of the transparency, with each successive graph progressing aft towards the frame and ending with the fourteenth resultant force distribution being immediately before and acting along the frame. The first of the remaining eight graphs characterizes the distribution of forces in the outboard direction along the centerline of the transparency, with each successive graph illustrating the distribution further outboard towards the aircraft sill.

The resultant forces calculated for the static analysis included the normal force, bending moment, and transverse shear forces. The method of computation is shown in Figure 15. The normal forces in the forward/aft direction, directly beneath the impact area, were in compression. Only the section of the transparency just forward of the impact area was in tension. Along the frame, aft of the impact area and just forward of the frame section, the normal forces were compressive indicating the path of the load as it travels through the windshield to the frame. The normal force distribution was compressive because the frame resisted the aft motion created by the applied forces acting in the aft direction. As the load traverses around the frame it became tensile until reaching the intersection of the frame and fuselage support, where it became compressive again. The normal forces in the outboard direction were also compressive and decreased in magnitude as the load traveled outboard along the transparency arch and approached the fuselage support structure. Typical normal force distributions in the forward and aft direction along the arch and along the transparency centerline are shown in Figures 24 and 25.

For the forward/aft direction, as the load progressed aft, the bending moment became more negative (compression in outer surface), attaining its maximum directly beneath the impact area.
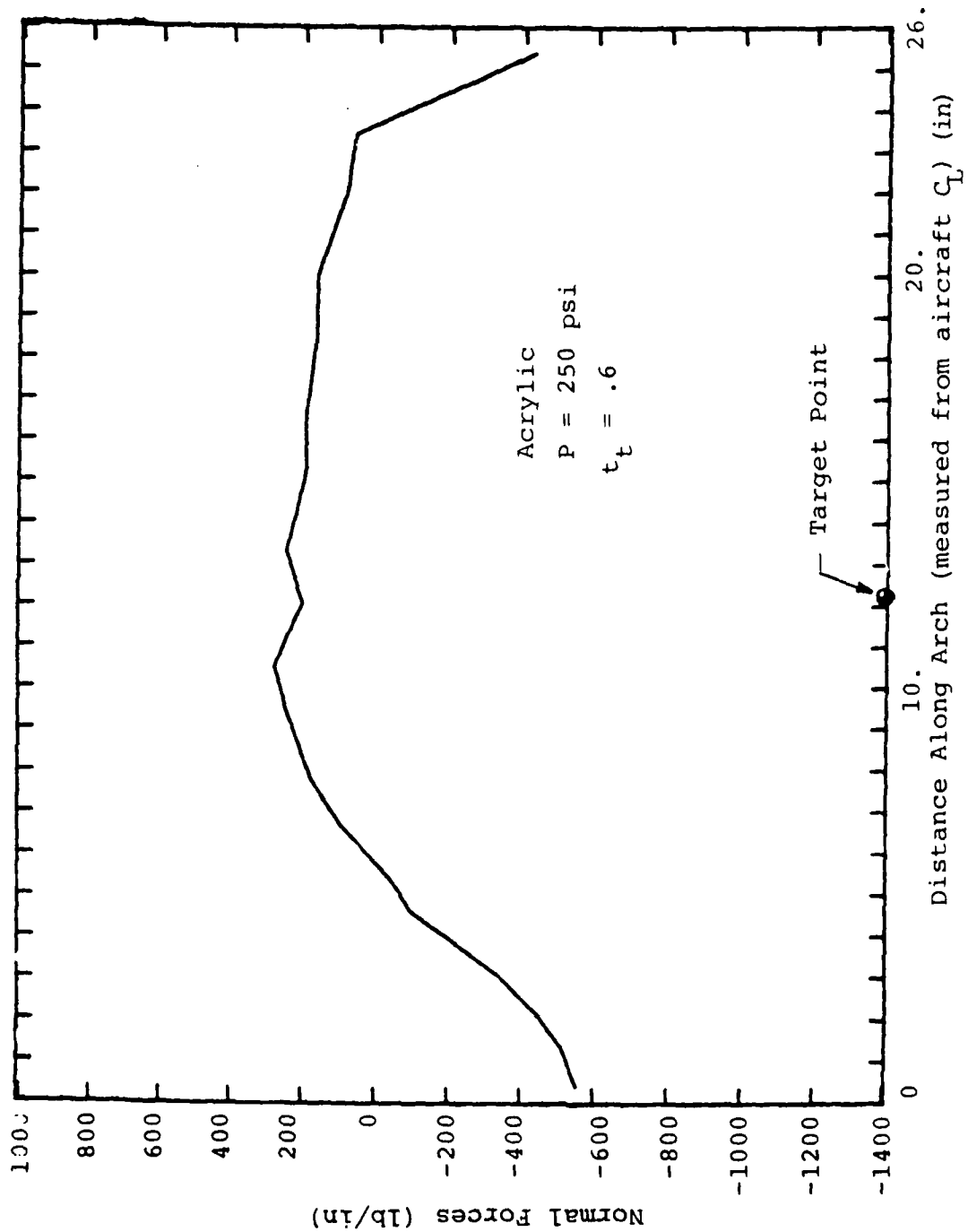
Figure 24. Normal Force Distribution Along Frame – Static Analysis.

46
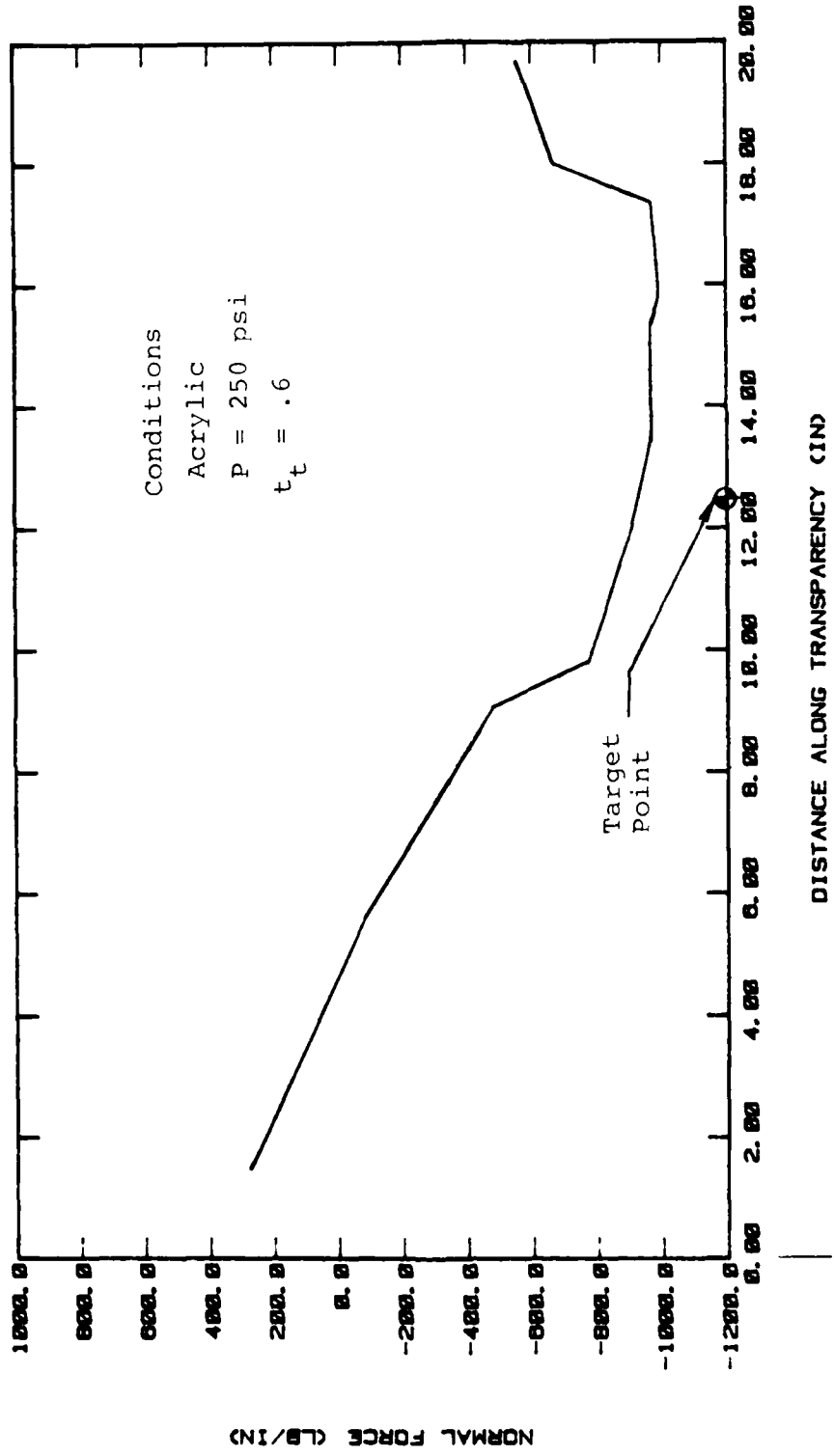
Figure 25. Normal Force Distribution Along Transparency Centerline - Static Analysis.

47

As the frame is approached a sign reversal takes place and the bending moment becomes positive. This occurred as a result of the frame's torsional and bending stiffness, which provides a partial restraint to transparency rotation. In the outboard direction the bending moment is again negative, directly beneath the impact location. The positive bending moment indicates tension in the top surface, compression in the bottom surface. Typical bending moment distributions in the forward and aft direction along the arch and along the transparency centerline are shown in Figures 26 and 27.

The graphical data for the transverse shear forces in the forward-aft direction indicate shear forces increasing in the aft direction, reaching a maximum directly underneath the impact area and reversing sign as the frame is approached. The load transfer mechanism in the outboard direction is primarily through bending and the normal forces. Typical transverse shear distributions in the forward and aft direction along the arch and along the transparency centerline are shown in Figures 28 and 29.

Peak bending, normal, and transverse shear forces along the frame are plotted versus stiffness for both static and dynamic analysis. This provides a good comparison between the stiffness parameter and the peak resultant forces as a function of load level. The data in Figures 30, 31, and 32 shows the effective load transfer to the frame for a static analysis. As the transparency stiffness is increased, the peak force transferred to the frame decreases. The only condition for which this did not occur is shown in Figure 30. The peak bending moment decreases for lower transparency stiffnesses when the load level increases due to nonlinearity of the transparency material. From this data one might associate a comparatively stiff transparency to an increase in birdstrike resistance. This is not necessarily a correct hypothesis. Failure criteria is not incorporated into the graphical data; only a comparison of the load transfer mechanisms is presented.
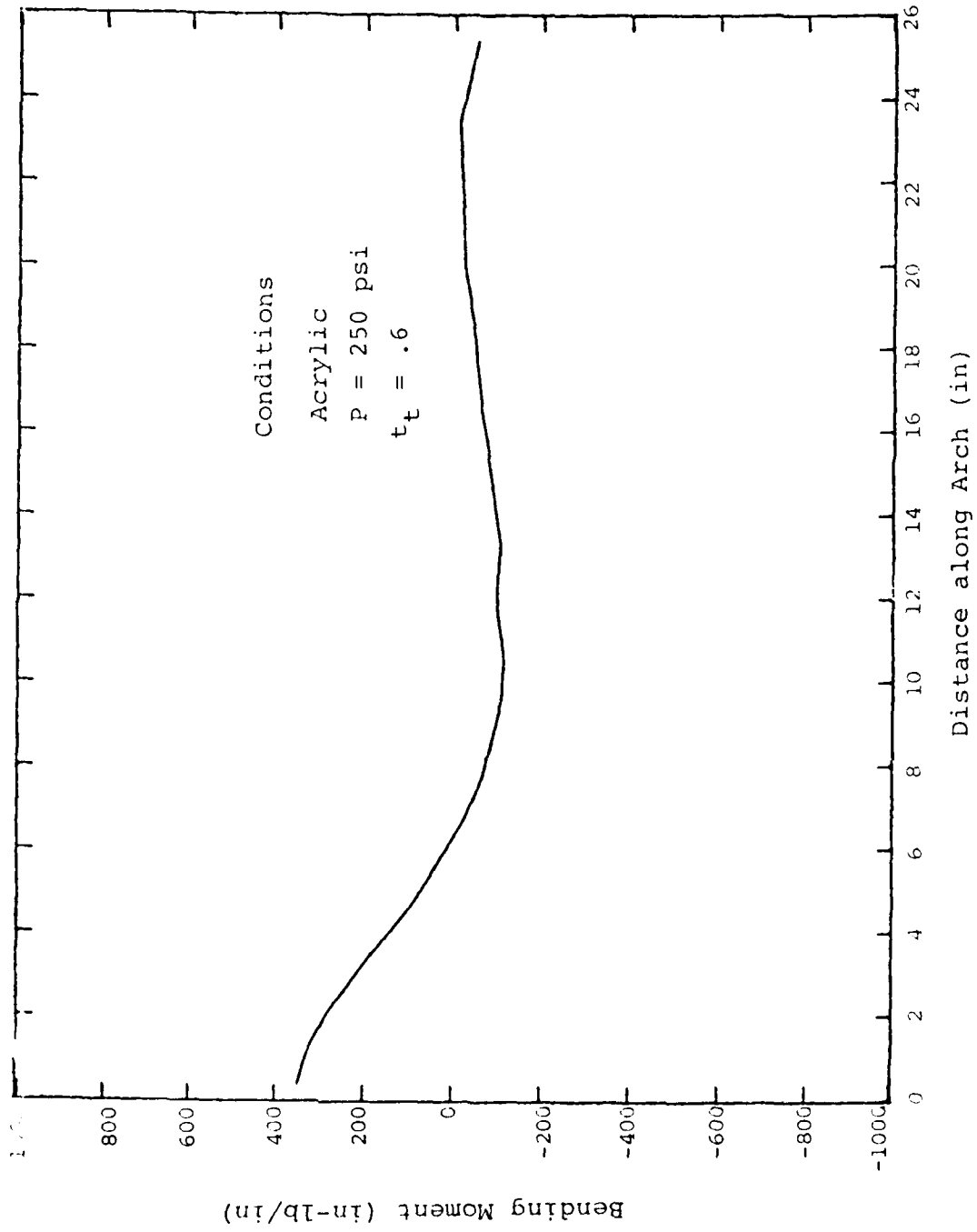
Figure 26. Bending Moment Distribution Along Frame - Static Analysis.

Conditions

Acrylic

P = 250 psi

t_t = .6

Distance along Arch (in)

Bending Moment (in-lb/in)
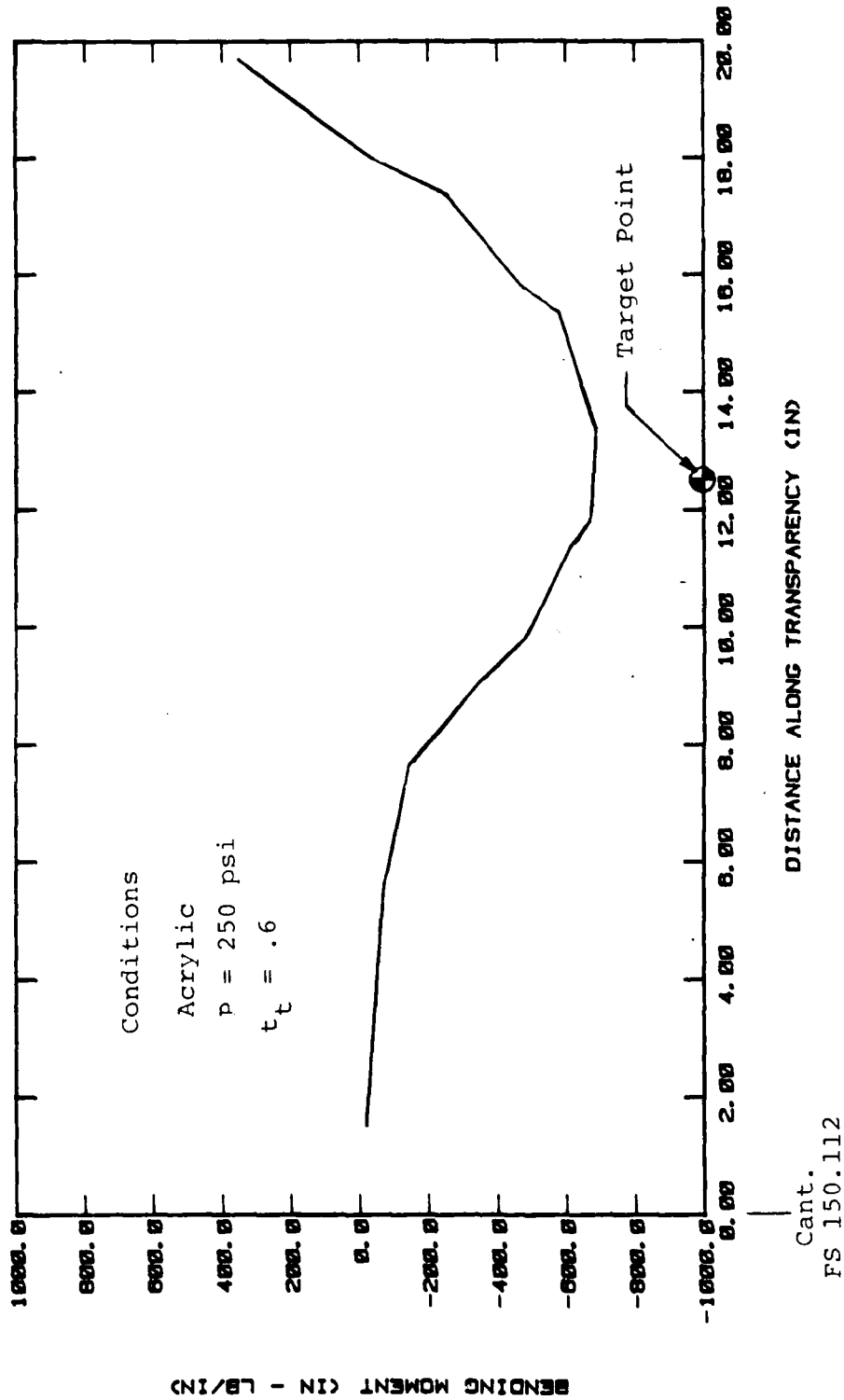
Figure 27. Bending Moment Distribution Along Transparency Centerline - Static Analysis.

50
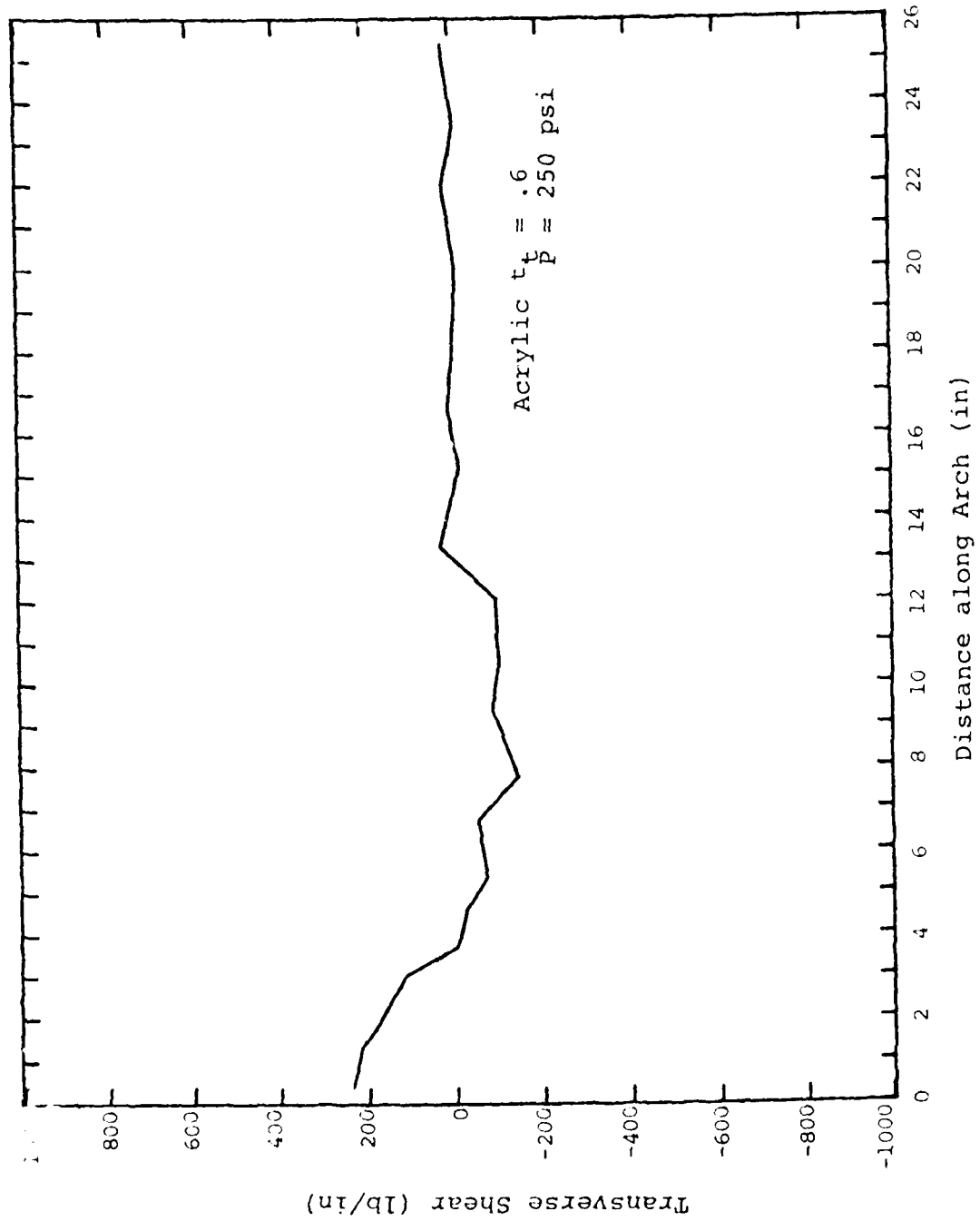
Figure 28. Transverse Shear Force Distribution along Frame - Static Analysis.
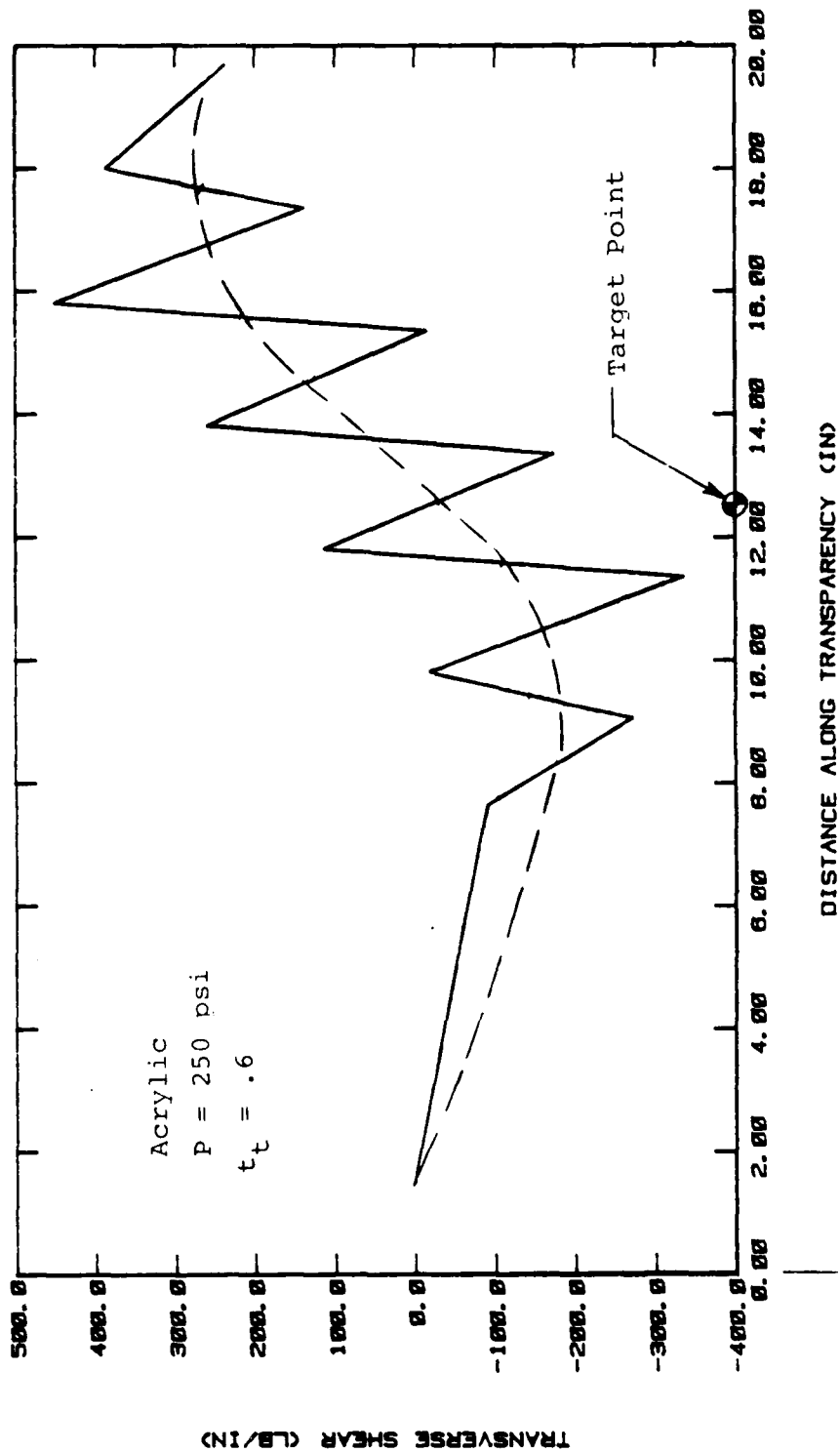
Figure 29.   Transverse Shear Force Distribution Along Transparency Centerline - Static Analysis.
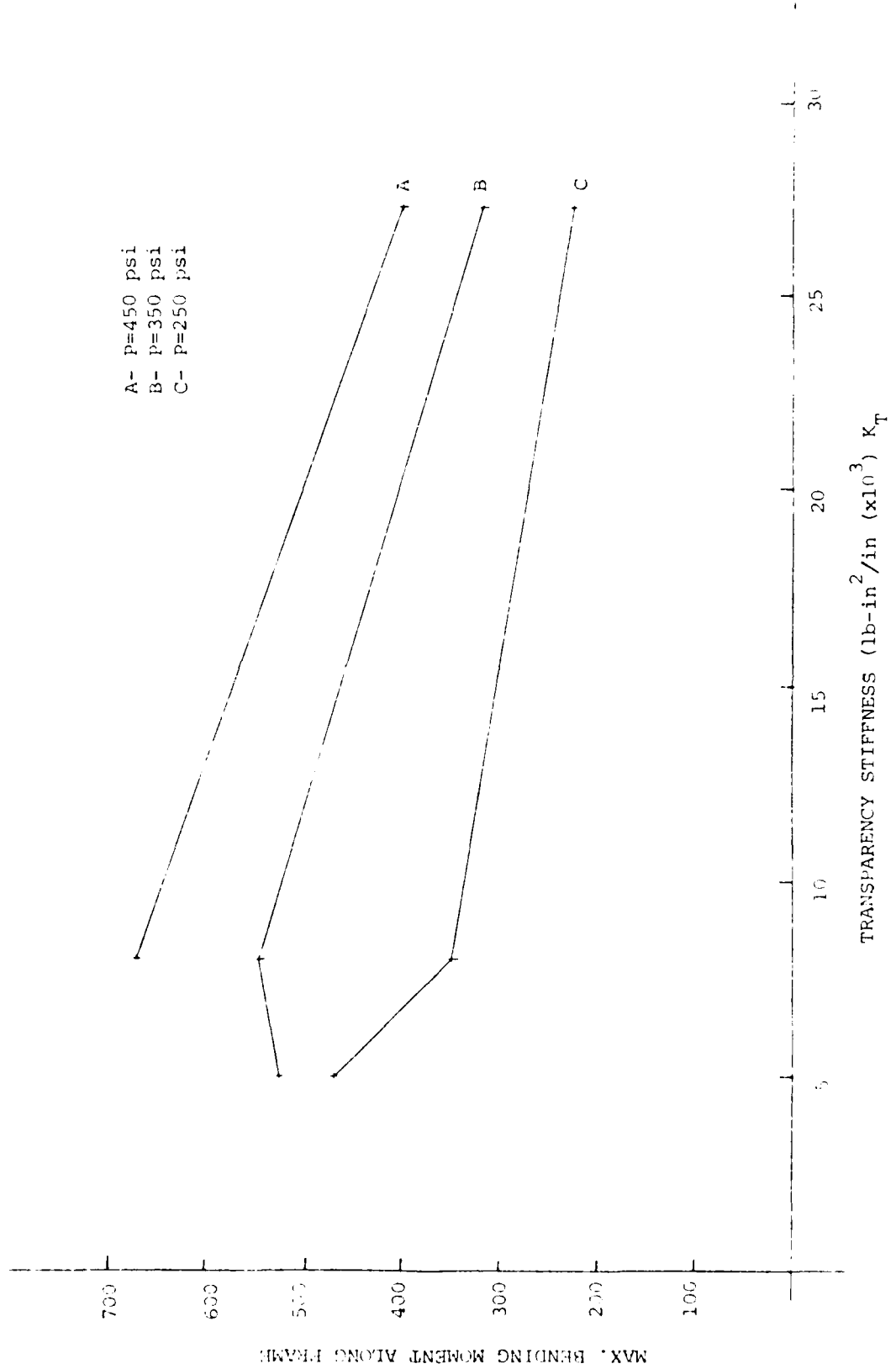
Figure 30. Peak Bending Moment Along Frame - Static Analysis.

A- P=450 psi
B- P=350 psi
C- P=250 psi

TRANSPARENCY STIFFNESS (lb-in^2/in (x10^3) K_T

MAX. BENDING MOMENT ALONG FRAME

53

Figure 31. Peak Normal Forces Along Frame - Static Analysis.

54

Figure 32. Peak Transverse Shear Force Along Frame – Static Analysis.
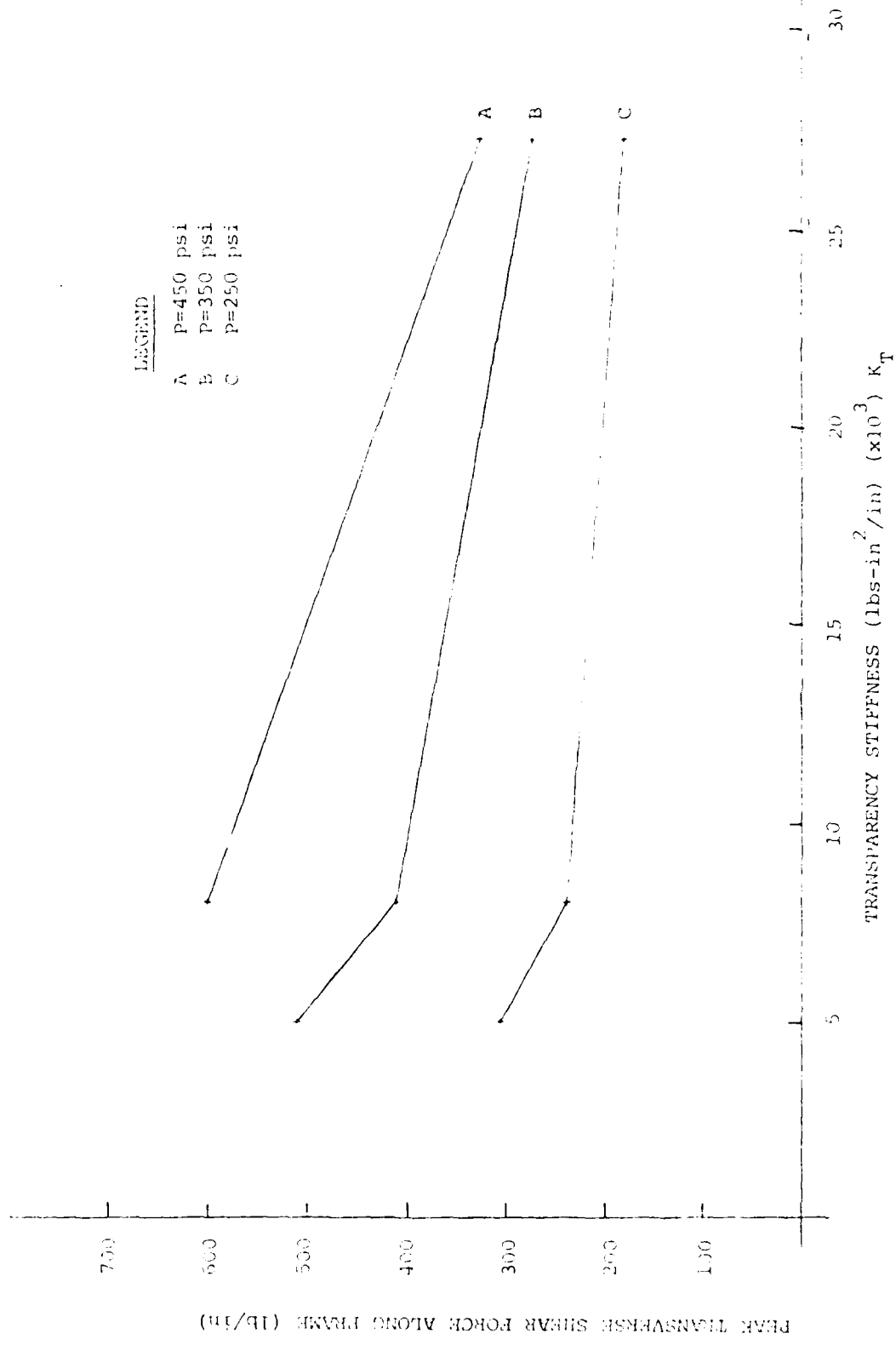
LEGEND

A   P=450 psi
B   P=350 psi
C   P=250 psi

TRANSPARENCY STIFFNESS (lbs-in^2/in) (x10^3) K_T

PEAK TRANSVERSE SHEAR FORCE ALONG FRAME (lb/in)

The effect on the windshield due to the applied load, for the dynamic analyses, is illustrated in the stress resultant graphical data presented in Section III of Reference 14. This data is similar to the static analysis in most respects; however, the normal forces were compressive only at the lower load levels. When the full momentum loads (P = 140 psi for the higher and P = 94 psi for the lower transparency stiffnesses) are applied to the system, tensile forces in the forward/aft direction arise along approximately a two inch band along the centerline of the transparency. Substantial normal forces are transferred in the outboard direction as compared to the forward/aft direction (see Reference 14). Typical normal force distributions along the arch and along the transparency centerline are shown in Figures 33 and 34.

The bending moments in the forward/aft direction were similar to the static analysis; compression in the top fibers and tension in the bottom fibers. Their magnitudes increase from the forward portion of the student windshield to the center of impact, then decrease to zero and reverse sign as the frame is approached, indicating tension in the top fibers and compression in the bottom fibers (see Reference 14). Again, this was the result of the frame imparting a partial restraint to the transparency. In the outboard direction the peak bending moment was approximately the same magnitude as in the forward/aft direction (see Reference 14). Typical bending moment distributions along the arch and along the transparency centerline are shown in Figures 35 and 36.

The transverse shear forces reverse sign under the applied load, indicating a transfer of load in both directions as expected. This is more pronounced for the more flexible transparencies because of the increased importance of local bending. Typical transverse shear distributions along the arch and along the transparency centerline are shown in Figures 37 and 38. The transverse shear forces calculated in the forward/aft direction, near the centerline of the transparency, are presented graphically
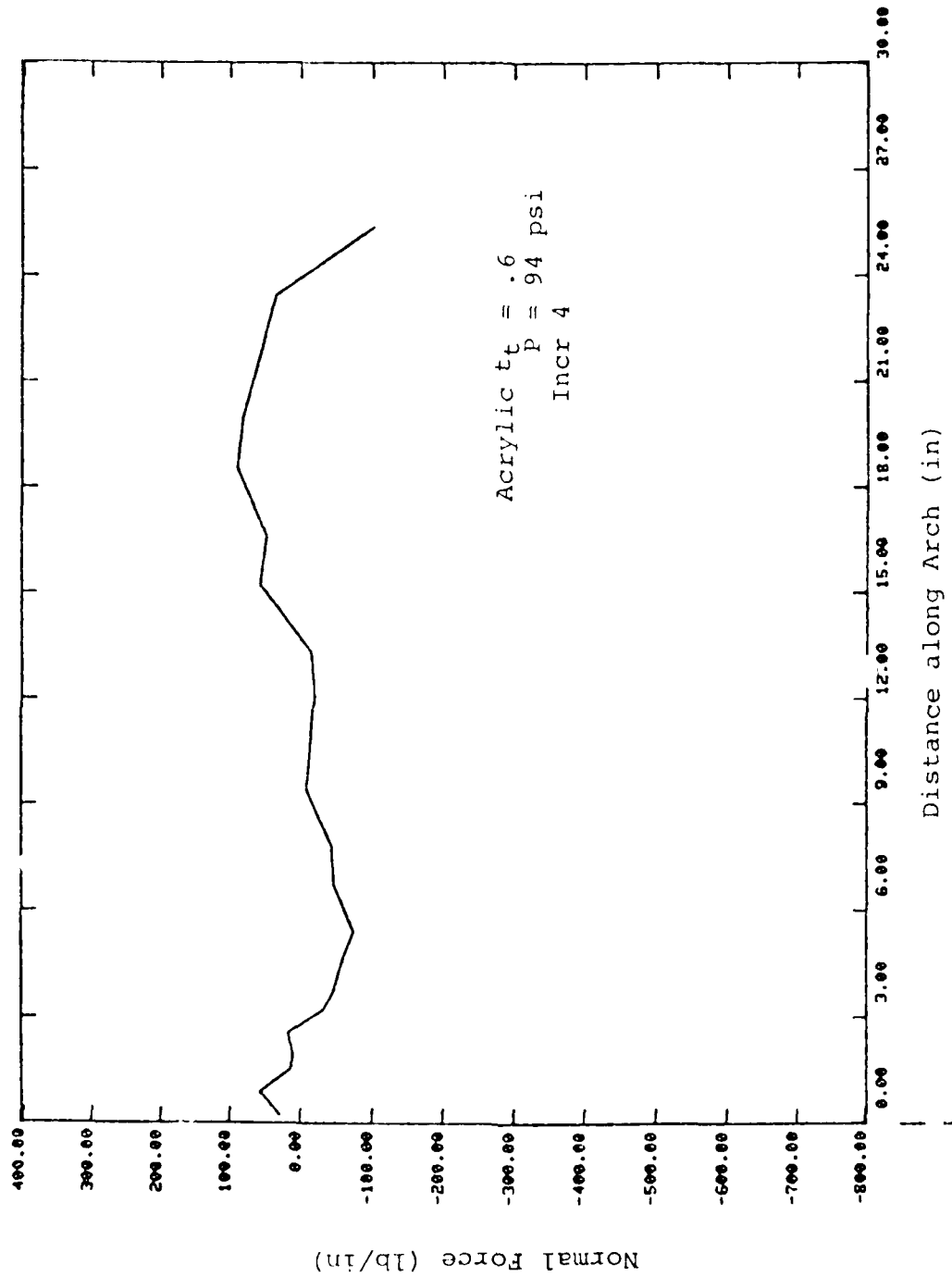
Figure 33. Normal Force Distribution Along Frame - Dynamic Analysis.
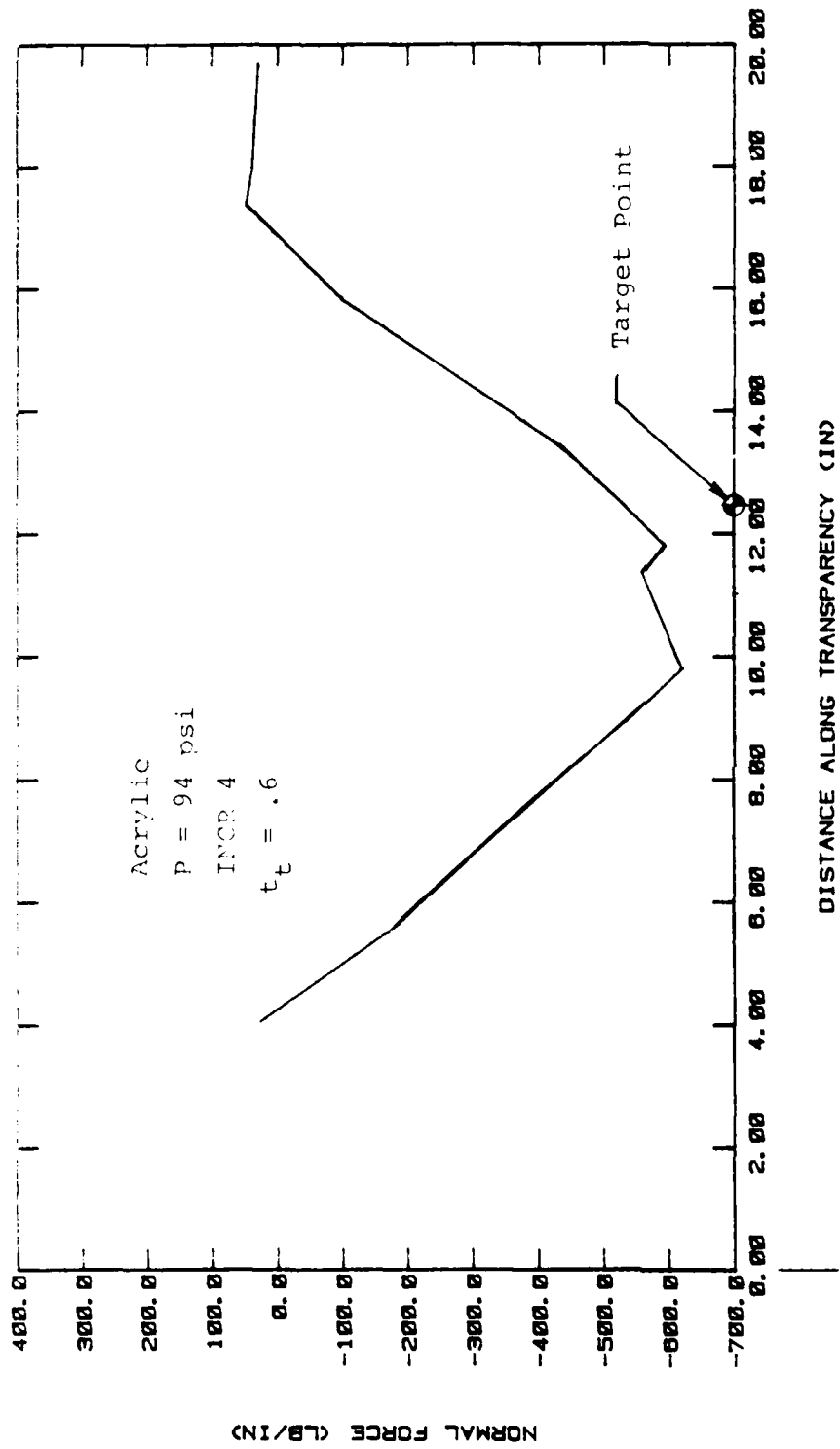
Figure 34. Normal Force Distribution Along Transparency Centerline - Dynamic Analysis.
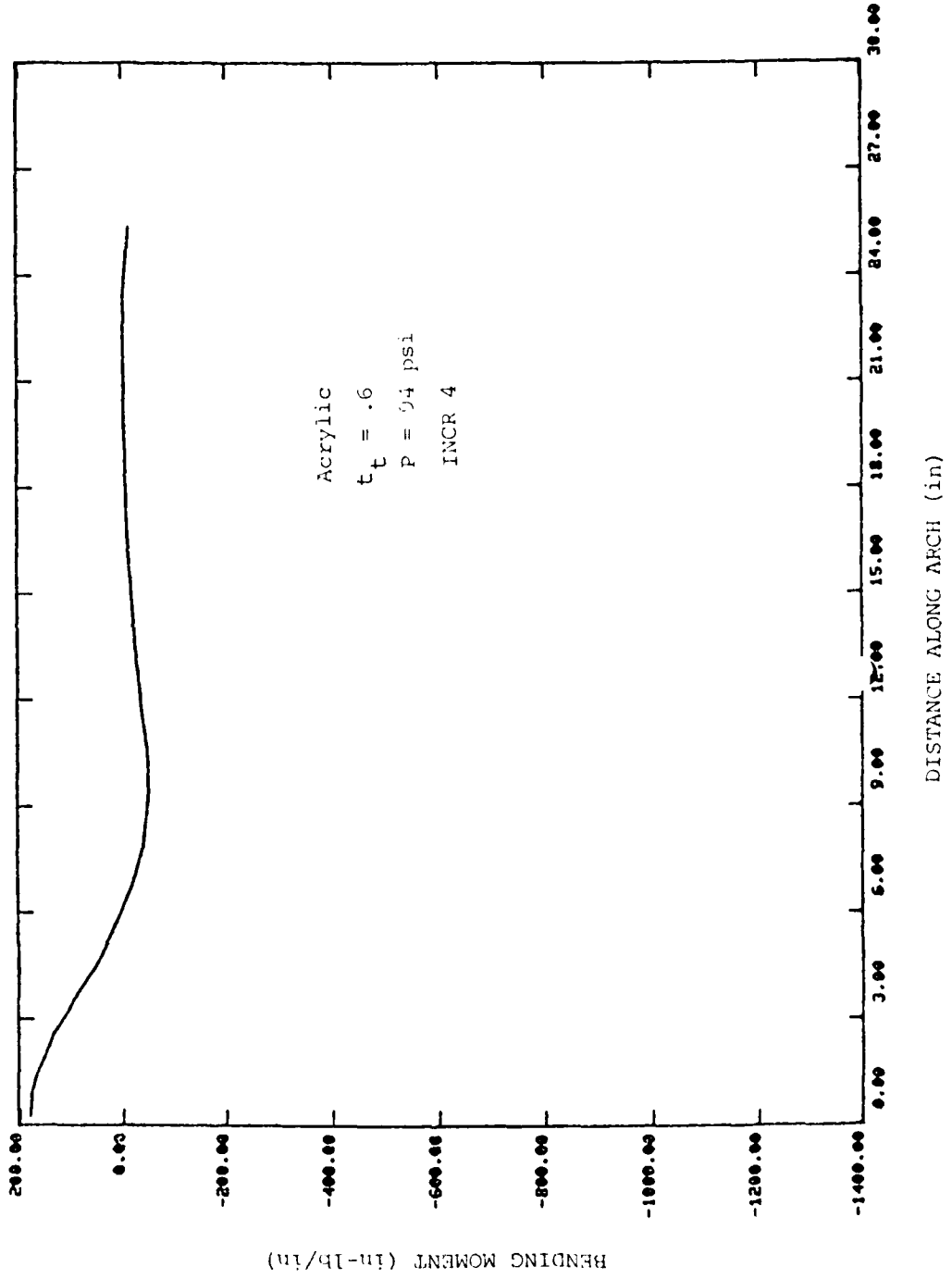
Figure 35. Bending Moment Distribution Along Frame – Dynamic Analysis.

Acrylic
$t_t = .6$
P = 94 psi
INCR 4

DISTANCE ALONG ARCH (in)
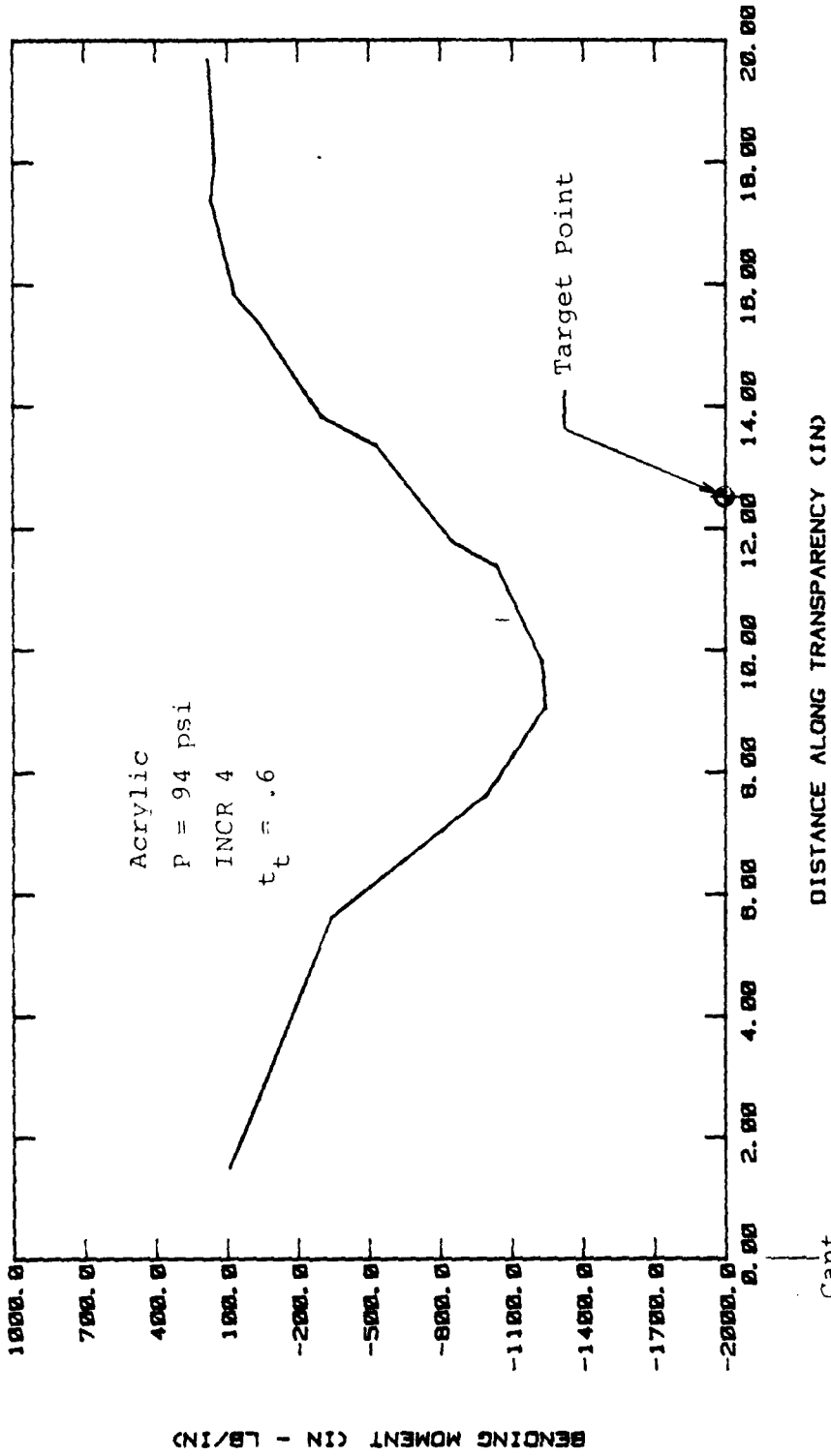
BENDING MOMENT (in-lb/in)

Figure 36. Bending Moment Distribution Along Transparency Centerline - Dynamic Analysis.

DISTANCE ALONG ARCH (in)

TRANSVERSE SHEAR (lb/in)

Acrylic
$t_t = .6$
P = 94 psi

INCR 4
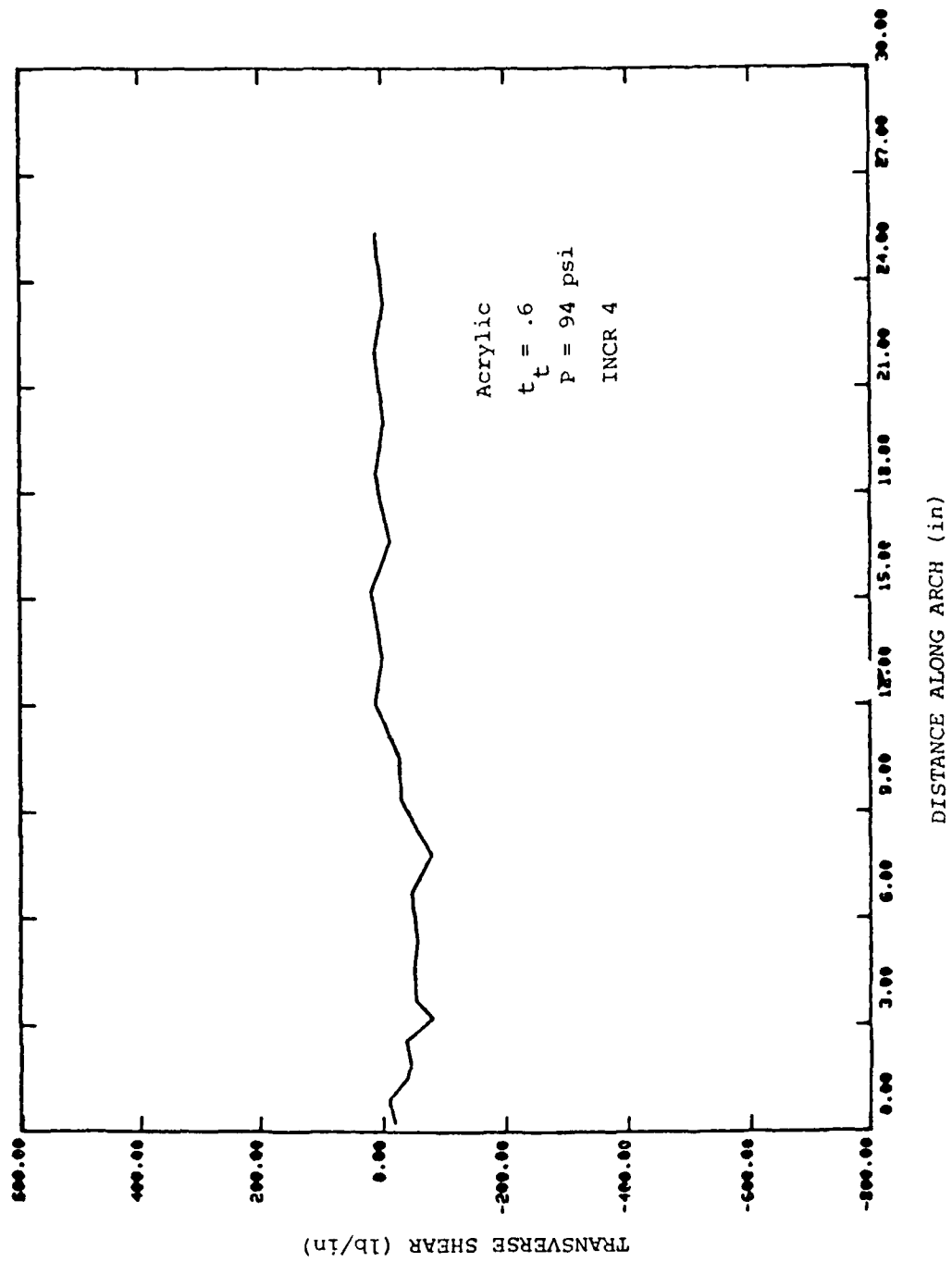
Figure 37. Transverse Shear Force Distribution Along Frame - Dynamic Analysis.

61
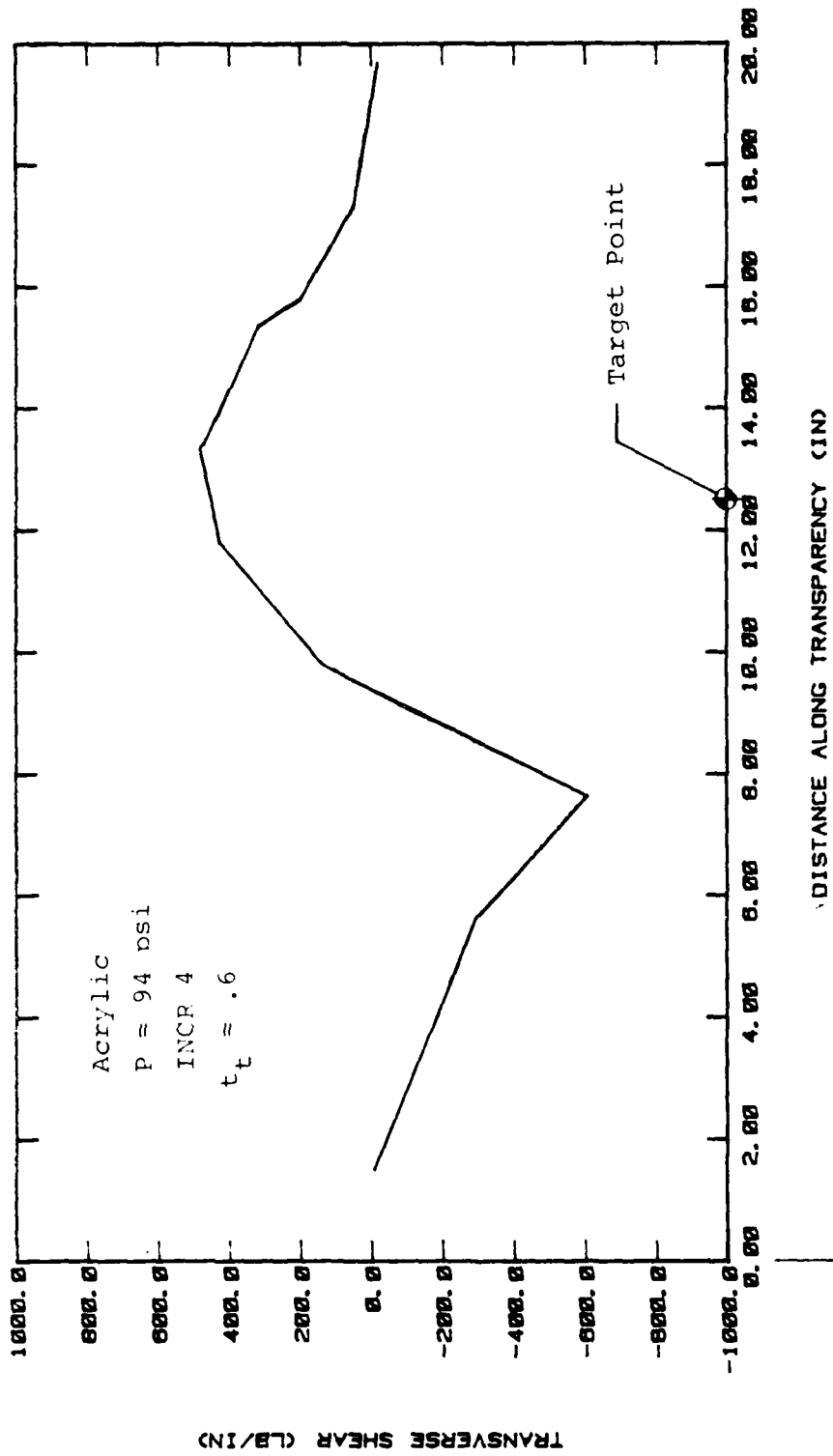
Figure 38. Transverse Shear Force Distribution Along Transparency Centerline - Dynamic Analysis.

in Figures 39, 40, and 41. Both increment two and four are
plotted on the same graph. Figure 39 presents data for the
0.45 inch polycarbonate material, Figure 40 presents data for
the 0.6 inch stretched acrylic, and Figure 41 presents data for
the 0.9 inch stretched acrylic. All three figures are very
similar; although their peak values are not the same, the shape
as a function of time indicates that the transverse shear forces
progress towards the aft arch at approximately the same speed.

The peak internal loads along the frame are plotted as a
function of transparency stiffness for the dynamic analysis.
They are presented in Figures 42, 43, and 44. The solid lines
indicate values for time increment 4 and the dashed lines indicate
values for increment 2. Notice that for increment 2 very little
bending moment or transverse shear force are being transferred
to the frame; only the transfer of normal forces are significant.
The normal force graphs also indicate the transition to tensile
forces as the applied load is increased. Until the deformation
becomes large, the normal forces in the transparency remain
compressive near the center area of the aft frame.

5.   DEFLECTION DATA

The static analysis deflection plots are presented in
Figures 45 through 50, and the dynamic analysis deflection plots
are presented in Figures 51 through 56 and in Section IV of
Reference 14. For the static analysis the transparency centerline
deflections were as expected. As the load increased, the trans-
parency and the frame deflection increased, with the transparency
deflection increasing at a faster rate. The deflection of the
frame became larger as the transparency stiffness was decreased,
indicating potential problems if the student windshield becomes
too flexible.

The dynamic analysis frame deflection plots indicate that
the frame was just beginning to absorb the bird impact energy
during the fourth time increment. The centerline deflection

63
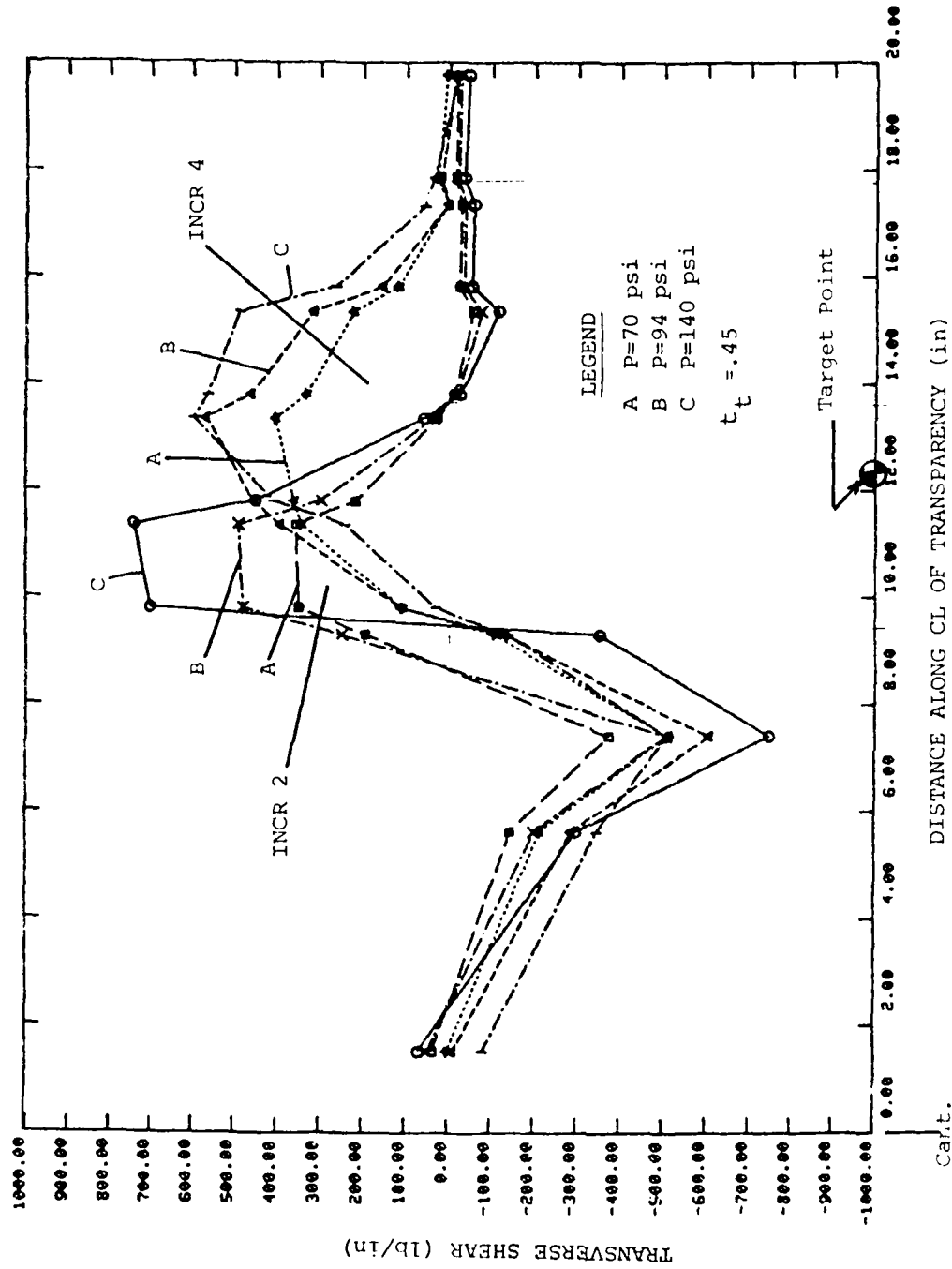
Figure 39. Polycarbonate ($t_t = .45$) Transverse Shear Force Distribution – Dynamic Analysis

64
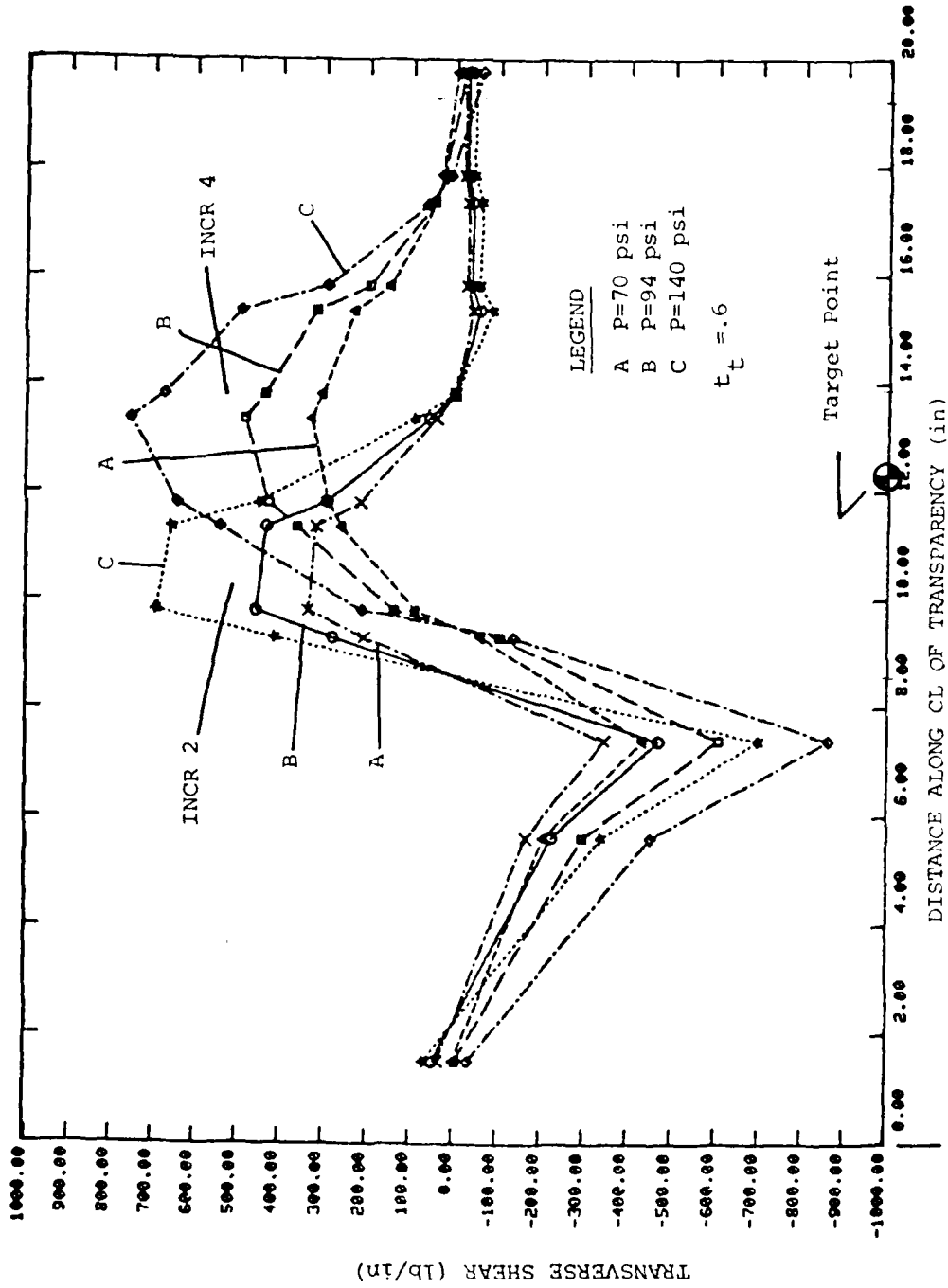
Cant.
PS 150.112

Figure 40. Acrylic ($t_t = .6$) Transverse Shear Force Distribution - Dynamic Analysis.

65
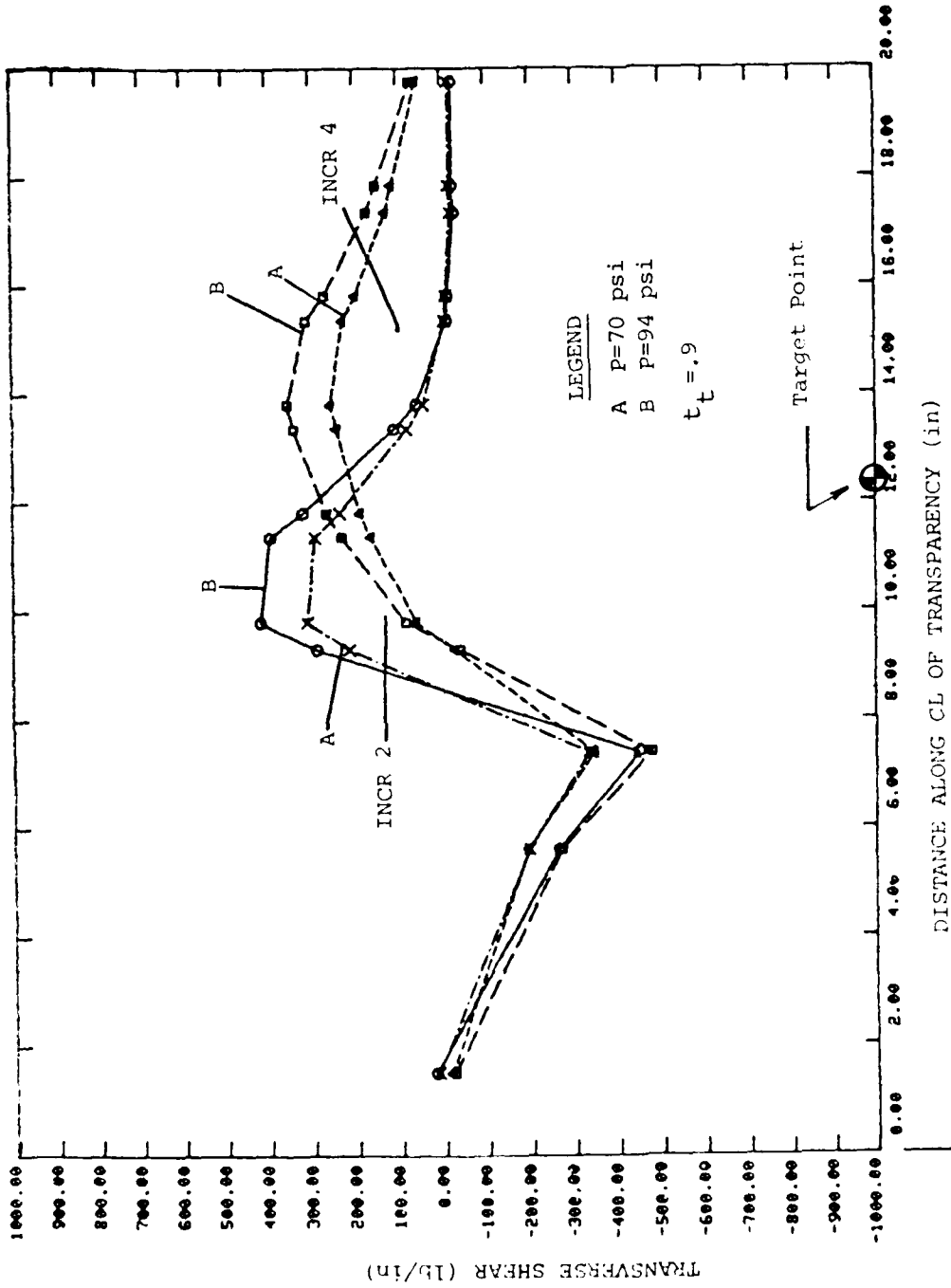
Figure 41. Acrylic ($t_t = .9$) Transverse Shear Force Distribution - Dynamic Analysis.
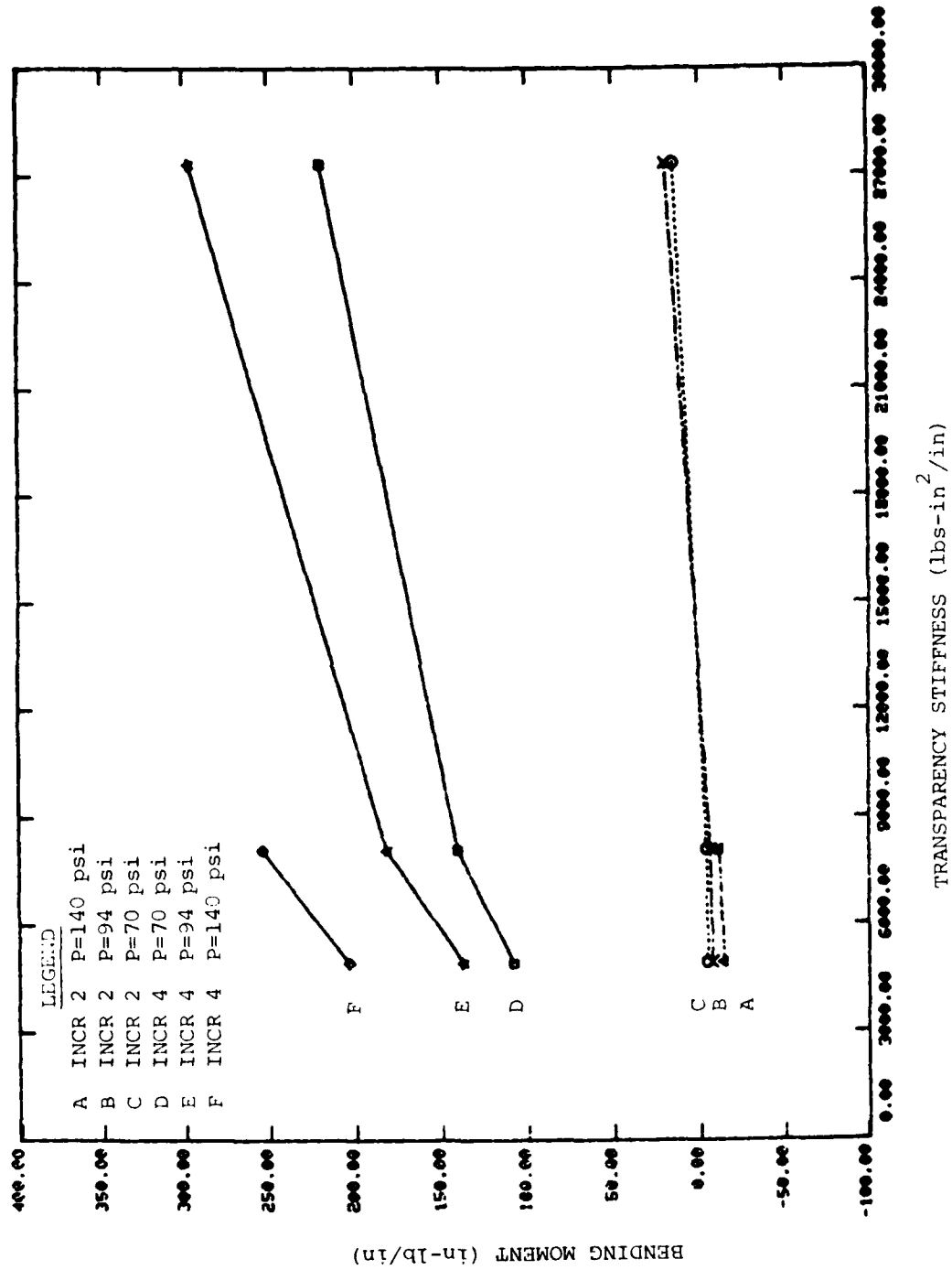
Figure 42. Peak Bending Moment Along Frame Versus Transparency Stiffness – Dynamic Analysis.
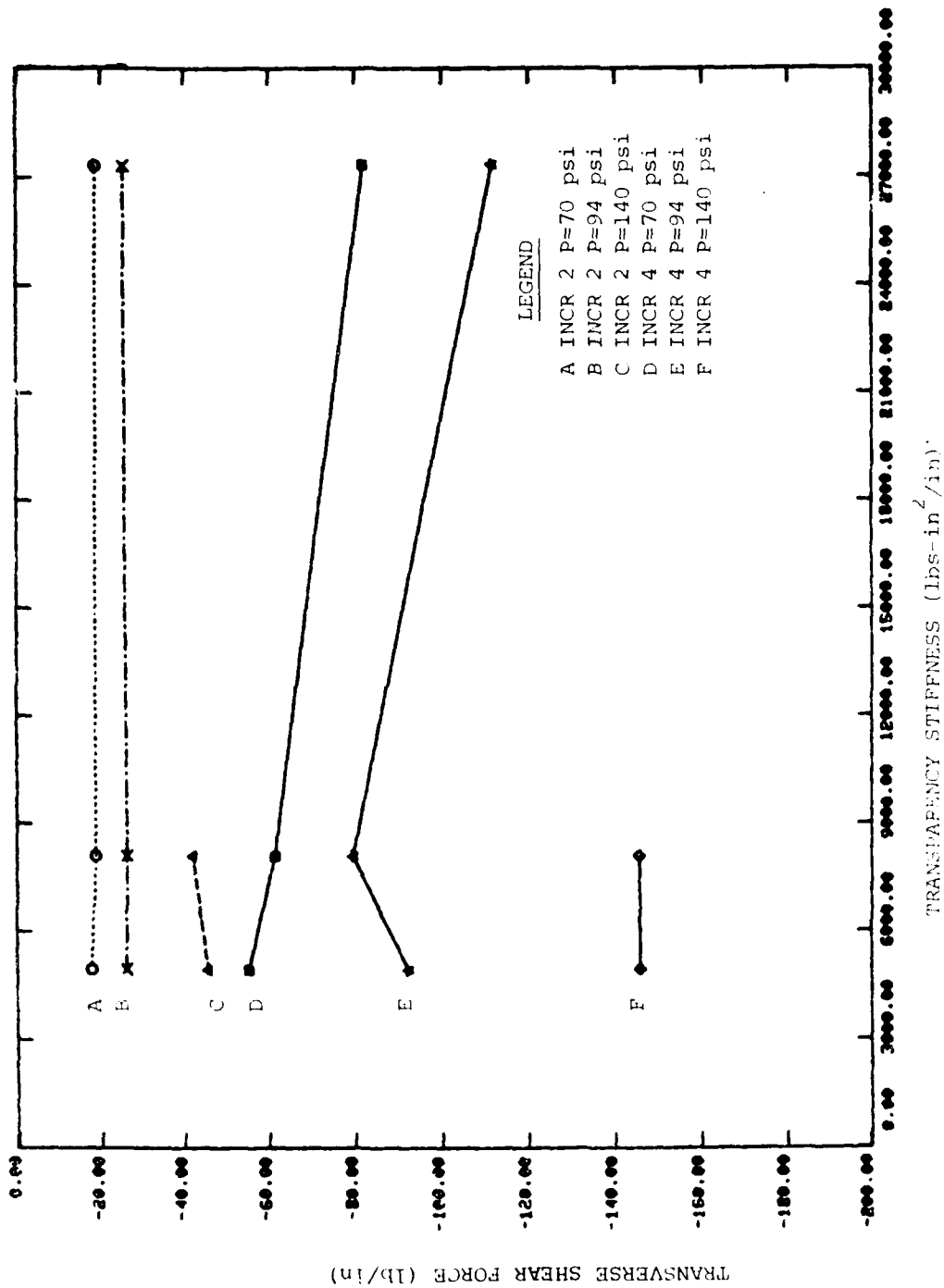
Figure 43. Peak Transverse Shear Force Along Frame Versus Transparency Stiffness - Dynamic Analysis.

68

TRANSPARENCY STIFFNESS (lb-in²/in)

NORMAL FORCE (lb/in)

LEGEND

A   INCR 2 P=70 psi
B   INCR 2 P=94 psi
C   INCR 2 P=140 psi
D   INCR 4 P=70 psi
E   INCR 4 P=94 psi
F   INCR 4 P=140 psi
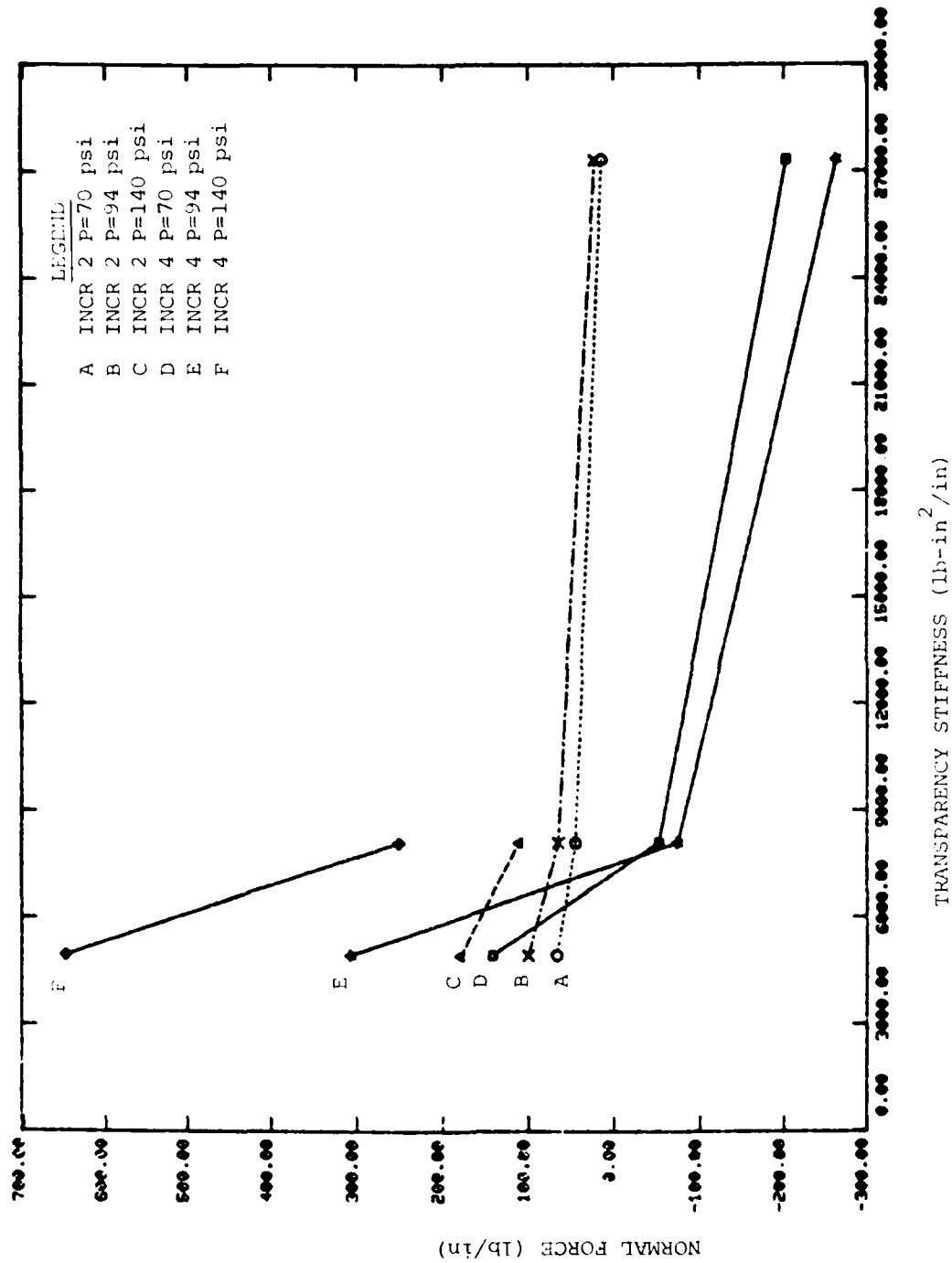
Figure 44.   Peak Normal Forces Along Frame Versus Transparency Stiffness -
Dynamic Analysis.

69
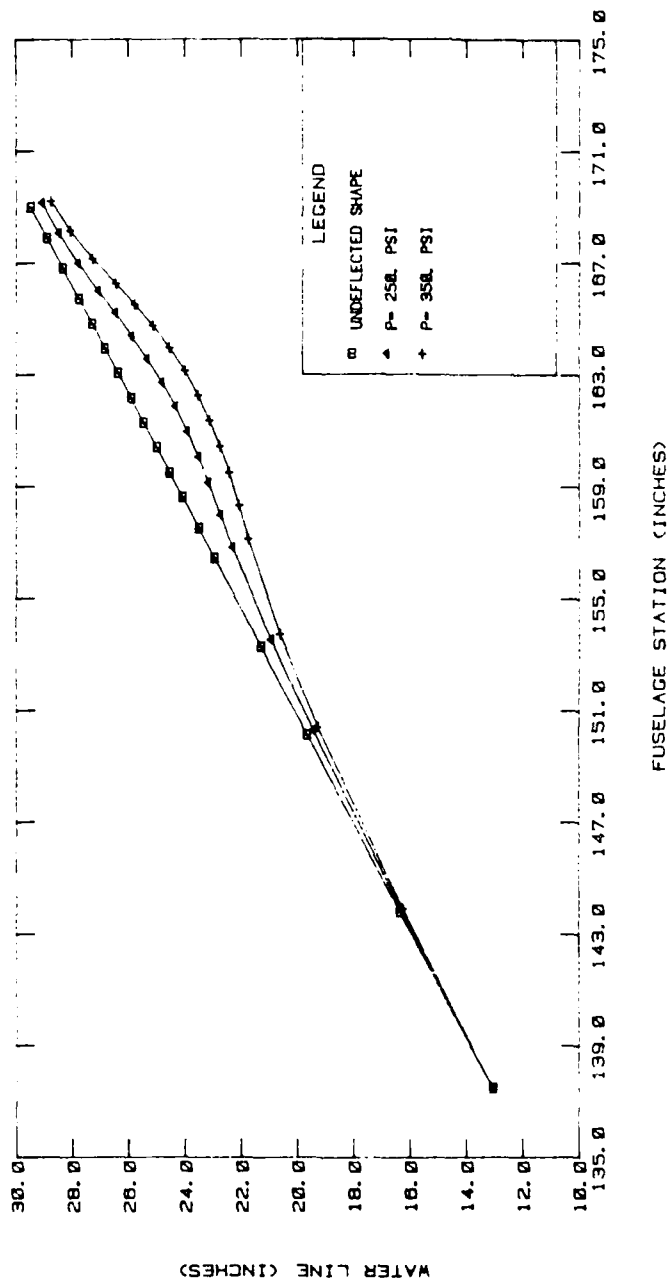
Figure 45. Centerline Deflection, Static Analysis t_t .45
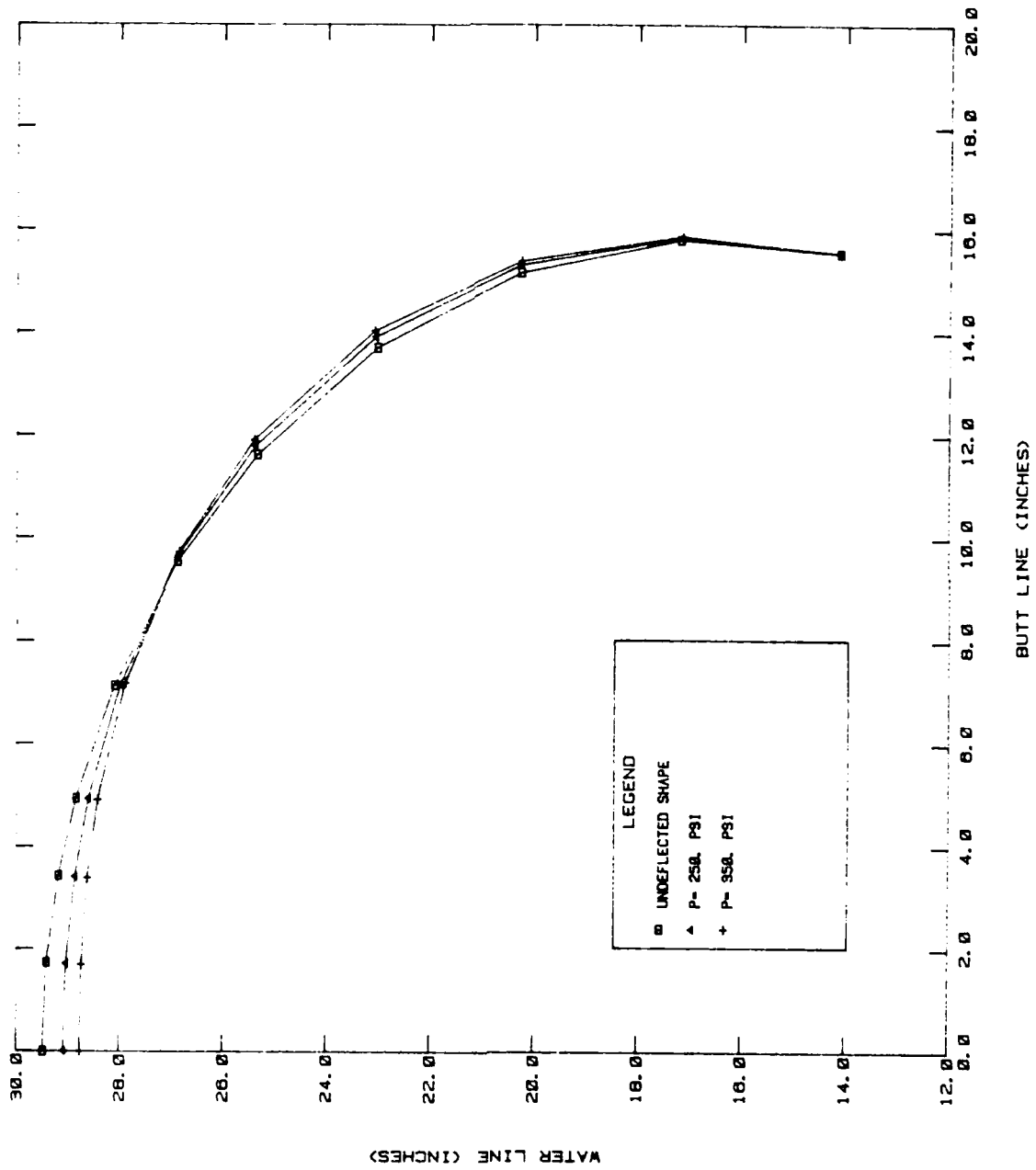
Figure 46. Frame Deflection – Static Analysis $t_t = .45$
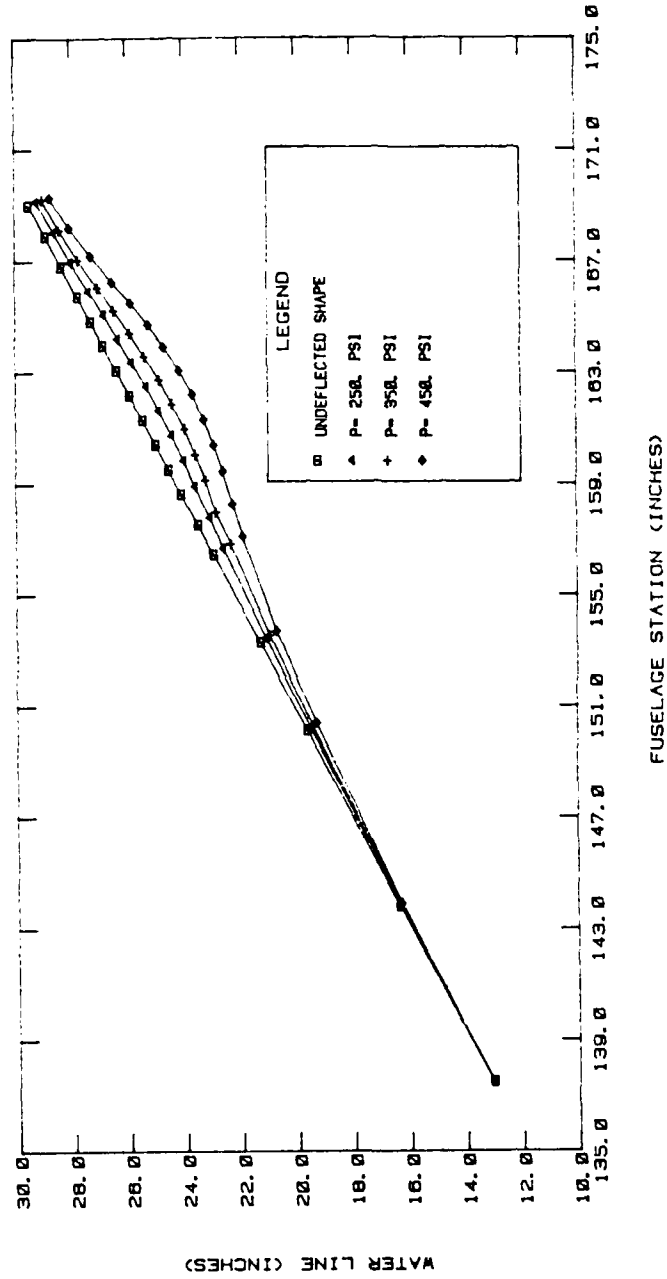
Figure 47. Centerline Deflection - Static Analysis $t_t = .6$

TH= .6 FRAME DEFL.
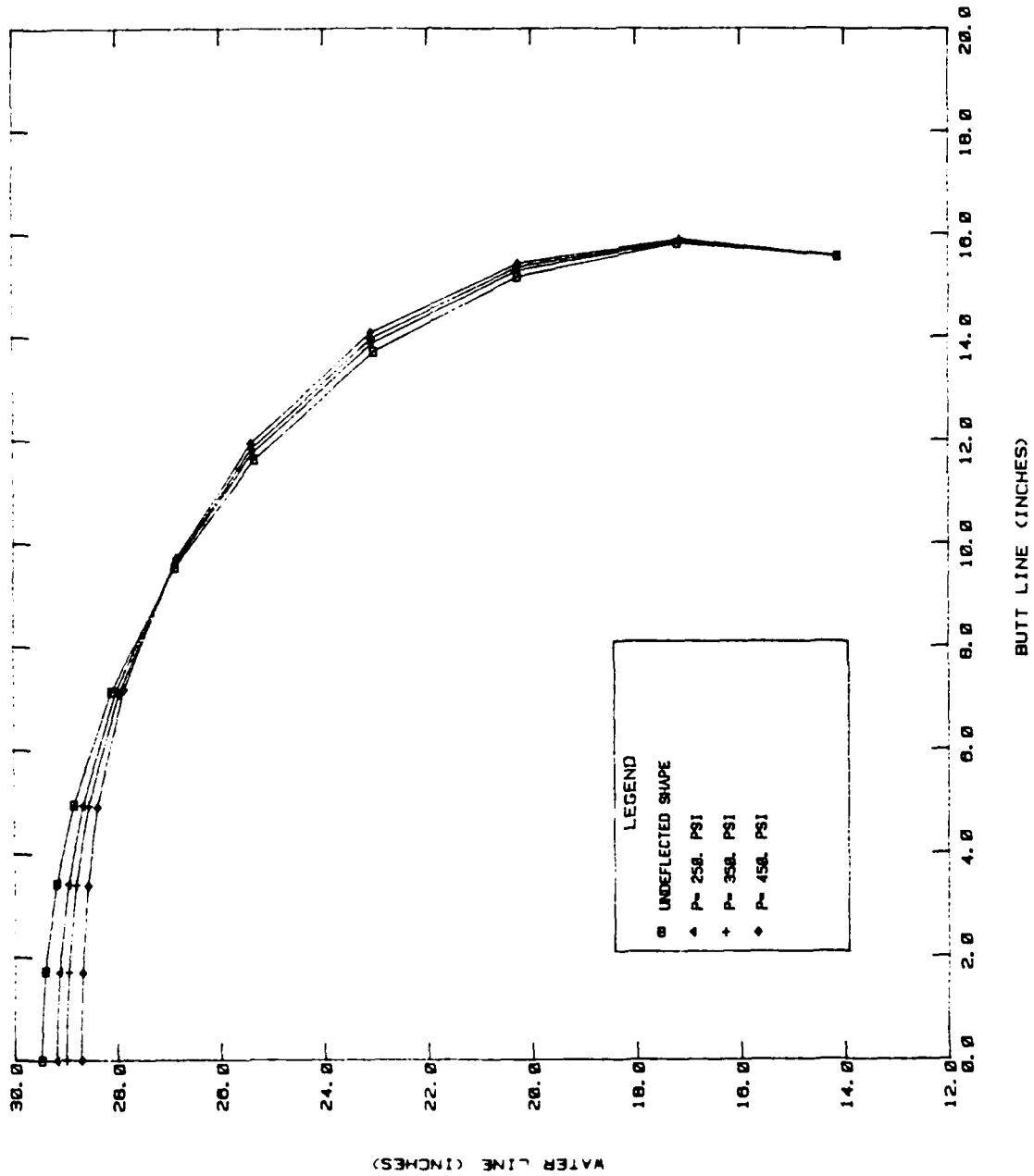
Figure 48. Frame Deflection - Static Analysis $t_t = .6$
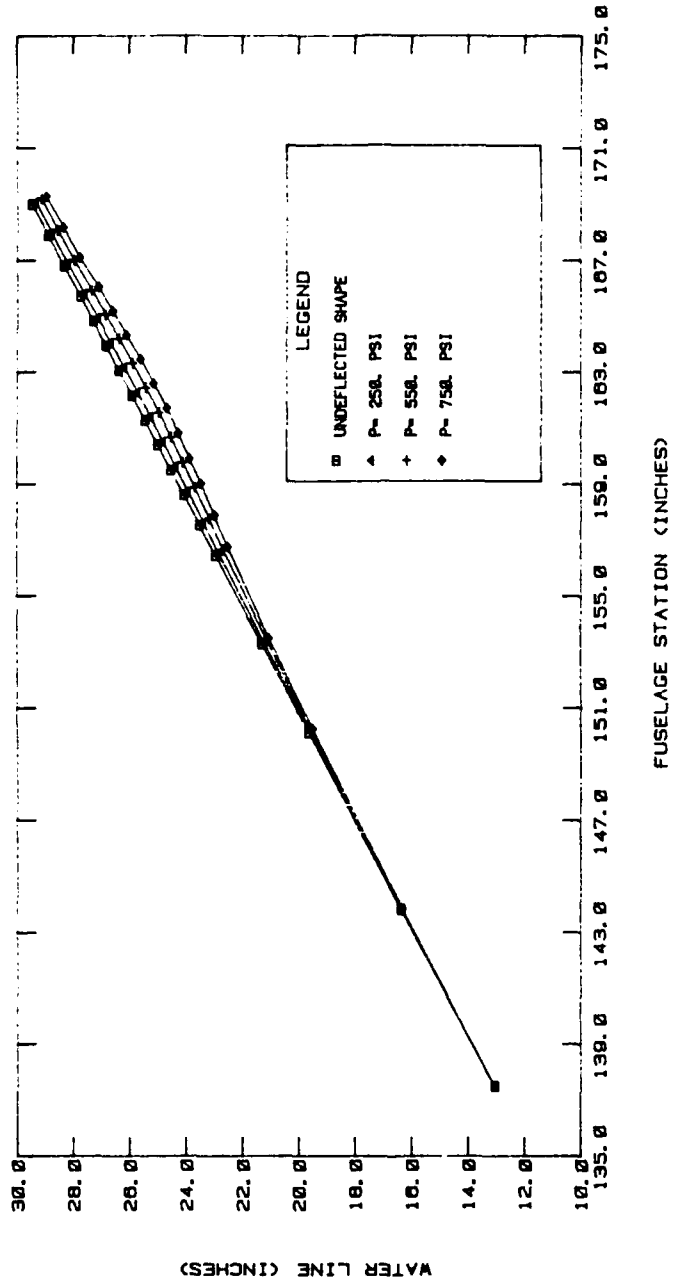
Figure 49.   Centerline Deflection – Static Analysis $t_i = .9$

74

Figure 50. Frame Deflection - Static Analysis $t_t = .9$
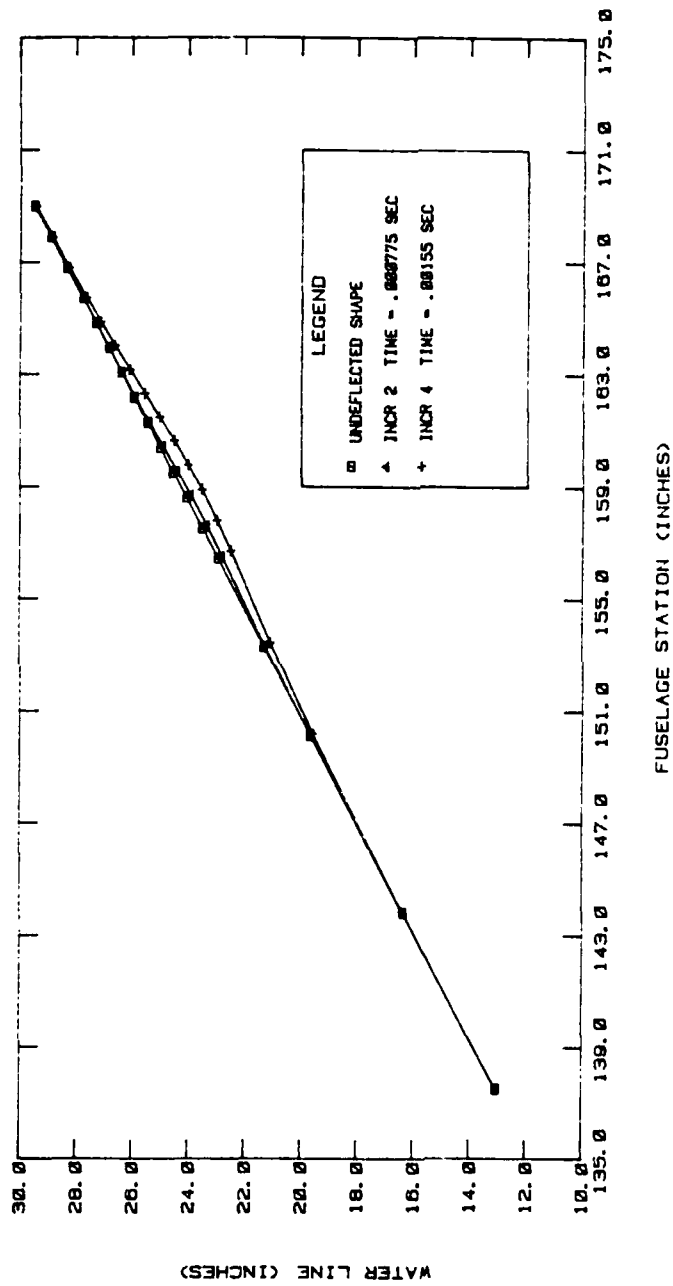
Figure 51. Centerline Deflection - Dynamic Analysis P=70 psi, $t_t = .6$
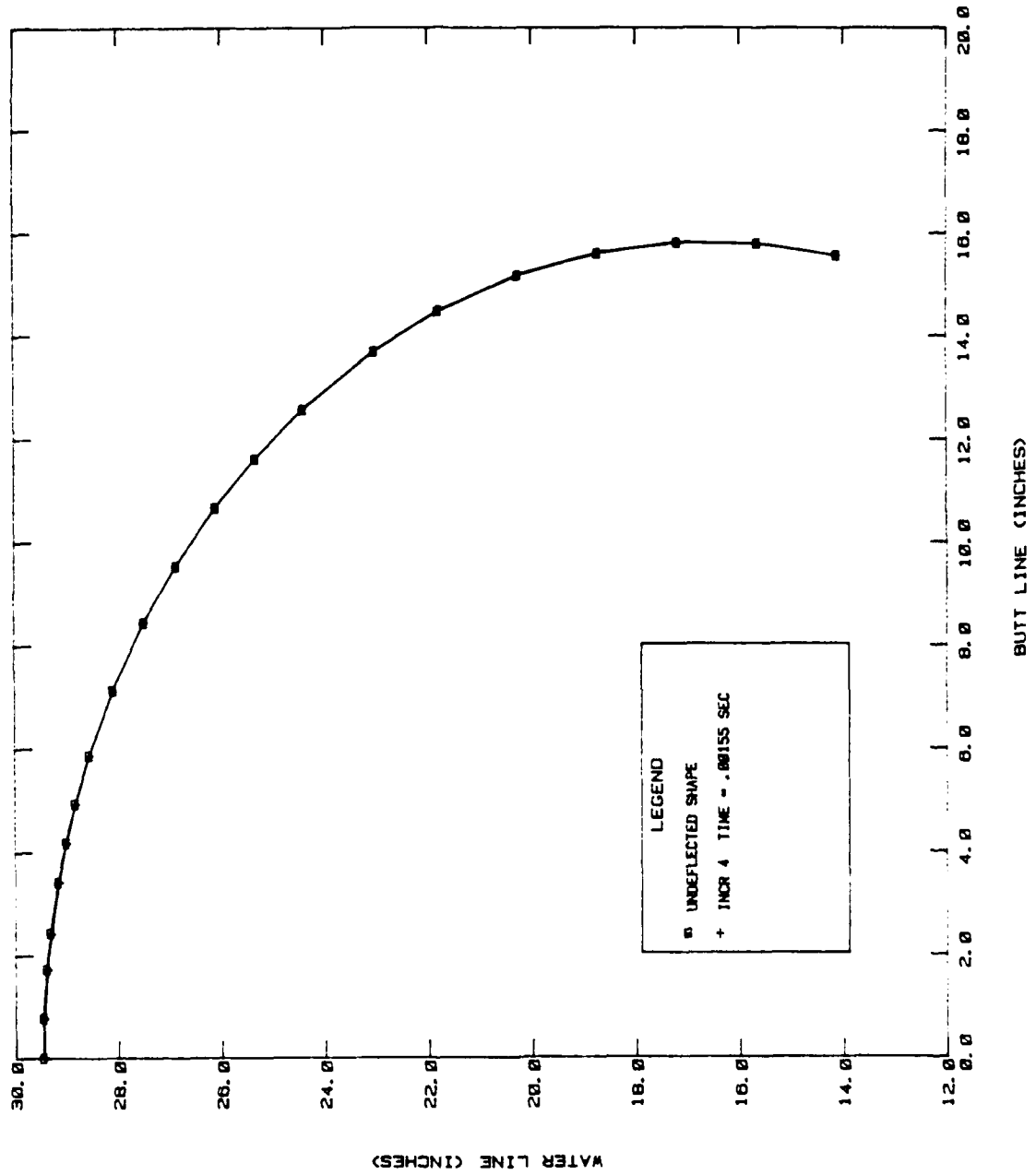
Figure 52.   Frame Deflection - Dynamic Analysis, P=70, t_t = .6
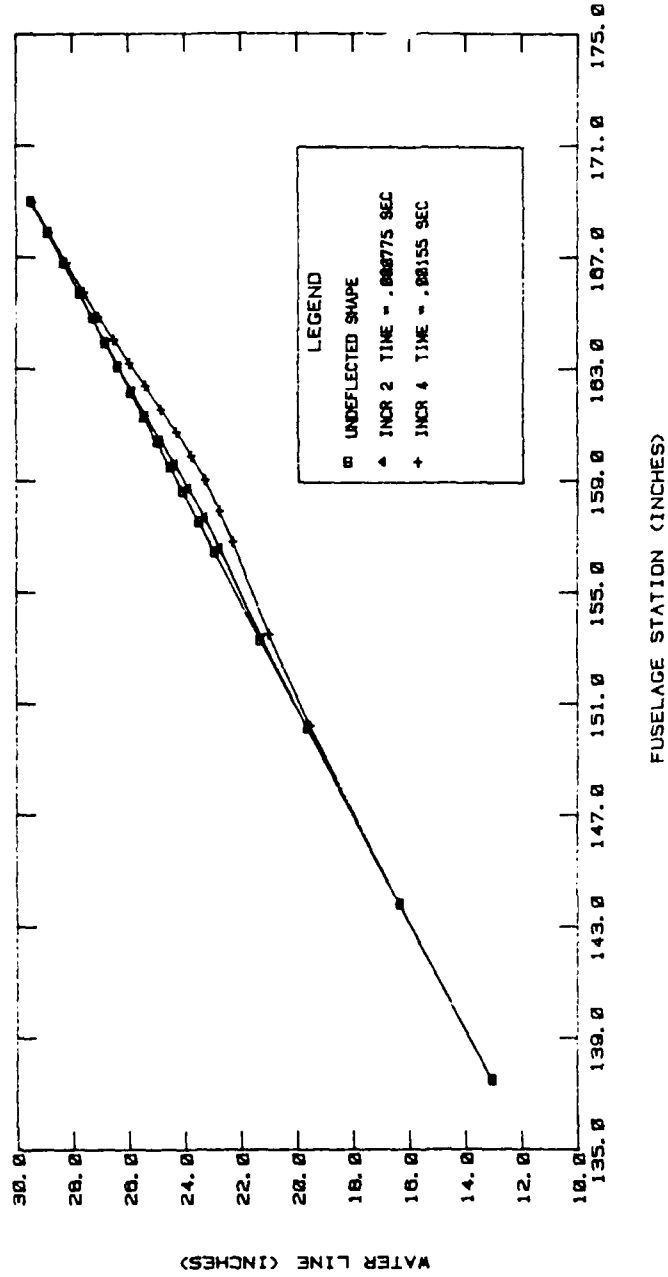
Figure 53. Centerline Deflection - Dynamic Analysis, P=94 psi, t_t = .6

Figure 54. Frame Deflection - Dynamic Analysis, P=94 psi, t_t = .6

TH= .6 P= 140. CL DEFL.

WATER LINE (INCHES)

FUSELAGE STATION (INCHES)

LEGEND
□ UNDEFLECTED SHAPE
▲ INCR 2 TIME = .088775
+ INCR 4 TIME = .00155 SEC
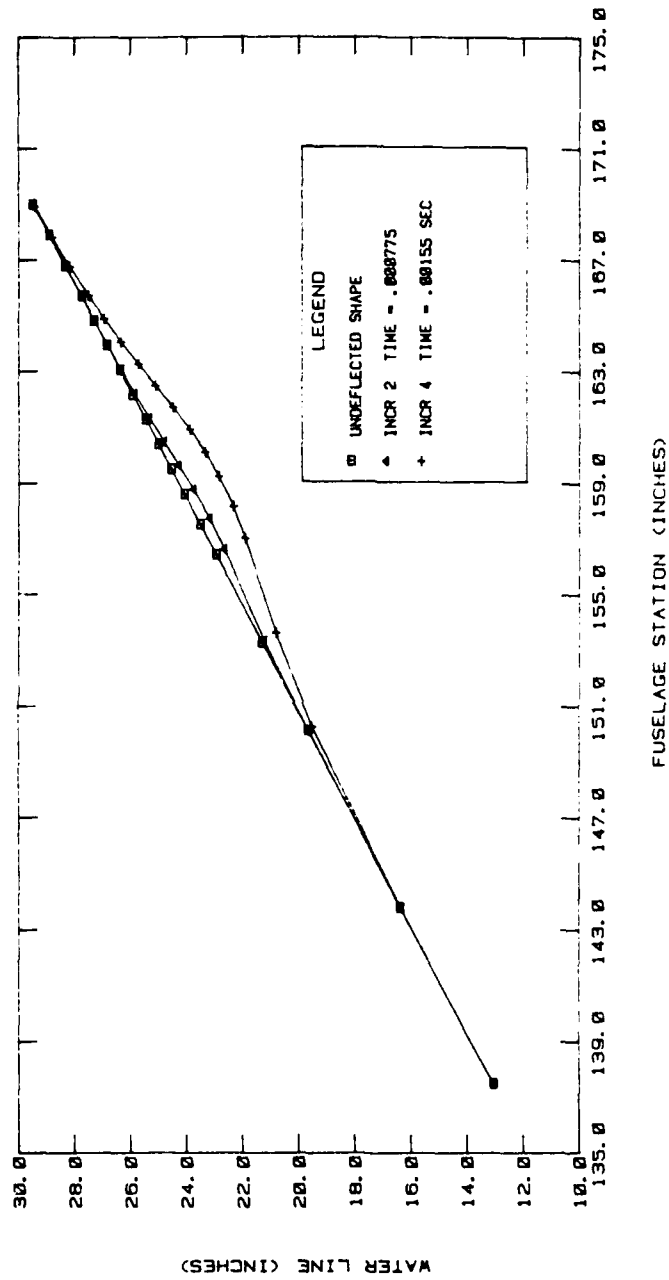
Figure 55. Centerline Deflection - Dynamic Analysis, p=140 psi, $t_t = .6$
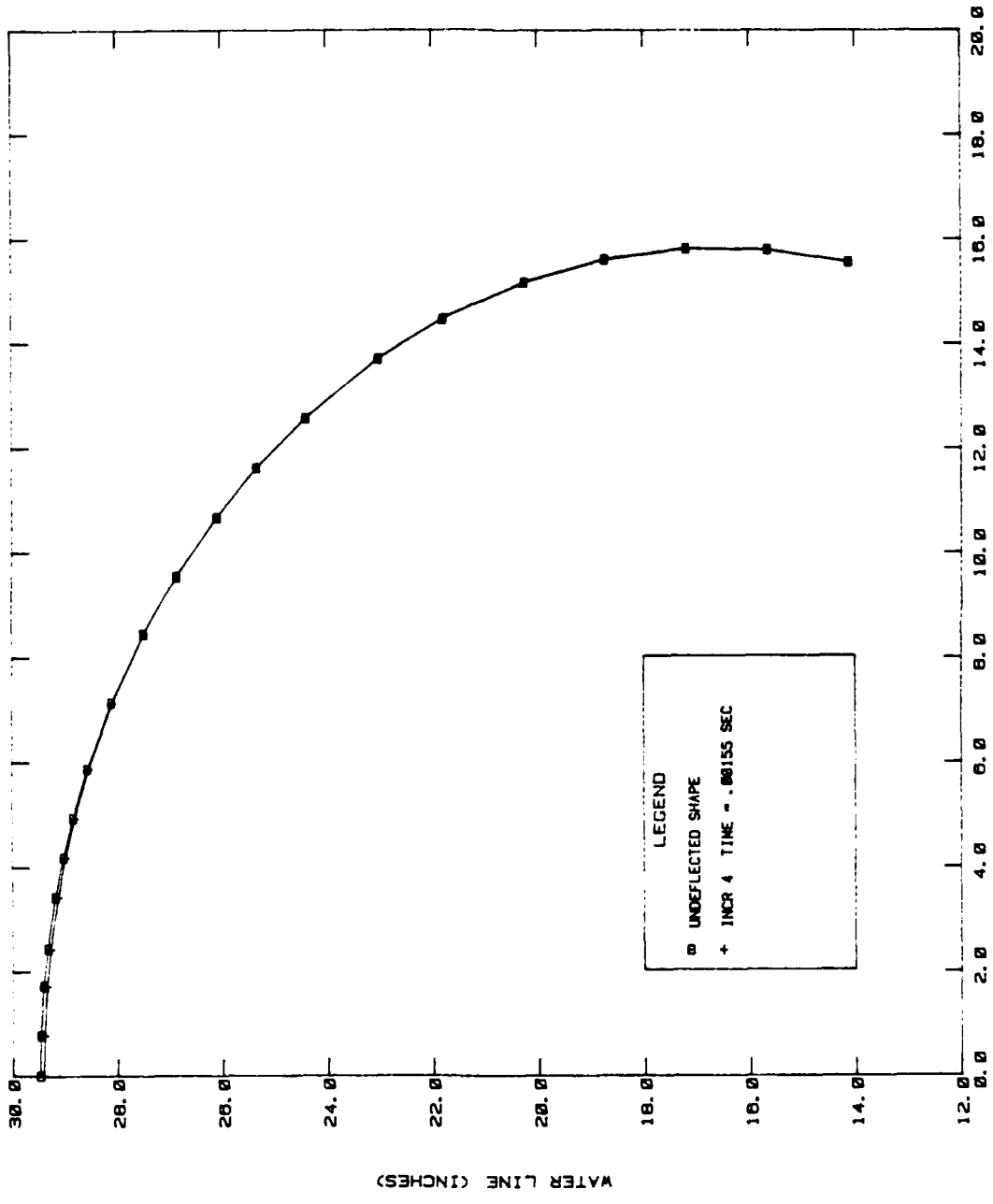
Figure 56. Frame Deflection - Dynamic Analysis, $p=140$ psi, $t_t = .6$

plots indicate the nonlinear aspects of the problem. For large transparency stiffnesses, the analytical results resemble a linear solution. The maximum deflection normal to the transparency is approximately 0.4 inch for the stiffest transparency at two-thirds momentum transferred. This contrasts with a 1.4 inch deflection for the 0.45 inch polycarbonate material at the same load level. All other deflections are relatively large compared to a linear solution, providing evidence of geometric and material nonlinearity along with the dynamic effects. As time progresses the transparency deflection increases to some maximum value and the deflection wave propagates in the direction of the frame. At time increment four the frame is just starting to deflect, indicating that the transparency deflection wave has progressed to the aft arch.

Typical contour plots of the z-axis deflection are presented in Figures 57 and 58. For increment two it is obvious that the frame is not absorbing much of the load. It is not until increment four that the load is being reacted by the frame.
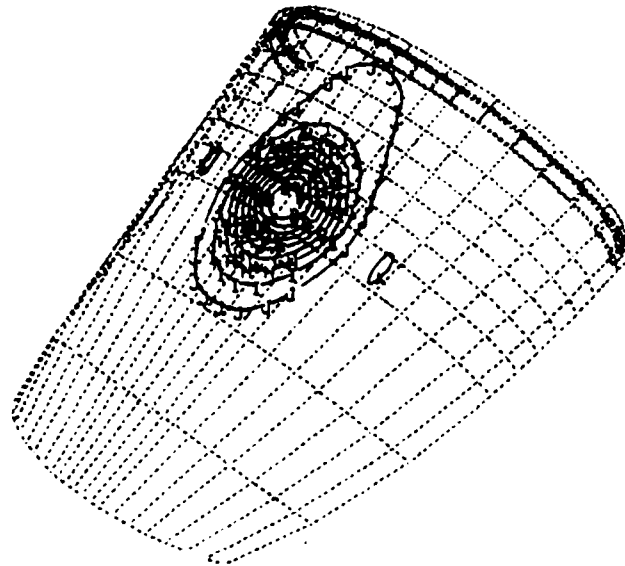
Figure 57.   Z Deflection Contours - Dynamic Analysis,
            Incr. 2.
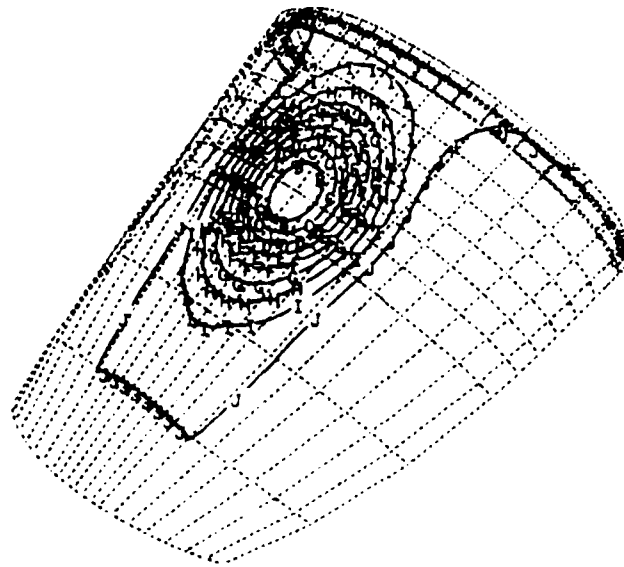
Figure 58.   Z Deflection Contours - Dynamic Analysis,
             Incr. 4.

84
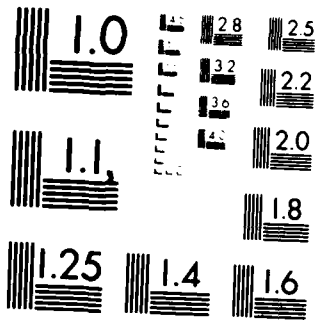
MICROCOPY RESOLUTION TEST CHART
NATIONAL BUREAU OF STANDARDS 1963 A

SECTION VI
RESULTS, CONCLUSIONS AND RECOMMENDATIONS

The studies conducted as a part of this effort have addressed the relative abilities of specific transparency systems to transfer and absorb a range of energy levels under static and dynamic conditions. The transparency materials have been identified as either polycarbonate or stretched acrylic. Good statistical data characterizing specific material properties as a function of strain rate for the two transparency materials is not available. Some work has been done to determine transparency material properties at conditions encountered during birdstrike. At high strain rates the polycarbonate elastic modulus from Reference 10 does not agree with the modulus used in this study, which was taken from MIL-HNDBK-17A (Table 2). The modulus used for the studies reported here is about twice as large as that in Reference 10 for large strain rates. If this reduced modulus were used, then the initial stiffness would be about half as much for the polycarbonate material and the resulting data would reflect this reduction in stiffness.

Interpretation of the finite element studies involved a number of considerations. Comparisons were made between deflection data along the centerline of the transparency and along the frame at the aft edge of the transparency for both the static and dynamic studies. For the static transparency study an attempt was made to establish linear relationships between significant parameters. The most relevant data derived from these studies includes calculation of the resultant forces around the impact area and along the frame for both static and dynamic solutions. This data provides some interesting insights into the behavior of the transparency structural system.

For the transient dynamic analysis, not only the compatibility of the respective stiffnesses but also the amount of energy, rate of loading, and time it takes to dissipate the energy will affect the ability of the transparency system to withstand the bird impact. For a brittle material such as the acrylic, the critical rupture

85

energy is smaller than for a ductile material such as the poly-
carbonate. When the strain energy builds up in any one area,
failure will occur. The structural limits for failure in these
finite element analyses were governed by the ability of the
transparency/support structure system to assimilate the energy
for the dynamic load condition, and by the aft frame yield
strength for the static load condition.

Load distribution, peak stress, and deflection data for
static and dynamic conditions were presented and discussed in
Section 5. Estimated failure data, using the failure criteria
described in Sections 2 and 5.2, is summarized in Tables 6 and
7 for the static and dynamic analyses. For the static analysis,
the 0.45 inch polycarbonate and the 0.9 inch stretched acrylic
show approximately the same capabilities. For the dynamic analysis
the peak stresses at the impact point were somewhat lower for
the 0.90 inch stretched acrylic. However, this is not conclusive
because of the known difference in the failure mode for the two
materials. Furthermore, based on past experience, failure at
the point of impact is an unlikely event in an uncoated polycarbonate
transparency during a birdstrike test. Frame failure, or frame-
induced failure in the transparency, was not evaluated because
the dynamic analysis was not carried out to large enough times to
define that portion of the response.

The parametric study to evaluate the effects of frame
stiffness was not completed. (Reference discussion in Section 4.2.)
To conduct a meaningful study in the material nonlinear range of
response would require the definition of specific design
configurations. Such an effort was judged to be beyond the
scope of this effort.

Additional conclusions and recommendations resulting from
this study are:

(1) Nonlinear dynamic analysis of a complex structure is
very time-consuming with respect to computer resources, calendar
time, and engineering person-hours.

TABLE 6
MATERIAL FAILURE ESTIMATES

STATIC ANALYSIS					
MATERIAL	STIFFNESS	THICKNESS	PRESSURE	TRANSPARENCY FAILURE MECH	FRAME FAILURE MECH
Poly	4.936×10^3b	.45	250	Plastic Range	Plastic Range
Poly	4.936×10^3b	.45	350	Plastic Range	Ductile Failure
Acry	8.1×10^3b	.6	250	Brittle Failure	Plastic Range
Acry	8.1×10^3b	.6	350	Brittle Failure	Plastic Range
Acry	8.1×10^3b	.6	450	Brittle Failure	Ductile Failure
Acry	2.734×10^4b	.9	250	Elastic Range	Elastic Range
Acry	2.734×10^4b	.9	350	Elastic Range	Plastic Range
Acry	2.734×10^4b	.9	450	Brittle Failure	Plastic Range
Acry	2.734×10^4b	.9	550	Brittle Failure	Plastic Range
Acry	2.734×10^4b	.9	750	Brittle Failure	Plastic Range
Low Stiffness Ductile Material	1.233×10^3b	.45	250	Elastic Range	Ductile Failure
High Stiffness Brittle Material	3.24×10^4b	.6	250	Brittle Failure	Elastic Range

TABLE 7
MATERIAL FAILURE ESTIMATES

TRANSIENT DYNAMIC					
MATERIAL	STIFFNESS	THICKNESS	INCR	PRESSURE	TRANSPARENCY FAILURE MECH.
Poly	$4.936 \times 10^3 b$	.45	2	70	Pass
Poly	$4.936 \times 10^3 b$	.45	4	70	Pass
Poly	$4.936 \times 10^3 b$	.45	2	94	Pass
Poly	$4.936 \times 10^3 b$	.45	4	94	Plastic-no failure
Poly	$4.936 \times 10^3 b$	.45	2	140	Plastic-no failure
Poly	$4.936 \times 10^3 b$	.45	4	140	Ductile failure
Acry	$8.1 \times 10^3 b$	.6	2	70	Pass
Acry	$8.1 \times 10^3 b$	.6	4	70	Brittle fracture
Acry	$8.1 \times 10^3 b$	.6	2	94	Pass
Acry	$8.1 \times 10^3 b$	.6	4	94	Brittle fracture
Acry	$8.1 \times 10^3 b$	.6	2	140	Brittle fracture
Acry	$8.1 \times 10^3 b$	.6	4	140	Brittle fracture
Acry	$2.734 \times 10^4 b$	.9	2	70	Pass
Acry	$2.734 \times 10^4 b$	.9	4	70	Pass
Acry	$2.734 \times 10^4 b$	.9	2	94	Pass
Acry	$2.734 \times 10^4 b$	.9	4	94	Pass

(2)   Much useful design information can be generated during a parametric study such as the one reported here.

(3)   There is a need for better definition of material properties and failure criteria as a function of strain rate for transparency materials.

(4)   A fully coupled loads model would facilitiate the performance of the dynamic response analysis.

(5)   Restart capability with MAGNA is necessary to conduct complex analyses of the type reported here.

(6)   The dynamic analysis studies reported here need to be extended to larger times (further into the impact event) to define the peak frame response.

(7)   A higher load intensity needs to be added to the dynamic analysis of the 0.90 inch stretched acrylic transparency.

(8)   The effect of support frame modification will have to be addressed for specific design recommendations to study the nonlinear material behavior of the frame.

(9)   Increased computer capability would greatly facilitate performance of the nonlinear dynamic analyses.

APPENDIX

BIRD LOAD CALCULATIONS

METHOD A (Reference 5,6)

$$F_{PEAK} = .705 \ W^{2/3} \ V^2$$

where W(Bird Weight) = 4 lbs
V (velocity, knots) = 400 knots

$$F_{PEAK} = 284238.19 \ lbs$$

METHOD B (Reference 3)

$$F_{PEAK} = K \omega^{2/3} V^2 \sin\theta$$

where $K = .0585$

$\omega = 4$ lbs

$V = 675.136$ ft/sec (400 knots)

$\theta = 27 \ 1/2°$

$$F_{PEAK} = 31025.395 \text{ lbs}$$

ASSUMPTIONS:

A) Normal incidence

B) Rigid impact structure

C) Soft bird

D) The bird mass is accelerated to the velocity of the structure in the time it takes the structure to traverse through an "effective bird dimension" ($\ell_{EFF} = 3.18\omega^{1/3}$). This acceleration is constant.

METHOD C (Reference 3)

$$F_{PEAK} = K \, \omega^{2/3} \, V^2 \sin\theta$$

where K = .245

ω = 4 lbs

V = 675.136 ft/sec (400 knots)

θ = 27 1/2°

$$F_{PEAK} = 129935.42 \text{ lbs}$$

ASSUMPTIONS:

A) Normal incidence

B) Rigid impact structure

C) The bird is a semirigid object deforming into a three-dimensional mound having a height of 1/4 of the effective bird dimension ℓ_{EFF}, the acceleration distance is then $3/8 \, \ell_{EFF}$. ($\ell_{EFF} = 3.18\omega^{1/3}$)

D) Acceleration of the bird is sinusoidal, the peak force is then $F_{PEAK} = \pi/2 \, F_{MEAN}$.

METHOD D (Reference 4)

$$F_{PEAK} = 2F_{AVE} = mV/T_s = 2m\ V^2\ \sin\theta/\ell_{EFF}$$

where m (bird mass) = 4 lbs/32.2 ft/sec^2

$$= .1242\ \frac{lbs\text{-}sec^2}{ft}$$

V = 675.136 ft/sec (400 knots)

θ = 27 1/2°

ℓ_{EFF} (effective length of bird) = 1.39 ft

F_{PEAK} = 37612 lbs.

ASSUMPTIONS:

A) The momentum normal to impact surface is transferred to the target.

B) Rigid impact structure.

C) The bird is a fluid body.

D) No deceleration of bird during impact ($T_s = \ell_{EFF}/V\ \sin\theta$) T_s is the squash up time.

E) The bird is a right circular cylinder with an effective length $\ell_{EFF} = \ell + d/\tan\theta$ where

ℓ = length of cylinder

d = diameter of cylinder

θ = angle between horizontal and transparency.

REFERENCES

1. Blaine S. West and Kenneth I. Clayton, "Alternate T-38 Transparency Development: Part I, Initial Analysis and Design," AFWAL-TR-80-3132, Air Force Wright Aeronautical Laboratories, Wright-Patterson Air Force Base, Ohio, November 1980.

2. Blaine S. West, "Alternate T-38 Transparency Development, Part II, Baseline Birdstrike Testing," AFWAL-TR-80-3132, Air Force Wright Aeronautical Laboratories, Wright-Patterson Air Force Base, Ohio, December 1980.

3. Don Kahle, Norm Phillips, and Blaine West, "Bird Impact Test Methodology," UDR-TR-75-46, University of Dayton Research Institute, Dayton, Ohio, 1976.

4. John P. Barber, Henry Taylor, and James S. Wilbeck, "Bird Impact Forces and Pressures on Rigid and Compliant Targets," AFFDL-TR-77-60, Air Force Flight Dynamics Laboratory, Wright-Patterson Air Force Base, Ohio, 1978.

5. Bruce F. Kay, "Helicopter Transparent Enclosures," Volume I, USARTL-TR-78-25A, 1979.

6. J. H. Lawrence, "Windshield Birdstrike Structure Design Criteria," AFFDL-TR-73-103, Air Force Flight Dynamics Laboratory, Wright-Patterson Air Force Base, Ohio, October 1973.

7. Blaine S. West and Robert Brockman, "Evaluation of Bird Load Models for Dynamic Analysis of Aircraft Transparencies," AFWAL-TR-80-3092, Air Force Wright Aeronautical Laboratories, Wright-Patterson Air Force Base, Ohio, 1980.

8. R. E. McCarty, "Finite Element Analysis of F-16 Aircraft Canopy Dynamic Response to Bird Impact Loading," 21st AIAA/ASME/ASCE/AHS Structures, Structural Dynamics and Materials Conference, Seattle, Washington, May 1980.

9. R. A. Brockman, "MAGNA: A Finite Element Program for the Materially and Geometrically Nonlinear Analysis of Three-Dimensional Structures Subjected to Static and Transient Loading," AFWAL-TR-81-3181, Air Force Wright Aeronautical Laboratories, Wright-Patterson Air Force Base, Ohio, March 1982.

10. G. E. Greene, "Testing for Mechanical Properties of Monolithic and Laminated Polycarbonate Materials, Part I, Test Results and Analysis," AFFDL-TR-77-96, Air Force Flight Dynamics Laboratory, Wright-Patterson Air Force Base, Ohio, 1978.

11.   Military Standardization Handbook, <u>Metallic Materials and Elements for Aerospace Vehicle Structures</u>, MTL-HNDBK-5C, AFML/MXE, Wright-Patterson Air Force Base, Ohio.

12.   Military Handbook, <u>Plastics for Aerospace Vehicles</u>, Part I and II, MIL-HNDBK-17A, Research and Technology Division (MAAE), Air Force Materials Laboratory, Wright-Patterson Air Force Base, Ohio.

13.   <u>Aerospace Structural Metals Handbook</u>, Mechanical Properties Data Center, Traverse City, Michigan, 1980.

14.   Richard A. Nash and Blaine S. West, "Alternate T-38 Transparency Development, Part V, Parametric Study Data," UDR-TR-82-37, University of Dayton Research Institute, Dayton, Ohio, 1983.

ATE
LME